UNIVERSITY OF CALIFORNIA,
IRVINE

Melanoma growth is regulated by the RhoJ GTPase

DISSERTATION

submitted in partial satisfaction of the requirements
for the degree of

DOCTOR OF PHILOSOPHY

in Biomedical Science

by

Rolando Ruiz-Vega

Dissertation Committee:
Associate Professor Anand K. Ganesan, Chair
Professor Bogi Andersen
Professor Xing Dai
Professor Marian Waterman
Assistant Professor Alex Boiko

2017

DEDICATION

To

my parents Francisco and Lilia Ruiz for their love and support throughout my graduate education. To my siblings Jenny, Janelly, Ricardo and Ronny for their encouragement.

I would also like to dedicate this dissertation to my grandfather who passed away in my final year of graduate school. He was the one who first sparked my interest in science.

TABLE OF CONTENTS

LIST OF FIGURES

LIST OF ABBREVIATIONS

6-4PP	6-4 pyrimidine pyrimidone
ACD	adrenocortical dysplasia homolog
AKT	protein kinase B
ARAF	V-Raf murine sarcoma viral oncogene homolog
ATP	adenosine triphosphate
ATR	ataxia telangiectasia
BAP1	BRCA-1 associated protein-1
BRAF	V-Raf murine sarcoma viral oncogene homolog B
cAMP	cyclic adenosine monophosphate
CD28	cluster of differentiation 28
CD80	cluster of differentiation 80
CD86	cluster of differentiation 86
CDK	cyclin-dependent kinase
CDKN2A	cyclin-dependent kinase inhibitor 2A
CK1	casein kinase 1
CPDs	cyclobutane pyrimidine dimers
CRAF	V-Raf1 murine leukemia viral oncogene homolog
CTLA-4	cytotoxic T lymphocyte-associated antigen 4
ERK	mitogen-activated protein kinase1/3
FLIM	fluorescence lifetime imaging
FTase	farnesyltransferase
GAP	GTPase activating protein

GDP	guanosine diphosphate
GEF	guanine nucleotide exchange factor
GGTase-I	geranylgeranyltransferase type I
GPCR	G-protein coupled receptor
GRB2	growth factor receptor-bound 2
GTP	guanosine triphosphate
GTPase	guanosine triphosphate binding protein
HRAS	V-Ha-Ras Harvey rat sarcoma viral oncogene homolog
IL-2	interleukin-2
INF-α	interferon alpha
INK4A	inhibitor of cyclin-dependent kinase
KRAS	Kristen rat sarcoma viral oncogene homolog
MAPK	mitogen activated protein kinase
MC1R	melanocortin-1 receptor
MEK1/2	mitogen-activated protein kinase kinase1/2
MITF	microphthalmia-associated transcription factor
MSH	melanocyte stimulating hormone
MYC	v-Myc avian myelocytomatosis viral oncogene homolog
$NAD(H)^+$	nicotinamide adenine dinucleotide
NADHP	nicotinamide adenine dinucleotide phosphate
NGS	next generation sequencing
NRAS	neuroblastoma RAS viral oncogene homolog
PAK	p21 activated kinase

PD-1	programmed death 1
PD-L1	programmed death ligand 1
PD-L2	programmed death ligand 2
PI3K	phosphoinositide-3-kinase
PIP_2	phosphatidylinositol (4,5)-diphosphate
PIP_3	phosphatidylinositol (3,4,5)-triphosphate
PKA	protein kinase A
PKG	protein kinase G
POT1	protection of telomere 1
PREX2	phosphatidylinositol-3,4,5-trisphosphate-dependent Rac exchange factor 2
PTEN	phosphatase and tensin homolog
RB	retinoblastoma protein
RhoGDI	Rho guanine nucleotide dissociation inhibitors
RhoJ	ras homolog family member J
RTK	receptor tyrosine kinase
SDH	succinate coenzyme Q reductase
SH2	src homology 2
SLK	STE20 like kinase
SOS	son of sevenless
SRC	proto-oncogene tyrosine-protein kinase
TCL	TC10-like Rho GTPase
TERF2IP	telomeric repeat binding factor 2
TERT	telomerase reverse-transcriptase

UVR	ultraviolet radiation
VEGFR	vascular endothelial growth factor receptor

ACKNOWLEDGMENTS

There are several people that I would like to thank because they were essential in making my graduate education an incredible journey. I would like to express the deepest appreciation to my committee chair, **Dr. Anand Ganesan**, who always challenged me in the most admiring way. His guidance and encouragement pushed me to new heights beyond the expertise of our own lab. He shaped me to become a critical scientist to move science forward in the right direction.

I thank my committee members, **Drs. Bogi Andersen, Xing Dai, Alex Boiko, and Marian Waterman**, whose questions during my committee meetings would always challenge me in new ways. They also supported me during the times I applied for funding. With their help, I was funded throughout my entire graduate education.

There are some undergraduate professors who also contributed to my advancement as a scientist. Drs. **Robert Koch** and **Amybeth Cohen** provided the foundation to prepare me to become a scientist. Their guidance during my undergraduate research motivated me to become a better scientist.

I would like to thank my entire lab, past and present, for the exciting times we had working together. **Dr. Elyse Paterson** for making me feel welcomed in the lab when I first started and for serving as a model during my photography sessions. **Dr. Hsiang Ho** for teaching me basic molecular biology techniques. **Dr. Amelia Hopkin** for also being a model during my photography sessions. **Francisco Espitia** who I first met at Del Obispo Elementary School and I came to encounter again many years later. His expertise helped move my project forward significantly. His motivation for working out was a constant reminder of the phrase “If you put your mind to it you can achieve it.”

Chi-Fen Chen provided so much valuable insight to various scientific questions and personal concerns. Collaborating with Chi-Fen has been an extremely valuable and amazing learning experience. **Priya Vasudeva** always available to have a conversation with during our down time. She was also extremely helpful during our single cell isolation days where we came in before the crack of dawn to lab. **Dr. Sohail Jahid** and **Jessica Flesher** for always providing guidance, support, and ideas to move my project forward. To all my summer high school students that came in through the Youth Science Fellowship Program and taught me the foundation of being a mentor. **Dr. Marc Liggins** always provided a unique perspective to life in lab and the world in general.

I would also like to thank all the amazing people in the **Biological Chemistry** department and in the **Cancer Research Institute** who helped me with all sorts of things both lab and non-lab related.

I thank all the funding agencies that funded my graduate education: **Stanley Behrens Foundation, FORD Dissertation Fellowship, National Science Foundation Graduate Research Fellowship, UCI MBRS program, UCI School of Medicine**.

I would like to especially thank all my family members for their support and encouragement throughout my graduate education. Without them I would not have become the scientist I am today. My brothers were always there to listen to my practice talks and I realized that if they can understand my talks then I am ready to present my work to my department, lab, or at a conference. My sisters were always curious about the experiments that I perform on my “patients”. My parents, who even though might not completely understand what I am doing they know that it is something not everyone can do. My significant other who always stood by my side even when I had to work long

hours. She always supported me even when a scientific outcome was not so positive. I thank all these people from the bottom of my heart.

CURRICULUM VITAE

Rolando Ruiz

EDUCATION

Ph.D. Biomedical Science, University of California, Irvine, (UCI) CA.

- Degree: June 2017

B.S. in Biological Science, California State University, Fullerton, (CSUF) CA.

- Degree: May 2010
- Area of Concentration: Cell and Developmental Biology

RESEARCH EXPERIENCE

University of California, Irvine Irvine, CA

Graduate Research, Mentor Dr. Anand Ganesan 2011-Present

- Elucidate the role of *RhoJ* in melanoma development and metastasis with inducible genetically engineered mouse models.
- Identify the downstream targets of *RhoJ* by utilizing RNAi technology and inhibitors.
- Determine the cell autonomous role of *RhoJ* in melanocytes.

Tufts University Sackler School of Biomedical Science Boston, MA

Post baccalaureate Research, Mentor Dr. Alain Charest 2010-2011

- Elucidated the role of p38 MAPK in glioblastoma multiform from cancer cells that originated in a genetically engineered mouse model.

California State University, Fullerton Fullerton, CA

Undergraduate Research, Mentor Dr. Robert A. Koch 2006-2010

- Identified the protein kinase C (PKC)-alpha and PKC-delta as the major subtypes and activators in *Ascidia ceratodes* sperm cells using various inhibitors.
- Identified the localization of PKC along the tail and mitochondrion of *A. ceratodes* sperm cells utilizing immunofluorescence.
- Defined plasma membrane microdomains as “lipid rafts” overlaying mitochondrion region in activated sperm cells by combining drug treatments with immunofluorescence, which are important for sperm activation.

Princeton University Princeton, NJ

Summer Undergraduate Research, Mentor Dr. Lynn Enquist 2008

- Determined the mechanism by which an attenuated Pseudorabies virus (PRV) strain spreads between mammalian neurons by utilizing a GFP-tagged attenuated strain of the virus that will encode for post-synaptic density (PSD-95-GFP) located at chemical synapses.

PUBLICATIONS

- Ruiz, R., Jahid, S., Harris, M., Marzese, D., Espitia, F., Vasudeva, P., Chen, C-F., de Feraudy, Wu, J., Gillen, D., Krasieva, T. B., Tromberg, B. J., Pavan, W., Hoon, D., Ganesan, A. (2017). The RhoJ-BAD signaling network: An achilles heel for BRAF mutant melanomas. *Plos Genetics,* Submitted.
- Chen, C-F.*, Ruiz, R.*, Vasudeva, P., Espitia, F., Krasieva, T., de Feraudy, S., Tromberg, B., Huang, S., Hoon, D., Garner, C., Wu, J., Ganesan, A. (2017). ATR mutations promote the growth of melanoma tumors by modulating the immune microenvironment. *Cell Reports, 18(10),* 2331-2342. *Co-first author.
- Geyfman, M., Kumar, V., Liu, Q., Ruiz, R., Gordon, W., Espitia, F., Cam, E., Millar, S. E., Smyth, P., Ihler, A., Takahashi, J. S., Andersen, B. (2012). Brain and muscle Arnt-like protein-1 (BMAL1) controls circadian cell proliferation and susceptibility to UVB-induced DNA damage in the epidermis. *Proc. Natl. Acad. Sci USA, 109(29),* 11758-11763.
- Acquaviva, J., Jung Jun, H., Lessard, J., Ruiz, R., Zhu, H., Donovan, M., Woolfenden, S., Boskovitz, A., Raval, A., Bronson, R. T., Pfanni, R., Whittaker, C. A., Housman, D. E., Charest, A. (2011). Chronic activation of wild type epidermal growth factor receptor and loss of Cdkn2a cause mouse glioblastoma formation. *Cancer research, 71(23)*, 7198-7206.
- Ruiz, R. and Koch, R. A. (2010). Localization and identification of protein kinase C subtypes in ascidian sperm activation. *Dimensions, 13,* 54-62.

PRESENTATIONS

- Ruiz, R., Jahid, S., Espitia, F., Chen, C-F., de Feraudy, S., Harris, M., Pavan, W., Gillen, D., Marzese., D., Hoon, Dave., and A. K. Ganesan. “RhoJ regulates the growth and development of BRAF mutant melanoma,” CSU Fresno, Fresno, CA (April, 2016; Oral Presentation)
- Ruiz, R., Jahid, S., Espitia, F., Chen, C-F., de Feraudy, S., Harris, M., Pavan, W., Gillen, D., Marzese., D., Hoon, Dave., and A. K. Ganesan. “RhoJ regulates the growth and development of BRAF mutant melanoma,” PanAmerican Society for Pigment Cell Research Conference, Orange, CA (September, 2015; Oral Presentation).
- Ruiz, R. and A. K. Ganesan. “Elucidating the role of RhoJ in melanoma chemoresistance,” Cancer Biology Training Grant Retreat, Palm Springs, CA (April, 2013; Oral Presentation).
- Ruiz, R. and J. Krowlewski. “TGF-β and TNF-α signaling in prostate apoptosis,” Minority Biomedical Research Support Symposium, UCI, Irvine, CA. (September, 2011; Oral Presentation).
- Ruiz, R. and A. Charest. “Elucidating the role of p38 MAPK in glioblastoma multiforme,” Molecular Oncology Research Institute Retreat, Dennis, MA. (June, 2011; Oral Presentation).
- Ruiz, R. and A. Charest. “Elucidating the role of p38 MAPK in glioblastoma multiforme,” New England Science Symposium, Harvard, Boston, MA. (April, 2011; Oral Presentation).
- Ruiz, R. and R. A. Koch. “Localization of Protein Kinase C and Identification of its Subtypes in Ascidian Sperm Activation,” Thesis Defense, CSUF, Fullerton, CA. (April, 2010; Oral Presentation).

- Ruiz, R. and R. A. Koch. “Localization of PKC Activity in Unactivated and Activated Ascidian Sperm,” California State University Program for Education and Research in Biotechnology, Santa Clara, CA (January, 2010; Poster Presentation).
- Ruiz, R., Allen, K., Lotfizadeh, A., and R. A. Koch. “Localization of PKC Activity in Ascidian Sperm Activation.” SACNAS-Advancing Hispanics/Chicanos and Native Americans in Science National Conference, Dallas, TX. (October 2009; Poster Presentation).
- Ruiz, R., Allen, K., Lotfizadeh, A., and R. A. Koch. “Localization of PKC Activity in Ascidian Sperm Activation.” West Coast Biological Sciences Undergraduate Research Conference, San Diego, CA. (April 2009; Poster Presentation).
- Ruiz, R., Allen, K., Lotfizadeh, A., and R. A. Koch. “Localization of PKC Activity in Ascidian Sperm Activation.” Natural Science and Mathematics Career Day, CSUF, Fullerton, CA. (April 2009; Poster Presentation).
- Ruiz, R. and R. A. Koch. “Localization of PKC Activity in Ascidian Sperm Activation: Enzymatic Characterization of Cellular Fractions.” MARC Pro-Seminar, CSUF, Fullerton, CA. (March 2009; Oral Presentation).
- Ruiz, R., Diaz, D., and R. A. Koch. “Characterizing Plasma Membrane Microdomains in *Ascidia ceratodes* Sperm Cells.” SACNAS (Society for the Advancement of Chicanos and Native Americans in Science) National Conference, Salt Lake City, Utah. (October 2008; Poster Presentation).
- Ruiz, R., Granstedt, A. and L. Enquist. “Constructing a recombinant PrV that expresses PSD-95-GFP to understand how it spreads between neurons” MARC Pro-seminar, CSUF, Fullerton, CA. (October 2008; Oral Presentation).
- Ruiz, R., Granstedt, A. and L. Enquist. “Development of a Pseudorabies Virus Strain to Label Synapses.” Lewis-Sigler Institute Summer Undergraduate Research Program Symposium, Princeton University, Princeton, NJ (August 2008; Oral Presentation).
- Ruiz, R., Diaz, D., and R. A. Koch. “Searching for microdomains (lipid rafts) in sperm cells of *Ascidia ceratodes.”* College of Natural Science and Mathematics Inter-Club Council Symposium, CSUF, Fullerton, CA (April, 2008; Poster Presentation).

FELLOWSHIPS/AWARDS/HONORS

- UC President’s Postdoctoral Fellowship 2017
- Stanley Behrens Fellow in Medicine 2016
- FORD Foundation Dissertation Fellowship, The National Academies 2016
- School of Medicine Outstanding Student Fellowship-UCI 2015
- National Science Foundation (NSF) Graduate Research Fellowship 2013-2016
- FORD Foundation Fellowship, The National Academies 2013
- Minority Biomedical Research Support (MBRS) Fellowship 2011-2013
- Post-Baccalaureate Research Program (PREP) Fellowship 2010-2011
- CSUF Dean’s List 2010
- Minority Access to Research Careers (MARC) Fellowship 2008-2010
- Alliance/Merck Ciencia (Science) Hispanic Award 2009

- Lewis-Sigler Institute Summer Undergraduate Research Fellowship 2008
- Associate Student Incorporated (ASI) Research Grant 2008
- Society for Advancement of Chicano and Native Americans in Science (SACNAS) Travel Award 2007-2009
- The Horatio Alger Association of Distinguished Americans Excellence Award and Scholar 2005-2009
- Laguna Niguel Rotary Club Excellence in Academics Award 2005-2008
- Educational Opportunity Program (EOP) Grant 2005-2010
- AVID (Advancement via Individual Determination) alumni Excellence in Academics Award 2006
- Links Mentoring Program book scholarship 2005
- Private Donor Excellence in Academics Award 2005
- Coral Thrift Shop Excellence in Academics Award 2005
- AVID (Advancement via Individual Determination) Excellence in Academics Award 2005
- Future Scholars Excellence in Academics Award 2005
- United Way Excellence in Academics Award 2005

TEACHING EXPERIENCE

University of California, Irvine Winter Quarter: 2015

Teaching Assistant-From Organisms to Ecosystems (Bio94)

- Trained students to look at a scientific finding and critically evaluate its validity.
- Coached students to propose evolutionary hypothesis.
- Developed interactive activities for this lower division course so students could distinguish biotic and abiotic factors.
- Worked with a diverse population of students, including many international students and ESL students, and developed strategies to meet the students' learning needs.
- Used online learning management systems to organize content and communicate with students outside of class to encourage clarity and transparency.

EduBoard

Online Tutor March 2015-Present

- Provide a personalized online student-centered tutoring experience for students in high school and college in the subjects of biology and algebra.

California State University, Fullerton Spring Semester: 2009, 2010

Teaching Assistant-Cellular Basis of Life Laboratory (Bio172L)

- Developed lectures on prokaryotic and eukaryotic cells including: evolutionary relationships; cell membranes; signaling and metabolic pathways; cellular reproduction; cell differentiation, and development.
- Designed and assessed student progress based on assignments and quizzes.

EXTRACURRICULAR AND VOLUNTEER ACTIVITIES

Horatio Alger Association 2014-Present

Mentor

- Listen, inspire, inform, guide, encourage, and support my Horatio Alger Scholar mentees with the goal of helping them to contribute to their personal and academic development.

UCI Cancer Research Institute Summers: 2014-Present

Youth Science Fellowship Program Coordinator

- Organize scientific workshops such as Next Generation Sequencing, graduate student panels, and seminars to encourage high school students in a path toward scientific research.
- Building the pipeline of high school students for the next generation of cancer researchers with lab experience.
- Mentor students in a laboratory by guiding them with a research project related to cancer and preparing them for a scientific talk about their work.

UCI Department of Biological Chemistry 2014-2015

Student Representative

- Served as a knowledgeable resource for graduate students, addressing their questions and concerns about on campus resources.
- Advised students to attend and participate in professional and personal development workshops.
- Organized social and networking events to strengthen community in the department.

Orange County Science and Engineering Fair 2013-present

Judge

- Encourage the youth of Orange County to learn about science and to consider a career in science or engineering.

Johns Hopkins Center for Talented Youth program at CSUF 2010

Teacher

- Organized and led a DNA lab activity for 120 academically gifted middle and high students where they gained a basic understanding of genetics.

PROFESSIONAL DEVELOPMENT

- E-Learning Instructional Design at University of California, Irvine Continuing Education 2017
- Foundations in Teaching Program at University of California, Irvine. 2015
- University Teaching 101 at Johns Hopkins University on Coursera. 2015
- Virtual Teacher Program at University of California, Irvine on Coursera. 2015

ABSTRACT OF THE DISSERTATION

Melanoma growth is regulated by the RhoJ GTPase

By

Rolando Ruiz-Vega

Doctor of Philosophy in Biomedical Science

University of California, Irvine, 2017

Associate Professor Anand Ganesan, Chair

The main function of the mammalian skin is to protect the organism against various deleterious environmental factors such as UVR. The skin contains specialized pigment producing cells, known as melanocytes, to protect against UVR. However, when melanocytes acquire mutations from excessive exposure to UVR or other factors, they transform into melanoma. Melanoma is the deadliest type of skin cancer that invades neighboring tissue during early tumor development. The BRAF oncogene is mutated in over 50% of human melanoma cases and therapies that target the BRAF signaling are effective at inducing tumor regression. Unfortunately, melanoma tumors acquire resistance and become unresponsive to BRAF therapy because of alterations in various signaling networks. Genes and pathways that allow cells to cope with oncogene-induced stress represent selective cancer therapeutic targets that remain largely undiscovered. In addition, melanomas accumulate a high burden of mutations that could potentially generate neoantigens, yet somehow suppress the immune response to facilitate continued growth. In order to better understand the signaling networks that drive BRAF mutant melanoma, we identified a RhoJ signaling pathway

that is a selective therapeutic target for BRAF mutant tumors. RhoJ is a small GTPase that cycles between an active-GTP bound state and an inactive-GDP bound state that regulates various physiological mechanisms. Previously we demonstrated that RhoJ is involved in chemoresistance in melanoma and in suppressing ATR activity. Using an autochthonous mouse model of melanoma, we determined that loss of RhoJ significantly prolonged the life of mice bearing $BRAF^{V600E}$ mutant melanomas by delaying tumor initiation and reducing metastasis. Transcriptome analysis revealed that RhoJ deletion in BRAF mutant tumors modulates the expression of the pro-apoptotic protein BAD as well as genes involved in cellular metabolism, generating tumors that grow more slowly and metastasize less avidly. PAK inhibitors induce apoptosis in melanoma cells in vitro via a BAD-dependent mechanism and induce the regression of BRAF mutant melanoma tumors in vivo. We also demonstrate that ATR mutant tumors accumulate multiple mutations and alter the immune system by decreasing T-cells to encourage tumor growth. Taken together, these studies identify the RhoJ-BAD signaling network as a therapeutic vulnerability for BRAF mutant tumors. Additionally, these studies also identify a novel mechanism by which melanoma cells modulate the tumor microenvironment to promote survival.

CHAPTER 1: Introduction

The Skin

The skin is a remarkable organ that is comprised of three major layers including the epidermis, dermis, and subcutaneous fat. The bottom most layer of the skin is the subcutaneous fat layer that helps insulate the body's temperature and provide energy when needed. The dermis is the middle layer that is relatively thick and mainly comprised of collagen, elastin, and fibrillin (1), components required for tissue to regain their shape after stretching or contracting. The dermis also contains several appendages including nerve endings, sweat glands, sebaceous glands, hair follicles, and blood vessels. The stratum corneum is the outermost layer of the epidermis that provides protection from foreign substances. The epidermis is relatively thin and mainly composed of keratinocytes that originate from the innermost layer within the epidermis known as the basal layer, which is comprised of basal cells. New keratinocytes slowly migrate to the top of the skin as older keratinocytes gradually shed off the skin leading to a stratified epithelium. Scattered within the basal layer, there are specialized cells called melanocytes that produce a pigment called melanin, which is a molecule whose concentration will dictate a person's skin color. Melanocytes' primary function is to provide protection from ultraviolet radiation (UVR) from the sun, which causes DNA damage and can lead to various skin cancers. These specialized cells are able to provide this protection because the melanin distributed throughout the skin absorbs most of the UVR.

Melanoblasts are melanocyte precursor cells that originate from the neural crest and migrate to the hair follicle and remain in a stem-cell-like state until they differentiate

and spread to the skin or hair (2). In human skin, one melanocyte is able to distribute melanin to approximately 15-25 keratinocytes in order to provide protection from UVR. Melanin is produced when neighboring keratinocytes produce the melanocyte-stimulating hormone (MSH) after UVR stimulation, which then binds to the melanocortin-1 receptor (MC1R) on melanocytes to initiate cyclic adenosine monophosphate (cAMP) signal transduction leading to the expression of microphthalmia-associated transcription factor (MITF), the master regulator of pigment production genes (3, 4). MITF expression regulates tyrosine accumulation resulting in the production of eumelanin and pheomelanin, which are transported to keratinocytes in melanosomes for UV protection. Amount of pigmentation produced is correlated with geographical locations such that higher pigmentation is observed near the equator and decreases as one moves away from the equator (5). Although melanocytes serve a specific function for the skin, any genetic alteration in these cells can lead to various skin disorders such as hypopigmentation, hyperpigmentation, and even skin cancers.

Causes of Melanoma Skin Cancer

Melanoma is the deadliest type of skin cancer that was first identified in the skin of Peruvian mummies (6). In the United States, there is an incidence rate of 19 per 100,000 persons in 2011 and unfortunately that number is on the rise (7). Melanoma initiation begins when melanocytes are transformed from either environmental or genetic factors. Environmental factors such as UVR (i.e. sun-tanning) contributes to melanoma incidences, and people who are fair skinned are more susceptible to this skin cancer because their melanocytes are being overexposed to UVR (8). UVR exists in three different wavelengths, UVA (320 to 400 nm), UVB (290 to 320 nm), and UVC (100

to 290 nm) but only some contribute to the development of melanoma. People are protected from UVC by the earth's ozone layer, which absorbs relatively short wavelengths. UVB is responsible for forming bulky DNA lesions known as cyclobutane pyrimidine dimers (CPDs) and pyrimidine (6-4) pyrimidone (6-4 PP) photoproducts, which cause mutations if not repaired correctly (9). CPDs are a product of two adjacent thymine nucleotides forming two C-C bonds with each other as oppose to with their corresponding adenine nucleotide. In contrast to CPDs, 6-4PP form a single bond between two thymine nucleotides. UVA is responsible for causing oxidative DNA damage that leads to double stranded DNA breaks (10). Melanoma usually occurs with intermittent exposure of UVR while basal cell carcinoma and squamous cell carcinoma, less deadly skin cancers, occur from constant UVR exposure (8).

Melanomas can be classified into stages depending on various prognostic factors established by the American Joint Committee on Cancer. The most important prognostic factor in melanoma is their movement to a regional lymph node. Alternatively, the degree of invasiveness is used as the prognostic factor in cases where melanoma has not traveled to the lymph node. The two systems used to predict patient outcome are the Clark level and Breslow thickness (11). Clark levels characterize melanomas based on their morphology within the epidermis, dermis, and subcutaneous fat layers of the skin (12). Breslow depth is the measure of the tumor thickness from the epidermis to the deepest tumor cell in the skin (13). Survival rate decreases when either the tumor has metastasized to the regional lymph node, the morphology of the tumor has invaded the subcutaneous fat, or when the depth of the tumor is greater than three millimeters. Their ability to invade deep into the skin and metastasize to other

tissues depends on the tumor's ability to proliferate and survive. Several genetic mutations have been shown to regulate pathways responsible for melanoma's aggressiveness.

Germline mutations

Genetic alterations and genomic instability are being identified with the current advances in next generation sequencing (NGS) and various genetically engineered mouse models. Both familial and sporadic mutations have been identified to drive melanoma development and progression. Familial mutations make up approximately 10% of melanoma cases (14) with the most common alteration being in the *Cyclin-dependent kinase inhibitor 2A (CDKN2A)* gene (15, 16). *CDKN2A* was connected with melanoma predisposition by linkage and by a positional cloning approach (15, 16). In humans, the *CDKN2A* gene encodes two different tumor suppressor proteins, INK4A (p16) and ARF (p14), which play a role in cell cycle regulation (17). INK4A (inhibitor of cyclin-dependent kinase) inhibits CDK4/6 (cyclin dependent kinase) from phosphorylating the retinoblastoma protein (RB) while ARF sequesters MDM2 preventing the subsequent degradation of p53 (17). The majority of mutations that occur on INK4A are loss-of-function missense mutations (15, 16). Mutations on CDK4 are very rare and only occur on arginine-24, which prevents INK4A association with CDK (18). In contrast to INK4A, ARF does not contain missense mutations but instead has entire gene deletions, insertions or splice mutations (19-21). Other familial mutations have been discovered more recently with the novel advances in sequencing technologies.

After 20 years of *CDKN2A* being the only familial gene that caused melanoma, current technologies have allowed for the discovery of a new set of familial genes that also lead to melanoma. MITF is the master regulator of melanocyte development and one of the first genes to be identified as a melanoma oncogene with NGS. Two different groups identified the same (E318K) mutation on MITF-M isoform, which changes its transcriptional activity by inhibiting sumoylation (22, 23). MC1R, which also plays a role in regulating pigments production, was also identified as a familial gene that leads to melanoma. Mutations on the *BRCA-1 associated protein-1* (BAP1) gene are more rare but occur in about 15% of familial cutaneous melanoma cases (24). It acts as a tumor suppressor in uveal melanomas (25), regulates melanocyte differentiation (26), and plays a role in DNA damage response (27). Another gene that was also recently discovered to be associated with familial melanoma is the *telomerase reverse-transcriptase* (*TERT*) gene. *TERT* is responsible for encoding a subunit of telomerase, the complex that maintains the length of telomere on DNA. It contains a mutation in the promoter region, which creates a new binding motif for transcription factors and increases the transcription of *TERT* (28). Whole genome sequencing identified somatic mutations -124bp and -146bp upstream of the initiation codon in 89% of melanoma cell lines (29). *Protection of telomere-1* (*POT1*) is another gene that forms a complex to protect telomere ends by binding to telomeric single stranded DNA (30). Exome sequencing identified *POT1* loss-of-function mutations and three missense mutations (Y89C, Q94E, and R273L) in melanoma (31). These mutations prevented *POT1* from binding to telomeric DNA and produce longer telomeres (31). Two other components of the telomerase shelterin complex, *Adrenocortical dysplasia homologue* (*ACD*) and

telomeric repeat binding factor 2 (*TERF2IP*), were also discovered to contain mutations in familial melanoma (32). Both mutations were associated with early tumor development and multiple primary melanomas. Unlike other mutations that are specific to melanoma, mutations in both *ACD* and *TERF2IP* can lead to other cancers such as breast, lung and colon cancer (14). The discovery of new mutations in melanoma cases has led to the development of novel therapeutic targets.

Somatic mutations

Somatic mutations also play a major role in melanoma development. The most prominent pathway that is known to drive melanoma is the mitogen-activated protein kinase (MAPK) signaling pathway (Figure 1.1.A). The MAPK signaling cascade consists of several kinases that regulate multiple cellular behaviors such as proliferation, growth, and differentiation (33). Various stimuli, such as UVR, can initiate signaling and activate the RAS family of proto-oncogenes (*NRAS*, *HRAS*, and *KRAS*). The RAS family proteins are low molecular weight GTP-binding proteins (GTPase) that cycle between active and inactive states depending on whether they are bound by guanosine triphosphate or guanosine diphosphate (GTP or GDP, respectively). NRAS (neuroblastoma RAS viral oncogene homologue) is mutated in 5-33% of melanomas cases (34-36) and are known to occur mainly above the neck region. HRAS (V-Ha-Ras Harvey rat Sarcoma viral oncogene Homologue) and KRAS (Kristen rat sarcoma viral oncogene homologue) mutations are observed in only 1% and 2 % of melanoma cases, respectively. The mutation observed in both NRAS and HRAS occur in glutamine-61 (37). These RAS proto-oncogenes then activate the RAF family of serine/threonine kinases (ARAF, BRAF, and CRAF). Mutations in both ARAF (V-Raf murine sarcoma

viral oncogene homologue) and CRAF (V-Raf1 murine leukemia viral oncogene homologue) are rare in all types of cancers and activating mutations in these kinases have only been observed in less than 1% of lung cancers (38). The *BRAF* (V-Raf murine sarcoma viral oncogene homologue B) oncogene is mutated in 40-60% of all melanoma cases (39) with the most common mutation being the valine-600 substitution with a glutamate (40). This mutation generates a constitutively active BRAF allowing the MAPK pathway to continuously propagate its downstream signaling. The next most common BRAF mutation is the valine-600 substitution with a lysine, which occurs in 20% of cases (41) due to chronic exposure to sun (42). The third and least common BRAF mutation occurs in 5-7% of patients where the valine-600 is substituted with an arginine (43). Although BRAF is the most common mutation in melanomas, it is not enough to drive tumors alone. Interestingly, this mutated oncogene is also found in benign nevi suggesting that other genetic alterations are required for melanoma progression. Upon mutation or activation of BRAF, it can then phosphorylate mitogen-activated protein kinase kinase1/2 (MEK1/2) and subsequently activate mitogen-activated protein kinase1/3 (ERK) kinases. Exome sequencing revealed that MEK1 and MEK2 have a mutation frequency of 8% (44) while ERK mutations are much more rare (45).

The PI3K-AKT kinase pathway is also crucial for proliferation and survival and is often altered in cancers including melanomas. The PI3K pathway is a signaling cascade that initiates with a growth factor binding to a receptor tyrosine kinase, which in turn activates PI3K (phosphoinositide-3-kinase). PI3K will then phosphorylate phosphatidylinositol (4,5)-diphosphate (PIP_2) and activate protein kinase B (AKT) where

it will localize to the cytoplasm in order to activate mTOR and lead to a cellular response (Figure 1.1.B). The activation of AKT by PI3K is highly regulated by the tumor suppressor *phosphatase and tensin homologue* (PTEN), which decreases intracellular phosphatidylinositol (3,4,5)-triphosphate (PIP_3) and prevents activation of AKT. Loss of PTEN occurs in 30-50% of melanoma cases (46-48) and cooperates with other mutations, such as BRAF, to drive melanoma (49). PTEN is also mutated in 10% of melanoma cell lines (50-52). AKT is has been shown to be constitutively activated in 60% of melanomas (53) while AKT3 has been shown to be overexpressed (54, 55). Since both loss of PTEN and activation of BRAF are observed with high frequency in melanoma, this suggests that both pathways are crucial for melanoma development.

Melanoma Treatments

The identification of all these mutations has led to the discovery of many therapeutic targets but no single agent has significantly increased survival rates. The chemotherapeutic drug Dacarbazine, an alkylating agent that causes DNA adducts, has been used to treat late stage melanomas since 1975. However, it only increases survival by 3-5% with an even lower durable response of <2% (56). Other chemotherapeutic agents have been used in combination with dacarbazine like cisplatin and vinblastine (57). Temozolomide is another alkylating agent that is similar to dacarbazine and used as a melanoma treatment, but unfortunately both drugs have comparable survival rates.

Over the past five to ten years, immunotherapy has greatly moved forward in treating late stage melanomas. The cytokines interleukin-2 (IL-2) and interferon alpha (INF-α) were the first immunotherapies used in the early 1990's and were shown to

have a median duration response of 8.9 months (58, 59). More recent efforts are aimed at inhibiting immune checkpoints. Immune checkpoints are numerous pathways that are directly associated with the immune system and are important for regulating immune responses in peripheral tissues to keep tissues functioning normally (60). Two monoclonal antibodies, ipilimumab and tremelimumab, have been developed to target the cytotoxic T lymphocyte-associated antigen 4 (CTLA-4). CTLA-4 is a negative regulator of T-cell activity that is expressed on the surface of T-cells. It counteracts the activating CD28 (cluster of differentiation 28) receptor but competes for the same two ligands: CD80 and CD 86. Blocking CTLA-4 with either ipilimumab or tremelimumab increases an immune response and recruits helper T-cells and both drug agents demonstrate significant improvements (61, 62). The breakthrough of CTLA-4 inhibition led to further research in other immune checkpoints. The programmed death 1 (PD-1) inhibitory T-cell receptor is another immune checkpoint that led to a significant breakthrough in immune therapy for melanomas. PD-1 ligands, PD-L1 and PD-L2 (programmed death ligand 1 and 2, respectively), are found in the tumor microenvironment, which suggests that PD-1 can provide a specific anti-tumor response (63). PD-1 limits T-cell activity in the neighboring tissues when an inflammatory response arises because of an infection and it also limits autoimmunity (64, 65). Two antibodies have been developed against PD-1 and PD-L1, pembrolizumab and nivolumab, for metastatic melanomas. A clinical trial for pembrolizumab demonstrated a response rate of 33% (66), while nivolumab had a response rate of 44% (67). These antibodies have shown promising results and phase III clinical trials are currently underway.

Kinase inhibitors have also been developed to target specific mutations in melanoma. A lot of focus has been placed on BRAF inhibitors because it is the most common mutation found in melanomas (39). Vemurafenib is a $BRAF^{V600E}$ specific kinase inhibitor that inhibits the MAPK signaling pathway and prevents cell proliferation, but it does not have an effect on melanomas that contain normal BRAF expression. Clinical trials have demonstrated that patients treated with Vemurafenib had a 53% response rate (68). Unfortunately, there is a small 10-15% population of patients that do not have positive effects from Vemurafenib (68, 69), which is most likely due to resistance mechanisms that tumors acquire. The most common resistance mechanisms lead to reactivation of MEK or ERK (45, 70-72), but there are other mechanisms such as upregulation of NRAS (73), $BRAF^{V600E}$ gene amplification (74), enhanced dimerization of $BRAF^{V600E}$ (75), and activation of alternative signaling pathways including PI3K pathway (76). With increased number of resistance mechanisms, Vemurafenib is becoming futile and needs to be used with other drugs as a combination therapy. Dabrafenib is a second BRAF inhibitor that was tested in clinical trials. Although Dabrafenib had a positive response rate on $BRAF^{V600E}$ patients (77), melanomas also acquired resistance with this drug. The resistance mechanisms that arose from BRAF inhibitors led to the development of other MAPK inhibitors. The MEK inhibitor, Trametinib, was developed and approved in 2013 for advanced stage melanoma cases with the BRAF mutation. Trametinib was far superior to chemotherapy but was not as effective as the BRAF inhibitors (78, 79). After the development of MEK inhibitors, combination therapy of kinase inhibitors became a promising option. Clinical trial using combination of BRAF and MEK inhibitors

demonstrated a median progression free survival of 9.4 months compared to patients on BRAF inhibitors alone who had a progression free median survival of 5.8 months (80, 81). Unfortunately, the advances made with kinase inhibitors do not provide a long-term solution for patients.

In addition to chemotherapy, immunotherapy, and kinase inhibitors, angiogenesis inhibition is another option that has been explored for melanoma and other cancers. This approach is directed at limiting or depleting nutrients essential for cancer growth by preventing the growth of blood vessels in tumors. Anti-angiogenic compounds target the vascular endothelial growth factor receptor (VEGFR) and prevent downstream signaling. Unfortunately, these drugs have had very little positive outcomes on melanoma cases (82) so they are not the primary method to treat melanoma.

GTPases

Many therapies have been developed for melanoma but very few provide a descent increase in survival, which indicates that more work needs to be done at the molecular level. In an attempt to develop different therapeutic targets, groups attempted to target the NRAS GTPase with little success because of their transitioning states. GTPases control a wide variety of cellular processes ranging from metabolism (83-85) to cell migration and invasion (86, 87). The most widely studied GTPases are the Rho family of GTPases, which are also a subfamily of the Ras superfamily like NRAS, HRAS and KRAS. The Rho GTPases includes six subfamilies which include the Rho subfamily (RHOA, RHOB and RHOC), Rac subfamily (RAC1, RAC2, RAC3 and RHOG), Cdc42 subfamily (CDC42, TC10/RHOQ, TCL/RHOJ, WRCH1/RHOU and WRCH2/RHOV), Rnd subfamily (RND1, RND2, RND3/RHOE, RHOD and RIF/RHOF),

RhoBTB subfamily (RHOBTB1, RHOBTB2, RHOBTB3 and RHOH/TTF) and the Miro subfamily (MIRO1/RHOT1 and MIRO2/RHOT2) (Figure 1.2.A). Many of these GTPases cycle between an active GTP state and an inactive GDP state where the exchange of GDP to GTP is mediated by guanine nucleotide exchange factors (GEFs), which causes the release of GDP from the GTPase (88) and the addition of GTP. Inactivation occurs via hydrolysis of GTP, which is aided by GTPase activating proteins (GAPs) (88). Rho guanine nucleotide dissociation inhibitors (RhoGDIs) also play a role in maintaining the GTPase conformation state by preventing them from undergoing nucleotide exchange or hydrolysis (89) (Figure 1.2.B). Rho GTPases have similar structural domains in order for proper GDP/GTP regulation, effector binding, and post-translational lipid binding (Figure 1.2.C). The switch I and switch II domains near the C-terminus undergo conformational change based on the binding of GDP and GTP and regulate the affinity of the effector domain (90). The effector-binding domain allows the binding of the effector to propagate a signal downstream. Post-translational modifications occur at the C-terminus in the hypervariable domain.

GTPases also undergo post-translational modifications during the "switching/cycling" process. Many GTPases undergo isoprenylation on the C-terminus, which was first studied in the RAS superfamily of GTPases. RAS GTPases, which include Rho, Rab, Arf, Rap, Ran, and Ras subfamilies, undergo farnesylation so that they can associate with lipid membrane (91, 92). Farnesyltransferase (FTase) is an enzyme that adds a 15-carbon isoprenoid to GTPases that contain a CAAX motif at the C-terminus, which is a four-amino acid sequence where C represents a cysteine, A is an aliphatic amino acid, and X is any amino acid. However, if the X residue is a leucine,

phenylalanine, isoleucine, or a valine then the GTPase will most likely undergo a geranylgeranylation, which is the addition of a 20-carbon isoprenoid by a geranylgeranyltransferase type I enzyme (GGTase-I). Members of the Rho GTPase family are mainly geranylgeranylated with the exception of Rnd GTPases, RhoJ (Ras homologue family member J) and RhoQ, which are farnesylated (93) even though their CAAX sequence suggests they should be geranylgeranylated. The process of membrane localization is not as important for the activation status of the GTPase but more for the downstream signaling that needs to take place (94-96).

Phosphorylation is another post-translation modification observed in very few GTPases including RhoA, RhoG and Cdc42. RhoA contains a serine at the C-terminal tail near the CAAX motif that is phosphorylated by protein kinase A (PKA), protein kinase G (PKG), and STE20 like kinase (SLK) (97, 98). This phosphorylation site is important in RhoA because it is necessary but not sufficient to dissociate it from the membrane (99), while a RhoGDI is also required for complete dissociation from the membrane. RhoG is also phosphorylated at the same serine by PKA, which is also near the CAAX motif (99). Other Rho family GTPases like Cdc42 have also been shown to be phosphorylated *in vitro* on tyrosine-64 by the proto-oncogene tyrosine-protein kinase (SRC) although its exact function has not been described (100). The closely related RhoJ and RhoQ GTPases also contain a serine near the CAAX motif but no studies have demonstrated that it gets phosphorylated. The other Rho GTPase, Rac1, gets phosphorylated at serine-71 by AKT but its function is also unknown (101).

RHOJ

Interestingly, RhoJ, previously known as TC10-like Rho GTPase (TCL), is a GTPase that is studied in melanoma and other cancers as a potential tumor driver. RhoJ belongs to the Cdc42 subfamily and shares 78% and 85% amino acid homology to Cdc42 and TC10, respectively (102). RhoJ is encoded by five exons and composed of 214 amino acids (102). Like other GTPases, RhoJ contains switch I and switch II p-loops near the N-terminus where GAPs and GEFs interact, respectively. Interestingly, RhoJ contains a CAAX motif that would suggest that it should get geranylgeranylated, but previous studies demonstrated that GGTase-I inhibitors did not prevent RhoJ from localizing to the plasma membrane but FTase inhibitors did suggesting it is farnesylated (93). RhoJ contains 20 amino acids more than Cdc42 at the N-terminus and a more recent study demonstrates that this 20 amino acid region also helps coordinates the location of and nucleotide exchange in RhoJ (103). RhoJ is highly expressed in the heart and to a lesser extent in the lung, liver, brain and spleen (102). Like other GTPases, RhoJ also plays a role in cytoskeletal reorganization (102), but initial studies of RhoJ also demonstrated that it is involved in clathrin-dependent endocytosis (104). Yeast and *in vitro* studies have determined that RhoJ binds to the CRIB domain of PAK and WASP, CIP4, Par6 and p50RhoGAP (102, 105).

More recent work has demonstrated RhoJ's role in mammalian cells. RhoJ regulates endothelial cell formation by influencing the ERG transcription factor and by regulating angiogenesis (106-112). RhoJ's ability to maintain angiogenesis for tumor vasculature made it a potential therapeutic target since suppression of RhoJ disrupts the formation of new tumor blood vessels in nude mice xenografts (108). Ganesan's group was the first to identify RhoJ's chemoresistant role in cancer, mainly melanoma

(113, 114), although others have now shown that it also plays a similar role in other cancers such as gastric cancer (115). With the progress made in mammalian systems, RhoJ was shown to interact with additional effectors such as the GIT-PIX protein complex, which stabilizes focal adhesions (116). In melanoma, RhoJ bind to PAK to regulate tumor invasion and migration (114). With the advances made in mammalian models, further studies need to be done to fully understand how RhoJ is driving melanomas and other cancers.

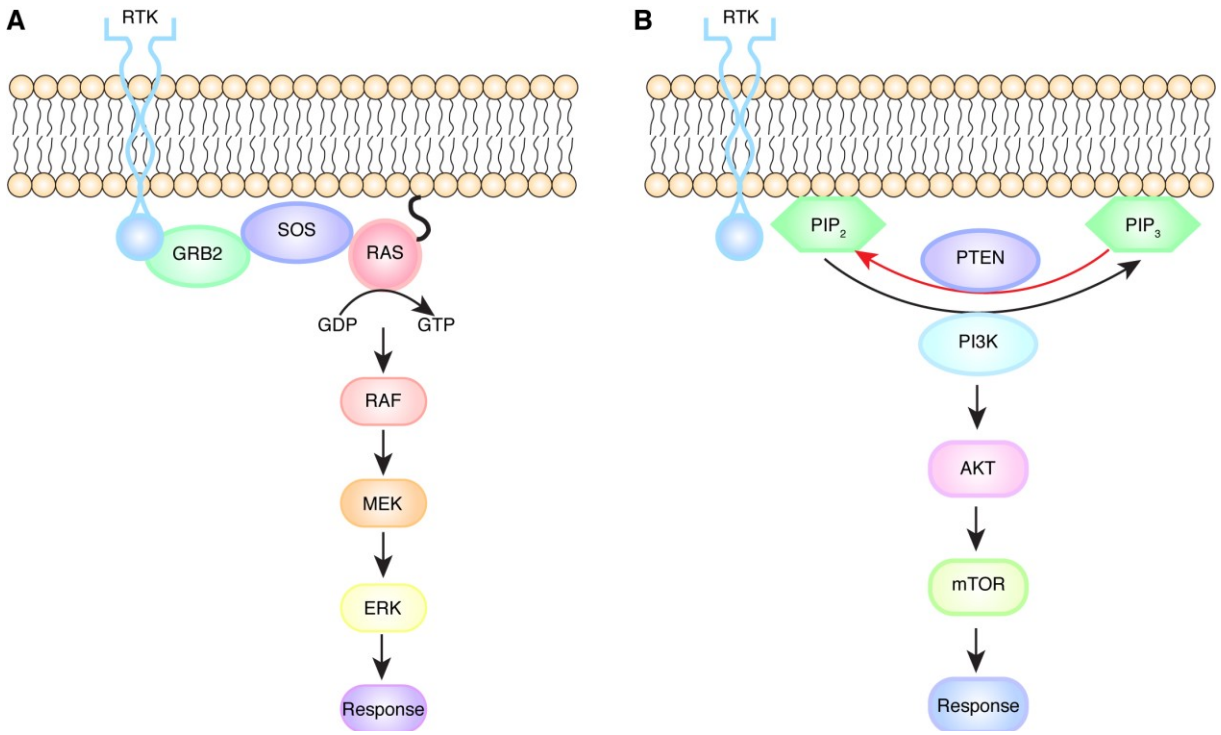

Figure 1.1. Signaling pathways affected in melanoma. (A) The MAPK signaling pathway initiates with a ligand binding to the RTK, which leads to dimerization. This event triggers the activation of the GRB2-SOS complex, which in turn activates RAS. RAS (NRAS, HRAS, KRAS) will then activate RAF (ARAF, BRAF, CRAF) and lead to the phosphorylation of MEK. MEK will lead to the activation of ERK and a cellular response. (B) The PI3K/AKT signaling pathway also initiates with activation of an RTK. This activation will lead to the phosphorylation of PIP_2 by PI3K to produce PIP_3. This phosphorylation event is also negatively regulated by PTEN. Upon phosphorylation of PIP_2, AKT is activated and leads to the phosphorylation of mTOR and a cellular response.

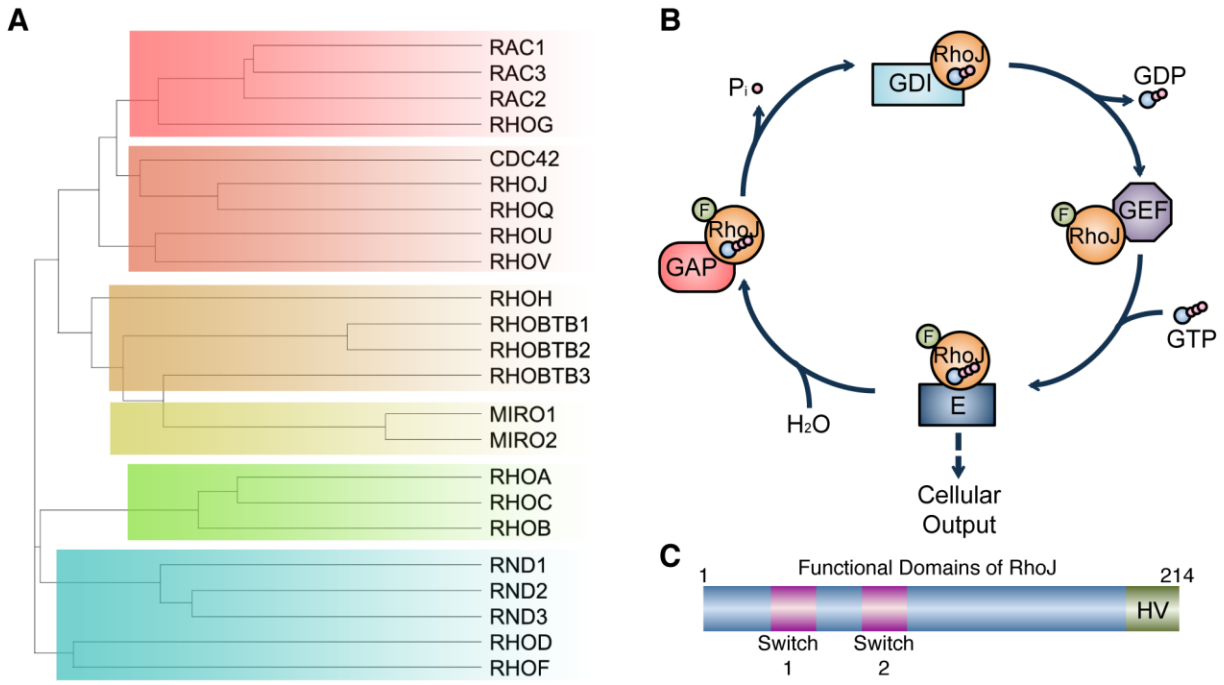

Figure 1.2. Characterization of RhoJ. (A) A phylogenetic tree demonstrating the homology between the six Rho GTPase subfamilies [modified from (117).] (B) RHOJ cycles between a

GTP bound (active) and GDP bound (inactive) conformational state. GEFs and GAPs regulate the guanine nucleotide exchange of GDP or hydrolysis of GTP, respectively, while the GDI lock RhoJ in its conformational state. E, effector; F, farnesyl isoprenoid; GEF, Guanine exchange factor; GAP, guanine adaptor protein; Pi, inorganic phosphate; GDI, guanine dissociation inhibitor. (C) A schematic representation of human RHOJ amino acid sequence. The switch I and II domains undergo conformational changes depending on guanine nucleotide bound. RHOJ is farnesylated at the carboxy-terminal hypervariable (HV) region that ends with a CAAX motif in order to associate with the membrane.

CHAPTER 2: The RhoJ-BAD Signaling Network: An Achilles Heel for BRAF Mutant Melanomas

Introduction

Oncogenes regulate cellular homeostasis in normal cells, and when mutated induce secondary physiological changes that stress cellular capacity for survival (118, 119). Paradoxically, oncogenes drive the uncontrolled growth of tumor cells (120) and represent some of the most effective cancer therapeutic targets (121). Unfortunately, inhibiting oncogene activity induces only short-lived tumor regression (122), eventually resulting in the regrowth of tumors that activate growth by other mechanisms (71, 73, 74). Recent studies have sought to define pathways that allow tumor cells to cope with oncogene-induced stress (123). Cancer cells are known to alter conventional signaling paradigms to skirt apoptotic stimuli (124). In addition to avoiding apoptosis, tumor cells rewire metabolism to further facilitate growth (125). An emerging approach to treat cancer is to identify non-mutated gene products critical for cancer cell and not normal cell survival and develop novel therapeutics to target these gene products (126). These “non-oncogene” dependencies have proven effective drug targets for breast cancer and could potentially be used in other cancers such as melanoma (127).

The BRAF oncogene is the most commonly mutated gene in human cutaneous melanomas (39), and this oncogene also drives tumor cell proliferation (128). BRAF mutations are not exclusive to tumors as they are also seen in common human nevi (129) that spontaneously arrest (119), and little is understood about what pathways allow BRAF mutant cells to proliferate to form nevi. Activating BRAF mutations and the loss of the tumor suppressor PTEN are events with a significant co-occurrence in

melanoma (130). These mutations result in the activation of MAPK and AKT signaling networks that accelerate melanoma development by promoting cell survival (49). While MAPK and AKT signaling play an important role in melanoma progression, it is currently not clear what other pathways suppress oncogene-induced stress in BRAF mutant cells to allow them to proliferate.

RNAi approaches have been used to uncover selective tumor dependencies and identify novel therapeutic targets (131). We previously used a genome-wide RNAi approach to identify RhoJ, a Cdc42 family GTPase, as a gene that allows melanoma cells to resist DNA damage stress *in vitro* (113). RhoJ activates group I p21-activating kinases (PAK) in melanoma cells and PAK inhibitors can sensitize melanoma cells to DNA damage (113, 114). In addition to modulating DNA damage stress, RhoJ modulates actin cytoskeletal dynamics in melanoma cells (114), and can regulate tumor angiogenesis in lung cancer xenografts (108). Intriguingly, while RhoJ modulates multiple pathways that may be involved in melanoma growth, it is not mutated in melanoma tumors, suggesting that it may represent a “non-oncogene” dependence in tumor cells. In this study, we utilize physiologically-relevant *in vivo* systems to examine the role that RhoJ and its downstream targets PAK-BAD play in nevus formation and cellular transformation. We reveal that RhoJ modulates the growth properties and apoptotic threshold of BRAF mutant melanocytes, accelerating both the formation of nevi and the growth and metastasis of melanoma tumors. Surprisingly, treatment of mice with PAK inhibitors before tumors developed or during the early phases of tumor growth inhibits tumor growth and metastasis, nominating PAK inhibitors as a novel treatment for early-stage cutaneous melanomas.

Materials and Methods

Mice.

RhoJ KO mice were generated as previously described (111). Briefly, the ES cells used to generate RhoJ knockout mice were derived from C57Bl/6N-*RhoJ*$^{tm1a(KOMP)Wtsi}$ and injected into C57B6/J mice to generate chimeric mice. The melanoma prone mice have the genetic background C57BL/6.Cg- *Braf*^{tm1Mmcm} *Pten*^{tm1Hwu} *Tg(Tyr-cre/ERT2)13Bos/BosJ* (*Braf*^{CA}, *Pten*$^{lox4-5}$, *Tyr::Cre*^{ERT2}) that have been previously characterized (49). Both mice strains were crossed to generate *Braf*^{CA}, *Pten*$^{lox4-5}$, *Tyr::Cre*^{ERT2}, *RhoJ*$^{-/-}$ mice. The entire survival study utilized a total of 19 males and 37 females. The pigmentation of the mouse paws were analyzed by measuring the area of the pigmented region in the paws and normalizing to the entire paw using ImageJ software. The quantification of the paws includes all the paws shown in the figures and supporting figures.

Multiphoton microscopy of mouse skin.

Tyr:Cre^{ERT2}; *Braf*^{V600E}; *RhoJ*$^{+/+}$ and *Tyr:Cre*^{ERT2}; *Braf*^{V600E}; *RhoJ*$^{-/-}$ mice were shave depilated at p50 (second telogen), euthanized, and immediately imaged ex-vivo (no labeling) with MPM to capture the fluorescence signal from keratin and melanin and second harmonic generated (SHG) signal from collagen using LSM 510 NLO Zeiss system. Fluorescence and second harmonic generation was excited by femtosecond Titanium: Sapphire (Chameleon-Ultra, Coherent) laser at 900 nm. Emission was detected at 390-465 nm for SHG channel (blue), and 500-550 nm (green) and 565-650 (red) fluorescence channels. Each animal was imaged at 8 to 10 randomly chosen locations on depilated skin of the lower back. Stacks of optical sections of 636μm x

636μm at different depths ranging from 0 to 240 μm (5 μm steps) were obtained to allow for 3-D volume reconstruction (LSM Image Browser, Carl Zeiss GMBH).

Activation of Tyr::Cre^{ERT2} transgene and treatment of mice with PAK inhibitors.

Braf^{CA}, Pten^{lox4-5}, Tyr::Cre^{ERT2} mice were genotyped as previously described (49). The Cre-specific primers are: forward 5'- GGTGTCCAATTTACTGACCGTACA-3' and reverse 5'- CGGATCCGCCGCATAACCAGTG -3'. Topical administration of 4-hydroxytamoxifen (4-OHT) to the back skin on pups and adults was performed as previously described (49). Paws of mice were also treated with 4-OHT at P2, P3, and P4. FRAX597 was administered to mice daily via oral gavage daily at a dose of 100 mg/kg (132) and prepared in 60%:40% PEG-400:DI water. Tumors in adult mice (P21) were induced for three days and allowed to progress for one week, at which point mice began FRAX treatment for six days. The veterinary staff was blinded as to the genotype of experimental animals utilized in the study, and monitored experimental animals on a daily basis. Animals were culled when tumor burden reached ethical limits and if the animals displayed signs of ill health or distress as determined by the veterinary staff. All mouse procedures were approved by UCI's IACUC regulations and standards. As an additional control for background strain variability, all survival comparisons were made between littermates.

RNA sequencing.

Total RNA from RhoJ WT 1-5 and RhoJ KO 1-5 was monitored for quality control using the Agilent Bioanalyzer Nano RNA chip (Santa Clara, CA). Samples with a RIN number >8 were used to construct libraries using the Illumina TruSeq RNA v2 kit. The input quantity for total RNA was 1μg and mRNA was enriched using oligo dT magnetic

beads. The enriched mRNA was chemically fragmented for four minutes. First strand synthesis used random primers and reverse transcriptase to make cDNA. After second strand synthesis the ds cDNA was cleaned using AMPure XP beads (Beckman Coulter, Beverly, MA) and the cDNA was end repaired and then the 3' ends were adenylated. Illumina barcoded adapters were ligated on the ends and the adapter-ligated fragments were enriched by nine cycles of PCR. The resulting libraries were validated by qPCR and sized by Agilent Bioanalyzer DNA high sensitivity chip. The concentrations for the libraries were normalized and then multiplexed together. The concentration for clustering on the flow cell was 12.5pM. The multiplexed libraries were sequenced on three lanes using paired end 100 cycles chemistry for the Illumina HiSeq 2500. The version of HiSeq control software was HCS 2.2.38 with real time analysis software, RTA 1.18.61.

Immunohistochemistry, immunofluorescence and immunoblotting.

RhoJ staining was optimized at 1:1000 using an Ab from Genetex (Irvine, CA). Slides were developed with either a horse-radish peroxidase liquid 3,3'-diaminobenzidine chromogen system (DAKO, Carpirteria, CA) or an alkaline phosphatase liquid permanent red chromogen system (DAKO), according to the manufacture's protocol. Fluorescence labeling was performed using SMA (Abcam 1:100) PMEL, KIT, DCT, and DAPI as described (133). The expression or phosphorylation of proteins was detected by western blotting using the following Abs: RhoJ (Abnova 1:250), Cdc42, Rac1/2/3, RhoA, actin, BAD, phospho-Bad^{Ser138}, and Vinculin (all from cell signaling 1:1000).

Cdc42 activity assays.

A Cdc42 activation assay was performed according the manufacturer's protocol (Cell Biolabs, San Diego, CA). Briefly, cell lysates expressing high RhoJ were unloaded of guanosine nucleotides and either loaded with GDP or GTPγS. Agarose beads conjugated with the PAK1 PBD domain pulled down Cdc42, Rac, or RhoJ only when GTP-bound. Lysates were then immunoblotted with indicated Abs.

Flow cytometric analyses for apoptosis.

Approximately 1×10^6 melanoma cell treated with FRAX-597 were trypsinized and washed with PBS, the single-cell suspensions were incubated with Alexa Fluor-Annexin V and propidium iodide (PI) (V13245; Invitrogen) per the manufacturer's protocol and were subjected to flow cytometric analysis. In all cases, cell debris was gated out based on forward scatter and side scatter analysis. Data was analyzed using FlowJo (Ashland, OR). Cells not treated with FRAX-597 were used to establish gating parameters. WM3248 cells were transfected with BAD^{S136E} (3582 pcDNA3 BAD^{S136E} Addgene #8800), with Lipofectamine 3000 (Invitrogen) according to the manufacturer's protocol. On the day of transfection, 14µg of DNA from the respective constructs were incubated with Plus Reagent in Opti-MEM to a volume of 350µL, and then mixed with 43µL lipofectamine in 350µL Opti-MEM and incubated for 20 min at room temperature. The DNA-Lipofectamine complexes were then added to each plate, and the cells were incubated at 37°C in a CO_2 incubator. The media was replaced after 24hrs and cells selected in G418.

Statistical Analysis.

The power and sample size calculations for the survival studies (Fig 1A and 1B) were based on a simulation of 1000 datasets utilizing SAS v9.2. To calculate the

power, the simulation under the alternative hypothesis made the following assumptions: 1.) No censoring data for both groups; 2.) The first event occurred on day 30 for the controls; 3.) The first event occurred on day 40 for RhoJ$^{-/-}$; 4.) Hazard ratios used were 1.5, 2, 4, 6; and 5.) Sample size of mice per group was 15, 20, 25, 30, 40, and 50. To calculate the type I error (alpha) under the null hypothesis the following assumptions were made: 1.) Data was not censored for both groups; 2.) The first event occurred on day 30 for both groups; 3.) Hazard ratio is 1; and 4.) Sample size of the mice per group was 15, 20, 25, 30, 40, and 50 (Data not shown).

Continuous outcomes were summarized via mean and standard error and tests of unadjusted means between groups were conducted using a two-sample t-test with unequal variances. Mean RhoJ expression levels adjusting for stage, age and gender were estimated and compared using multiple linear regression analysis. Residual diagnostics were performed in order to assess the functional form of continuous covariates included in the model and to identify potentially influential subjects. Estimated mean differences, corresponding Wald-based 95% confidence intervals, and p-values corresponding to the test of no association in RhoJ levels were reported for all model covariates. No deviations in model fit or influential observations were observed.

The TCGA analysis was performed as follows. The skin cutaneous melanoma (SKCM) TCGA Exome-sequencing and RNA-sequencing datasets were downloaded June 2016. Single nucleotide variants (SNVs) at the position 1799 of the BRAF gene (c.1799T>C) leading to a non-synonymous alteration at the amino acid 600 of the BRAF protein were annotated as BRAFV600E. Additional, RhoJ expression assessed by RNA-sequencing was normalized using the z-score and the statistical difference on

mean expression between BRAF wt and BRAFV600E was assessed by the Student's t-test.

Study Approval

Mice were housed and maintained by the University Laboratory Animal Resources. All animal experiments were approved by the University of California, Irvine's Institutional Animal Care and Use Committee. Melanoma tumor microarray tissues were collected and processed with approval from the Providence Saint John's Health Center and John Wayne Cancer Institute joint Institutional Review Board and Western Institutional Review Board.

Results

RhoJ regulates melanoma progression

To evaluate the role of RhoJ in melanoma development, constitutive RhoJ knockout (KO) mice were crossed with a previously described autochthonous mouse model of melanoma that carries a *Tyr:Cre*^{ERT2} allele, a *Braf*^{CA} allele, and one or two copies of a *Pten*$^{lox4-5}$ allele (49) (Figure 2.1.A). Initial studies validated that RhoJ knockout mice lacked RhoJ expression (Figure 2.1.B). RhoJ deletion significantly inhibited the growth of melanoma tumors that expressed either no PTEN ($p<0.0001$, Log-rank; Figure 2.1.C) or had one functional copy of PTEN ($p<0.0001$, Log-rank; Figure 2.1.D), suggesting that RhoJ drives tumor growth by amplifying BRAF and not AKT signaling. Melanoma tumors from RhoJ KO mice metastasized to the lung at a lower rate as compared to RhoJ wild type (WT) mice ($p=0.003$, Student's t-test; Figures 2.1.E, 2.1.F), suggesting that RhoJ regulates tumor progression, metastasis, or both. To determine whether RhoJ regulates tumor progression, tumors were induced on the

paws of experimental mice and the kinetics of tumor growth was measured. There was a significant delay in tumor progression in RhoJ KO mice as compared to RhoJ WT mice. RhoJ KO mice developed early stage tumors (as measured by pigmented area) a week later than RhoJ WT tumors (Figure 2.1.G, 2.1.H), indicating that RhoJ promotes the growth of developing melanoma tumors.

RhoJ modulates signaling pathways that control melanocyte differentiation and survival

In order to better understand how RhoJ promotes tumor growth, the whole genome expression profiles of *Braf^{V600E};Pten$^{fl/+}$;RhoJ$^{+/+}$* tumors and *Braf^{V600E};Pten$^{fl/+}$;RhoJ$^{-/-}$* tumors were examined (Figures 2.2.A, 2.2.B). Transcriptomics analysis revealed that RhoJ modulates the expression of pigment genes such as premelanosome protein (*Pmel17)* and Oca2 melanosomal transmembrane protein (*Oca2)* (Figure 2.2.A). As a preliminary validation of the pathways identified in our transcriptomics experiments, we sought to determine whether RhoJ deletion affects melanogenesis. Initial observations revealed that RhoJ KO mice exhibit a greater number of white hairs as compared to RhoJ WT mice (Figures 2.2.C, 2.2.D), indicating that RhoJ modulates postnatal melanogenesis. Immunofluorescence studies revealed that RhoJ KO mice contained fewer melanocytes that express Pmel17 (Figures 2.2.E, 2.2.F) yet have similar if not higher numbers of DCT-positive melanocyte stem cells within the hair follicle (Figures 2.2.G, 2.2.H) when compared to RhoJ WT mice. These results suggest that RhoJ influences pigmentation by modulating melanocyte differentiation, not by modulating the number of melanocyte stem cells.

Interestingly, pathway enrichment analysis revealed that *RhoJ* deletion in mouse tumors modulated pathways that have previously been shown to be regulated by BRAF, such as cellular bioenergetics (oxidative phosphorylation) (134), RAF and PI3 kinase signaling pathways (135), UVB-induced MAPK signaling pathways (136), and p53 signaling pathways (113) (Figure 2.2.I). Notably cytokines, immune regulators, and angiogenesis regulators were not identified in our bioinformatics analysis, suggesting that RhoJ regulates melanocyte growth in a cell autonomous manner. *FoxC2*, a gene that regulates the expression of multiple mitochondrial genes (137), was up-regulated in RhoJ KO tumors as compared to RhoJ wild type tumors as demonstrated by both RNA-seq results (Figure 2.2.A) and by western blotting (Figure 2.2.J). BRAF mutant cells are known to suppress AKT and BAD signaling to promote their growth *in vivo* (76). Intriguingly, we observed that the expression of the proapoptotic protein BAD was elevated in RhoJ KO tumors (Figure 2.2.K), consistent with the hypothesis that RhoJ downregulates BAD signaling. Taken together, these observations suggest that RhoJ modulates the growth of tumors by altering the metabolism and apoptotic threshold of BRAF mutant melanocytes (Figure 2.2.L).

RhoJ regulates the development of melanocytic nevi via a cell autonomous mechanism

Our preliminary studies made the novel observation that RhoJ modulates melanocyte differentiation (Fig 2.2.C). Previously published studies determined that RhoJ is expressed in endothelial cells in developing retinas (106), and RhoJ knockout mice exhibit delayed radial growth of the retinal vasculature without other discernible angiogenesis phenotypes (111). Our transcriptomics analysis did not identify

angiogenesis genes as a class that is modulated in RhoJ knockout tumors (Figure 2.2.I), in contrast to previous studies that identified RhoJ as critical regulator of angiogenesis in xenograft models (108). Analysis of the vasculature from RhoJ KO melanomas revealed no difference in the number of blood vessels per unit area in comparison to RhoJ WT melanomas (Figures 2.3.A, 2.3.B), indicating that RhoJ deletion does not significantly affect tumor angiogenesis in our autochthonous mouse model. To further analyze the effects of RhoJ on melanocytes, RhoJ KO mice were crossed with a nevi mouse model that carries a *Tyr:Cre*^{ERT2} allele and a *Braf*^{CA} allele (49). Nevi were quantified microscopically with multiphoton microscopy (MPM), a techniques that utilizes intrinsic fluorescent signals to generate a three-dimensional image of nevi (138), at the second telogen (p50) after the hair was removed. *Tyr:Cre*^{ERT2}; *Braf*^{V600E}*; RhoJ*$^{-/-}$ mice had reduced the number of microscopic nevi that could be visualized from the skin surface as compared to *Tyr:Cre*^{ERT2}; *Braf*^{V600E}*; RhoJ*$^{+/+}$ mice (Figures 2.3.C, 2.3.D), a result that neared statistical significance (p=0.059). Similarly, less nevi were visualized macroscopically in RhoJ knockout mice as compared to RhoJ wild type mice as visualized by a dissecting microscope (p=0.07, Figures 2.3.E, 2.3.F). Our observations indicate that although *RhoJ* is a global KO, its deletion has no detectable effect on the angiogenesis of autochthonous melanomas nor does it influence the number of stem cells in the hair follicle (Figures 2.2.G, 2.2.H). RhoJ deletion does affect the growth of melanoma tumors, the formation of nevi, and has subtle effects on melanocyte differentiation. Taken together, these findings indicate that RhoJ specifically modulates the growth and survival of BRAF mutant melanocytes.

RhoJ is activated in a specific subset of melanoma tumors

Although RhoJ is highly expressed in the heart and to a lesser extent in the liver (102), its expression in cutaneous melanoma has not been extensively analyzed. We examined the expression of RhoJ in a panel of human melanoma cell lines (Figure 2.4.A) and determined that RhoJ expression levels varied widely in $BRAF^{V600E}$ and $BRAF^{WT}$ cells lines. Additional studies sought to determine whether RhoJ signaling was activated in melanoma cells that express high levels of RhoJ. Our previously published studies showed that RhoJ regulates PAK activity in human melanoma cell lines (113, 114). Group I PAK kinases contain a p21-binding domain (PBD) where small GTPases, like Cdc42, RhoJ, and Rac, can bind when they are in their GTP-bound-active state (102). We utilized a Cdc42-PAK functional assay to better evaluate the activation of this family of GTPases in melanoma and determined that RhoJ, Cdc42, and Rac1/2/3 interact with PAK in melanoma cells when they are GTP-bound but not when they are loaded with GDP (Figure 2.4.B). Interestingly, we observed that RhoJ and Cdc42 bind to PAK conjugated agarose beads even when they are not loaded with GTP, suggesting that RhoJ and Cdc42 but not Rac1 are intrinsically activated in RhoJ highly expressing cells (Figure 2.4.B, “prior to unloading” lane).

To verify that RhoJ plays a role in the growth of human melanomas, we optimized a RHOJ Ab for immunohistochemistry (Figure 2.4.C) and examined the expression of RHOJ in AJCC stage III and stage IV melanoma tumors using two well-annotated melanoma tissue FFPE microarrays (139). Stage III melanoma tumors expressed significantly higher levels of RHOJ than stage IV melanoma tumors (Figure 2.4.D, 2.4.E). Integration of the Cancer Genome Atlas (TCGA) melanoma RNA-

sequencing and exome-sequencing datasets confirmed a higher expression of RHOJ in $BRAF^{V600E}$ as compared to $BRAF^{WT}$ melanoma tissues (Figure 2.4.F). Moreover, 27% of all tumors examined in a human melanoma tissue microarray had both the $BRAF^{V600E}$ mutation and expressed high levels of RHOJ (Figure 2.4.G). Taken together, these studies indicate that RHOJ is expressed in about half of stage III and stage IV melanoma tumors harboring $BRAF^{V600E}$ mutation.

PAK inhibitors selectively blocks the growth of RhoJ expressing melanomas by suppressing BAD phosphorylation

Our initial studies demonstrated that RhoJ deletion slows the initiation and progression of BRAF mutant melanoma tumors *in vivo* (Figures 2.1, 2.3). To determine whether blocking RhoJ signaling would be an effective method to inhibit the growth of melanoma tumors, we first examined whether blocking RhoJ signaling pharmacologically was sufficient to induce apoptosis *in vitro*. Melanoma cell lines were treated with a Group I selective PAK inhibitor, FRAX597 (132). FRAX597 induced apoptosis in BRAF mutant cell lines that expressed high levels of RhoJ (WM3248 and WM983B), but not in BRAF wild type cell lines that expressed less RhoJ (WM1366, Figure 2.5.A). Moreover, FRAX597 induced low levels of apoptosis in cells where RhoJ was undetectable, independently of the BRAF mutation status (Figure 2.5.B). Previously published studies have defined doses of Vemurafenib and Trametenib that can induce apoptosis in a majority of treated cells *in vitro* after 72 hours (70). FRAX597 induced more apoptosis than Vemurafenib and Trametenib after 24 hours in cell lines that expressed detectable levels of RhoJ (Figure 2.5.A). PAK is known to inhibit apoptosis by inducing the phosphorylation of BAD at serine 136, which inhibits the

ability of BAD to suppress the function of the anti-apoptotic protein BCL2 (140). FRAX597 effectively inhibited the accumulation of BAD phosphorylated at Ser136 in a dose dependent manner (Figure 2.5.C). Overexpression of a BAD^{S136E} phosphomimetic (141) protected cells from PAK-induced apoptosis (Figure 2.5.D), indicating that PAK inhibitors induce apoptosis by blocking BAD phosphorylation.

To determine whether PAK inhibition could block the growth of early stage melanoma tumors, tumors were induced in adult mice as previously described (49) and treated with FRAX597 for six days either one week after tumors were induced or two weeks after tumor induction when tumors are first visible. Mice treated with FRAX597 for a short period of six days before tumors were visible significantly prolonged the survival of mice by 30 days ($p<0.0021$, Log-rank; Figure 2.5.E), consistent with a role for RhoJ and PAK1 in the growth of nascent tumors. Treating mice with FRAX 597 for six days after tumors were first visible resulted in fewer tumors in FRAX597 treated mice as compared to vehicle treated mice (Figure 2.5.F) as measured by the pigmented area (Figure 2.5.G). Taken together, these results identify PAK inhibitors as agents that can block the progression of early stage, BRAF mutant, RhoJ expressing melanomas by modulating BAD signaling.

Discussion

Oncogene-induced senescence and apoptosis play an important role in inhibiting tumorigenesis by maintaining homeostasis (119). In order to bypass homeostasis, tumors acquire mutations in oncogenes, such as BRAF, but also alter conventional signaling paradigms to facilitate growth. In this study, we sought to identify signaling pathways that allow melanoma cells to survive $BRAF^{V600E}$ induced oncogenic stress.

We identify a novel role for the Cdc42 family member RhoJ in resisting the effects of oncogene-induced stress. RhoJ deletion had mild effects on normal melanocyte differentiation, resulting in the accumulation of an increased number of grey hairs without modulating the accumulation of melanocyte stem cells. RhoJ played an even more important role during the process of nevus formation and most significantly affected tumor development and metastasis. While previously published studies have defined a role for Cdc42 in regulating melanoma cell movement (142), this study represents the first identification of a specific Cdc42 signaling network that cooperates with BRAF to regulate melanocyte growth *in vivo.* The observation that RhoJ is not mutated in melanoma but yet plays a more important role in the growth of BRAF mutant cells ranging from nevi to tumors indicate that RhoJ is part of a normal signaling pathway that is co-opted to speed tumor development (Figure 2.5.H).

To better understand how RhoJ and PAK regulate tumor formation, we examined how RhoJ deletion affected gene expression in transformed melanocytes. Transcriptomic studies revealed that RhoJ knockout tumors had increased expression of genes involved in oxidative phosphorylation and the transcription factor FoxC2, which controls the expression of metabolic pathways. Deregulation of cellular energetics, a hallmark of cancer (143), has been postulated to be a mechanism to avoid oncogene-induced stress in melanoma (144). Previous studies have also shown that biguanides such as metformin and phenformin, electron transport chain complex I inhibitors, when combined with BRAF inhibitors induce tumor regression in $BRAF^{V600E}/PTEN^{fl/fl}$ mouse model of melanoma (145). The observation that RhoJ modulates the expression of complex I components (Figure 2.2.L) but does not affect tumor angiogenesis in our

model (Figure 2.3.A) identifies RhoJ signaling as a novel regulator of metabolic adaptation in BRAF mutant melanoma cells.

In addition to modulating the expression of oxidative phosphorylation genes, loss of RhoJ also led to an upregulation of the pro-apoptotic gene BAD. PAK is known to activate BAD phosphorylation, promoting BAD binding to 14-3-3τ instead of Bcl2, resulting in increased survival (140). Overexpression of a BAD phosphomimetic mutant protected cells from the effects of a PAK inhibitor (Figure 2.5.E), verifying that PAK inhibitors modulate cell survival by regulating BAD activity. We observed that RhoJ knockout tumors induced BAD expression, while acute inhibition of PAK modulated BAD activity but not BAD levels. These results are likely a consequence of chronic versus acute inhibition of RhoJ and PAK signaling, respectively. Anoikis occurs when cells can no longer adhere to the extracellular matrix and undergo apoptosis (146). Migrating cancer cells leave the primary niche and avoid anoikis because they express mutated oncogenes and other genes that block apoptosis induction (147). Previous studies have demonstrated that the BRAF oncogene protects melanoma cells from anoikis by modulating BAD signaling (148). Similarly, PAK activation, which is overexpressed in breast cancer, is known to protect MCF10A cells from undergoing anoikis (149). Taken together, our studies identify RhoJ and PAK as critical regulators of both metabolic adaptation and apoptosis evasion, key events required to establish the tumorigenic platform.

To validate whether the RhoJ-PAK signaling network influenced the growth of BRAF mutant tumors, we determined whether PAK inhibitors could block the growth of BRAF mutant autochthonous mouse melanomas during early phases of development.

The PAK inhibitor FRAX597 inhibits the growth of nascent tumors *in vivo* after only six days of treatment (Figure 2.5.E) and induces apoptosis *in vitro* after 24 hours (Figure 2.5.A) by blocking BAD phosphorylation (Figure 2.5.C). Moreover, administering FRAX597 after tumors were visible also affected tumor growth (Figure 2.5.G), suggesting that PAK and RhoJ modulate both the phases of tumor initiation and tumor progression. The results presented here are more dramatic than other studies which demonstrated that the BRAF inhibitor PLX4720, the precursor derivative of Vemurafenib, only moderately inhibited tumor growth *in vivo* without inducing tumor regression (150) or preventing relapse (76). Of note, while the MEK inhibitor PD325901 can induce tumor regression and prolong survival in transgenic mouse models, this requires long-term treatment (six weeks) (49). Previous studies have documented that PAK1 is amplified in BRAF wild type tumors (151) and identified PAK inhibitors as agents that can slow the growth of melanoma xenografts (152) and synergize with BRAF inhibitors to kill melanoma cells (153). In contrast, the studies presented here define a role for RhoJ signaling in regulating the growth of BRAF mutant melanocytes at all stages (Figure 2.5.H), and result in the remarkable observation that early, limited treatment with PAK inhibitors is effective in halting tumor growth. Our tissue microarray studies determine that RhoJ is more highly expressed in stage III disease as compared to stage IV disease, suggesting that RhoJ is likely a better therapeutic target in early stage melanomas. Future studies will involve assembling tissue collections of early stage melanomas to verify that RhoJ is an ideal therapeutic target for early stage disease.

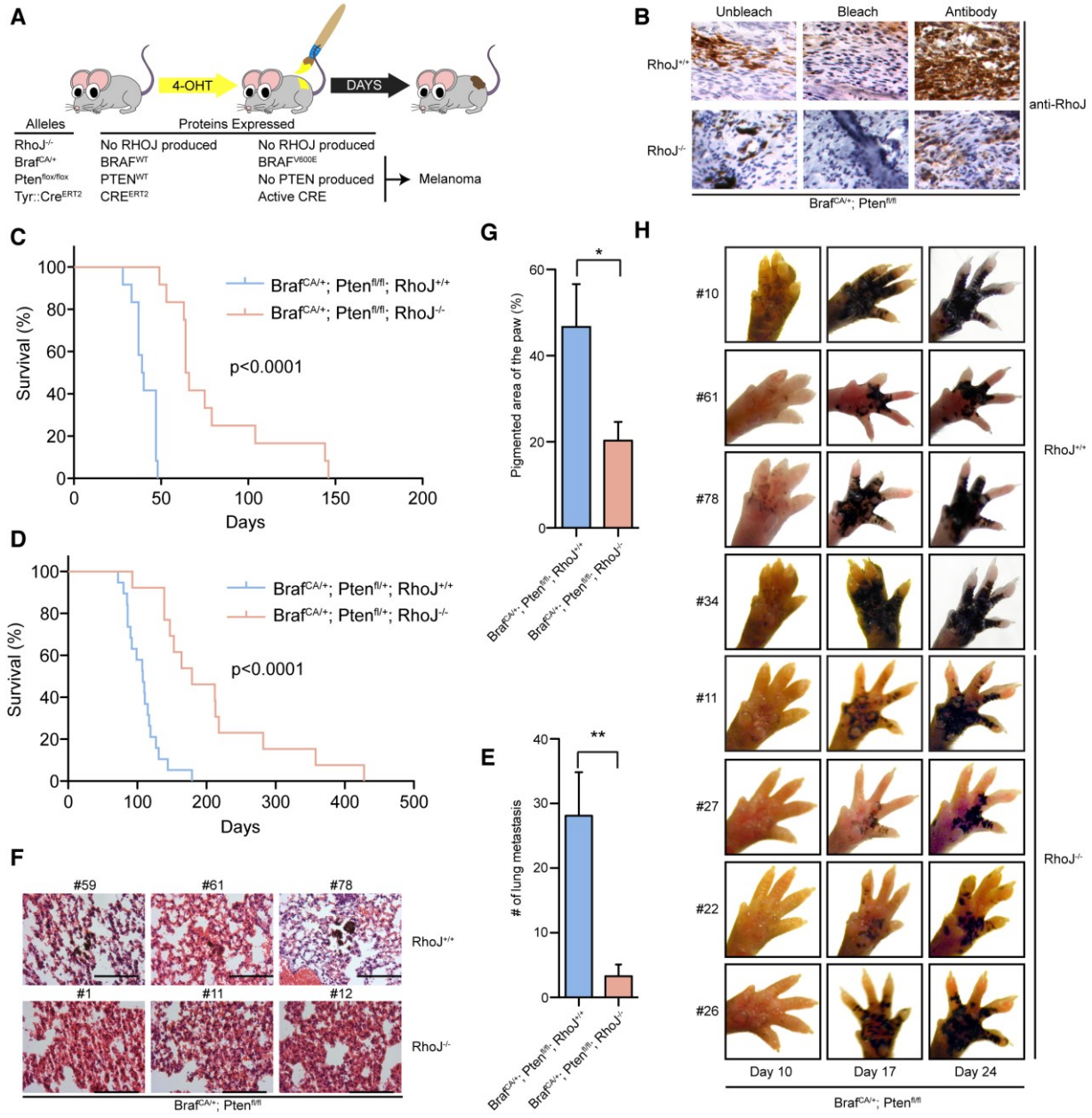

Fig 2.1. **RhoJ regulates melanoma tumor development.** (A) Inducible melanoma mouse model containing Braf mutation (mt), loss of Pten and RhoJ. Mice carrying *Braf$^{CA/+}$, Pten$^{fl/fl}$ and Tyr:Cre^{ERT2}* alleles were crossed with constitutive RhoJ KO mice. Activation of Cre^{ERT2} by 4-OHT leads to a Braf^{V600E} mutation and Pten loss. (B) RhoJ is not expressed in RhoJ KO mice. Formalin-fixed paraffin embedded mouse melanoma

skin was bleached with 3% hydrogen peroxide (overnight) to remove melanin and analyzed for expression of RhoJ. (C) Loss of RhoJ prolongs survival of $BRAF^{V600E}$ and PTEN null tumors. Kaplan-Meier survival analysis of 4-OHT treated *$Braf^{CA/+}$; $Pten^{fl/fl}$;Tyr::Cre^{ERT2}; $RhoJ^{+/+}$* (n=12) and *$Braf^{CA/+}$; $Pten^{fl/fl}$;Tyr::Cre^{ERT2}; $RhoJ^{-/-}$* (n=12) mice. Log-rank test demonstrates significant difference between *$Braf^{CA/+}$; $Pten^{fl/fl}$;Tyr::Cre^{ERT2}; $RhoJ^{+/+}$* and *$Braf^{CA/+}$; $Pten^{fl/fl}$;Tyr::Cre^{ERT2}; $RhoJ^{-/-}$* ($p<0.0001$). (D) RhoJ deletion prolongs the survival of mice carrying $BRAF^{V600E}$ and PTEN haploinsufficient tumors. Kaplan-Meier survival curves of 4-OHT treated *$Braf^{CA/+}$; $Pten^{fl/+}$;Tyr::Cre^{ERT2}; $RhoJ^{+/+}$* (n=19), and *$Braf^{CA/+}$; $Pten^{fl/+}$;Tyr::Cre^{ERT2}; $RhoJ^{-/-}$* (n=13) mice. Log-rank test demonstrates significant difference between *$Braf^{CA/+}$; $Pten^{fl/+}$;Tyr::Cre^{ERT2}; $RhoJ^{+/+}$* and *$Braf^{CA/+}$; $Pten^{fl/+}$;Tyr::Cre^{ERT2}; $RhoJ^{-/-}$* ($p<0.0001$). (E) RhoJ deletion reduces lung metastasis. Lung metastases were compared in aged-matched (P30) mice using a dissection microscope (**p=0.003, n=8, Student's t test). Error bars represent standard error of mean (SEM). (F) RhoJ KO mice have reduced number of lung metastases. Representative lungs from aged-matched mice (P30) were stained with H&E in *$Braf^{CA/+}$; $Pten^{fl/fl}$;Tyr::CreER; $RhoJ^{+/+}$* (top panels) and *$Braf^{CA/+}$; $Pten^{fl/fl}$;Tyr::CreER; $RhoJ^{-/-}$* (bottom panels) animals. Melanoma cells were identified by their pigmentation characteristic. Scale bar is 200μm. (G) RhoJ deletion inhibits melanoma development. The amount of pigment present on the paws at day 17 was analyzed with ImageJ (*p=0.04, n=5, T-test). Error bars represent SEM. (H) Paws of 4-OHT treated mice were imaged at 10, 17, and 24 days post birth.

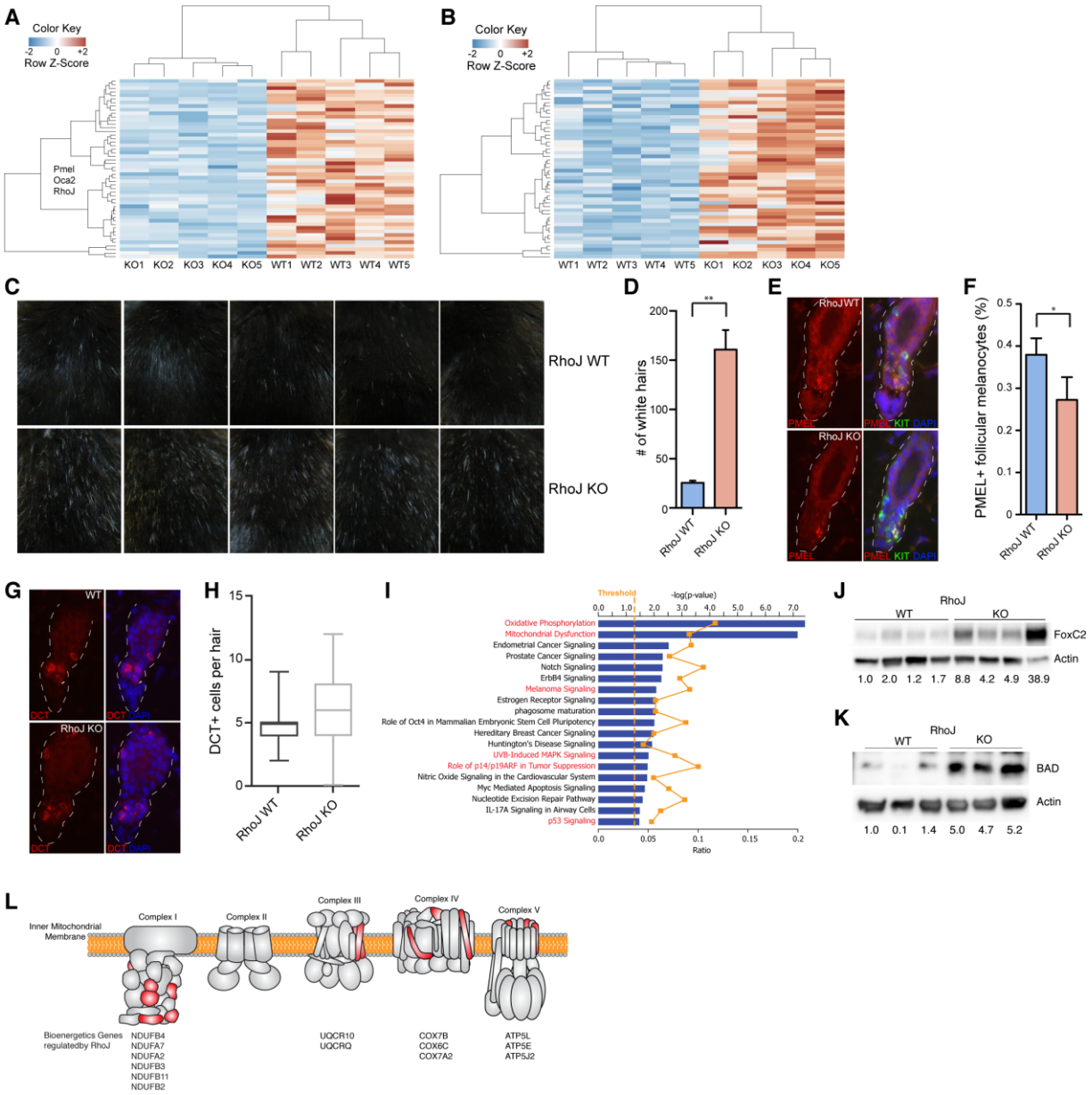

Figure 2.2. RhoJ modulates various signaling pathways to promote tumor growth.

(A) Heat map plot of the top 50 down-regulated genes upon loss of RhoJ. Hierarchical clustering of RNA-seq normalized read counts ranging from less frequently expressed (dark blue) to overexpressed (dark red) genes. (B) Heat map of top 50 up-regulated genes upon loss of RhoJ. Hierarchical clustering of RNA-seq count reads ranging from less frequently expressed (dark blue) to overexpressed (dark red). (C) RhoJ KO mice have a greater number of white hairs than RhoJ WT mice. Images of 8-month old mice

show that loss of RhoJ induces accumulation of white hairs. (D) The number of white hairs over an area of $1in^2$ was counted and quantified using ImageJ (**p=0.002, Student's t-test). Error bars indicate SEM. (E) Loss of RhoJ results in fewer PMEL17+ follicular melanocyte stem cells. Double labeling for the melanosome protein PMEL17 (red) in hair follicle melanocyte stem cells (KIT+, green) at telogen demonstrates a noticeable reduction in the intensity and extent of PMEL expression in RhoJ KO mice. White dashed line indicates the extent of the hair follicle. (F) Quantification of the immunolabeling described in D demonstrates a statistically significant difference between RhoJ WT and RhoJ KO hairs (*p=0.03, Student's t test). Error bars indicate standard deviation of the mean. (G) Melanocyte stem cells reside in the hair germ of RhoJ KO hair follicles. Both RhoJ WT and RhoJ KO skins exhibit telogen-stage hair follicles that contain DCT+ (red) McSCs. White dashed line indicates the extent of the hair follicle. (H) Quantitative analysis of DCT+ cells that reside in the hair follicle or RhoJ KO and RhoJ WT mice are represented as a box and whisker box plot. The box plot is the 25-75^{th} percentile and the whiskers are the min and the max. (I) RhoJ regulates oxidative phosphorylation, melanocyte differentiation, and MAP kinase signaling. Based on the differentially expressed genes between melanoma tumors from RhoJWT and RhoJKO mice, Ingenuity Pathway Analysis (IPA) generated an enrichment of canonical pathways regulated by RhoJ based on the literature (pathways potentially regulated by BRAF are highlighted in red). Bars indicate the negative logarithm of the enrichment p-value. The orange dotted line indicated the statistical threshold ($p<0.05$) for the enrichment canonical pathways. The orange squares indicate the ratio (value of molecules in a given pathway that meet the cutoff criteria, divided by total number of

molecules that make up that pathway) for each canonical pathway. (J) FoxC2 is up regulated in mouse tumor samples. Melanoma tumor lysates were prepared for western blot and probed for the indicated Abs. (H) BAD is up regulated in RhoJ KO mouse tumor samples. (L) Bioenergetic genes, found throughout the electron transport chain, upregulated when RhoJ is absent are shown. Note the number of genes that are present in complex I.

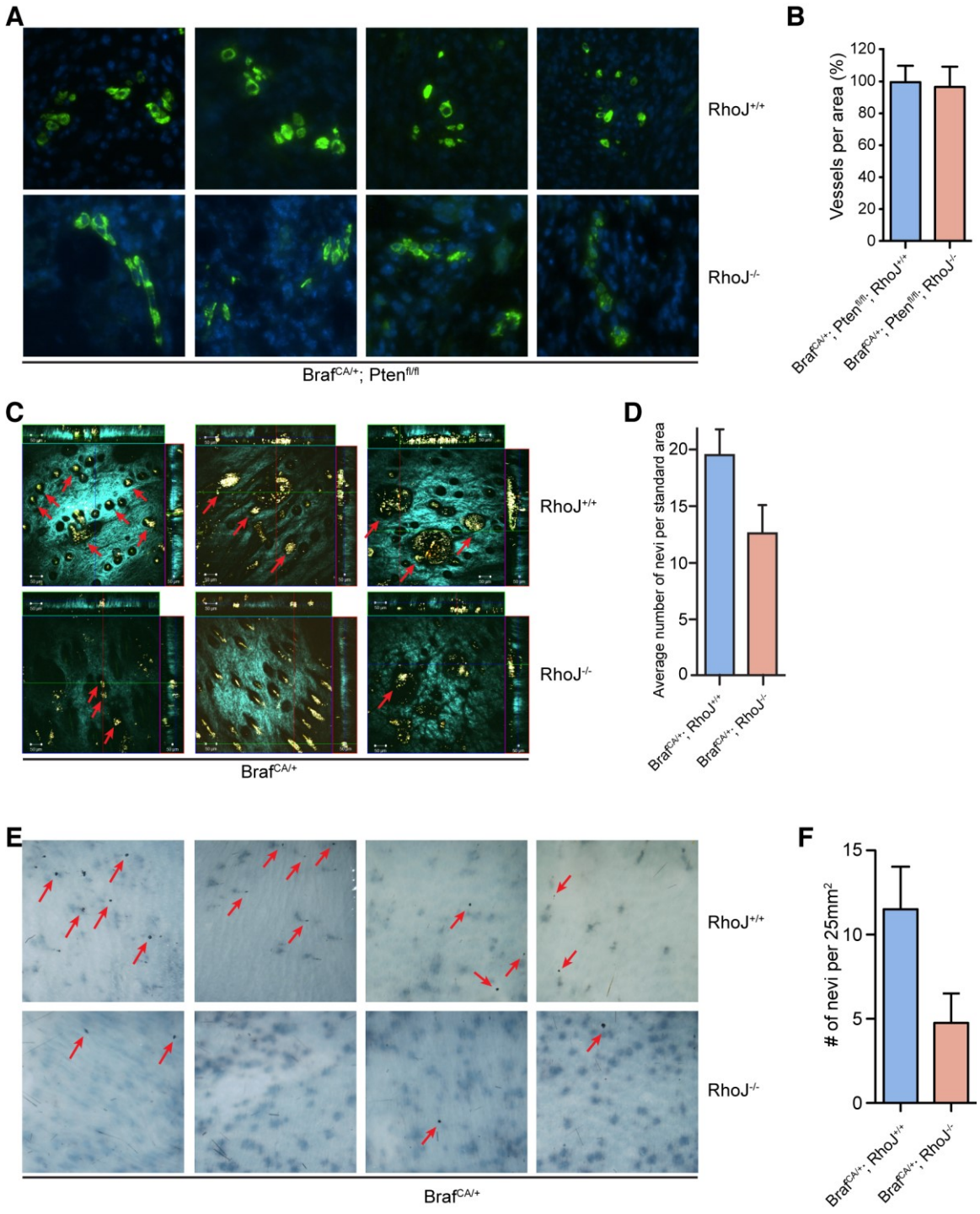

Figure 2.3. RhoJ regulates the formation of BRAF mutant nevi. (A) RhoJ deletion does not significantly affect the angiogenesis of BRAF mutant autochthonous melanoma tumors. Tumor sections from age matched (post-natal day 30) $BRAF^{V600E}$ and PTEN null RhoJ KO or RhoJ WT mice were stained with smooth muscle actin Ab

followed by Alexa-488 secondary Ab to visualize blood vessels. Representative immunofluorescence sections are shown. (B) RhoJ KO and RhoJ WT melanomas have similar numbers of vessels. The number of blood vessels in RhoJ WT and RhoJ KO per unit area (412μm x 412 μm) were quantified. The number of blood vessels were not significantly different (p=0.8, n=6 (mice) and 3 areas per tumor were counted). (C) RhoJ deletion inhibits nevus formation. MPM images were captured as described in materials and methods from *Tyr:Cre^{ERT2}*; *Braf^{V600E}; RhoJ$^{+/+}$* and *Tyr:Cre^{ERT2}*; *Braf^{V600E}; RhoJ$^{-/-}$*. Colored lines indicate positions being displayed as xy (blue), xz (red) and yz (green) planes. Field of view is 636μm x 636μm Cyan: SHG of collagen; Green: fluorescence of keratin; Yellow and Red – fluorescence of melanin. Nevus indicated by red arrows. (D) Nevi were quantified within the upper 50μm from 3-D skin reconstructions. Fewer microscopic nevi could be visualized from the skin surface in RhoJ KO skin as compared to RhoJ wild type skin (p=0.059, ANOVA, n=10). (E) RhoJ deletion reduced the number of macroscopic nevi visualized from the skin surface. Skin samples were fixed in 10% formalin for 36 hours and dehydrated in a series of increasing alcohol concentrations, and nevi were visualized by a dissecting microscope. Red arrows indicate pigmentation that could be visualized on the skin surface. (F) Macroscopic nevi were quantified on skin samples that measured 25mm^2. RhoJ KO samples contained fewer nevi (p=0.07, Student's t-test, n=4).

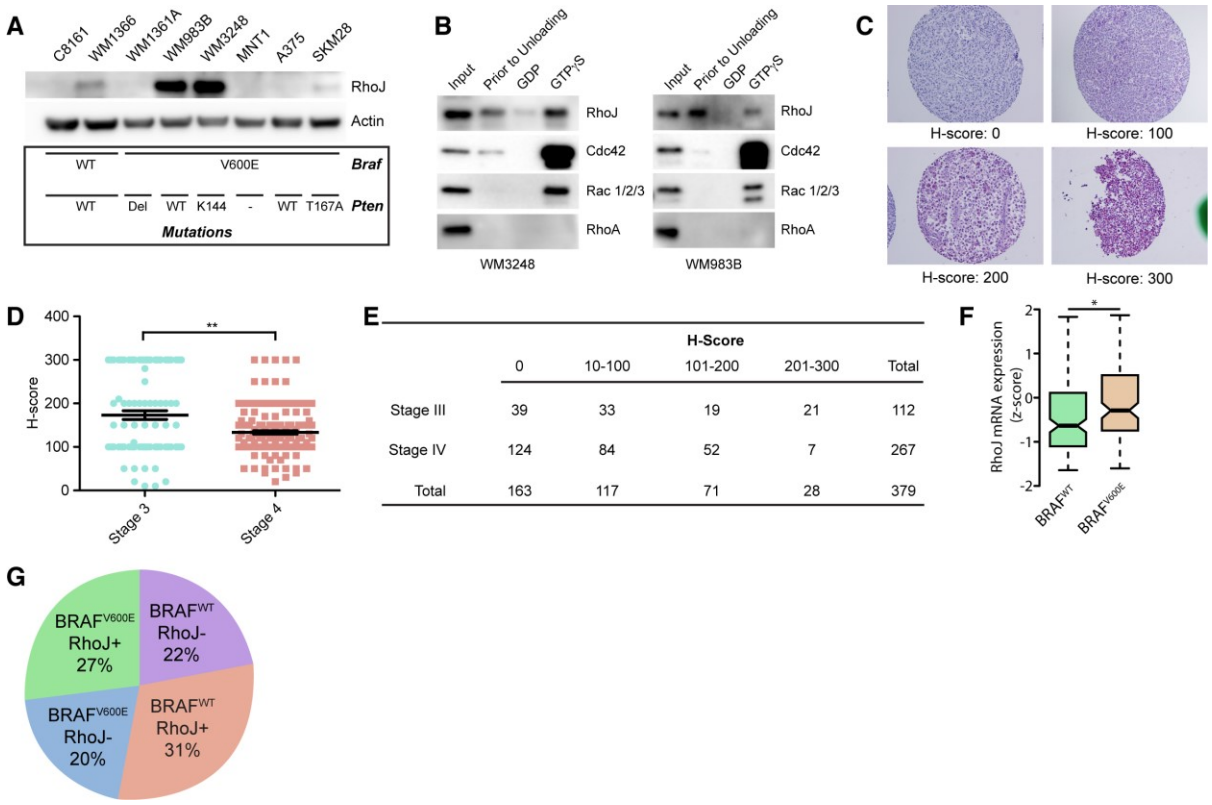

Figure 2.4. RhoJ signals through PAK1 and is expressed in a subpopulation of Braf mutant human tumors. (A) RhoJ is expressed in melanoma cell lines containing $BRAF^{V600E}$ mts. Lysates from various melanoma cell lines containing WT BRAF or $BRAF^{V600E}$ mt were prepared and immunoblotted with the indicated Abs. BRAF and PTEN status are indicated below each cell line. (B) RhoJ is activated in melanoma cells. Melanoma cell lysates were analyzed in their initial state ("prior to unloading" lane) or after exchange and reloading with either GDP or GTPγS. Protein lysates were then incubated with PAK-PBD Agarose beads and precipitated. Precipitated lysates were subjected to immunoblotting using the indicated Abs. (C) Optimization of RhoJ antibody for immunohistochemistry evaluation of AJCC stage III and IV TMAs. Human melanoma tumors were stained with an optimized RhoJ Ab and developed with liquid

permanent red. Representative samples with the indicated H-score were determined by a dermatopathologist. (D) RhoJ is expressed higher in stage III melanoma tumors. Tumors were scored for RhoJ expression and quantified using a standard H score criteria (**$p<0.001$). (E) Over 50% of human melanomas express RhoJ. Quantification of RhoJ+ tumors based on H-score. (F) RhoJ expression is higher in $BRAF^{V600E}$ melanoma clinical specimens. TCGA SKCM RNA-seq data for RhoJ expression was compared between $BRAF^{WT}$ (n=168) and $BRAF^{V600E}$ (n=130) melanoma specimens (*$p=0.02$, Student's t-test). (G) $BRAF^{V600E}$ and RhoJ status among AJCC stage III and stage IV melanoma tumors. Tissue microarrays were stained with an anti-BRAF mutant specific anti-S100, and an anti-RhoJ Abs as indicated. The percentage of tumors that stained with S100 (positive control) Ab and also stained with RhoJ and/or the mutant BRAF Ab was calculated. RhoJ + designates tissue that expresses RhoJ while RhoJ – tissues do not express RhoJ.

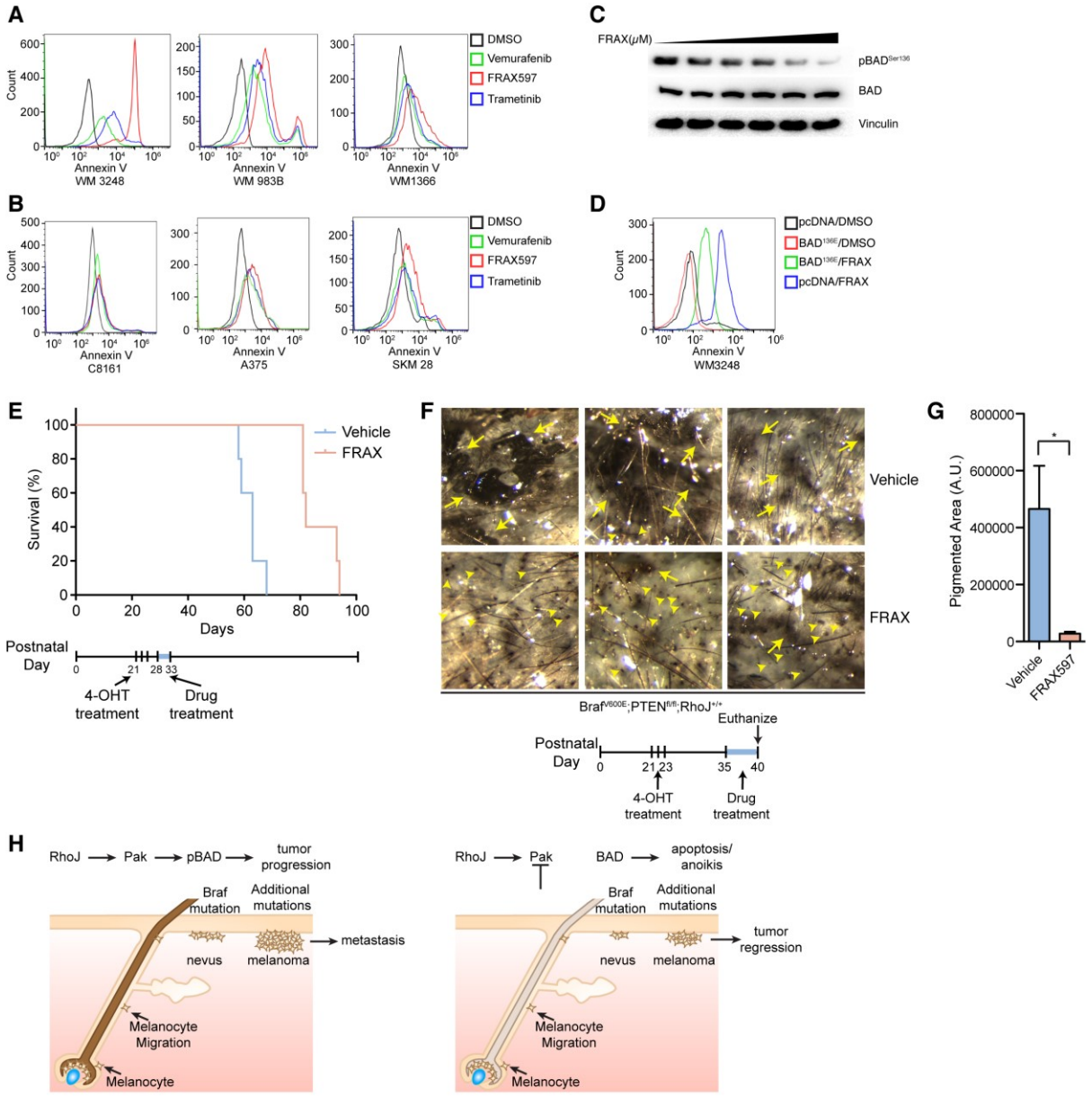

Figure 2.5. PAK inhibition induces apoptosis via BAD and blocks the progression of BRAF mutant melanomas. (A) FRAX597 inhibits PAK1 activation and induces apoptosis in BRAF^{V600E} melanoma cell lines. Apoptosis was quantified with annexin V labeling and flow cytometry. (B) FRAX597 does not induce apoptosis in cell lines that do not express detectable RhoJ. Flow cytometry analysis of melanoma cell lines treated with vehicle, vemurafenib (5μM), FRAX597 (1μM), or trametinib (0.1μM). (C) PAK inhibition decreases the phosphorylation of BAD$^{Ser\ 136}$. Melanoma cell lines

harboring the $BRAF^{V600E}$ mutation were treated with an increasing concentration of FRAX597 (0μM, 0.2μM, 0.5μM, 1μM, 2.5μM, 5μM) and immunoblotted with the indicated antibodies. (D) Over expression of pcDNA3 BAD^{S136E} phosphomimetic rescued survival after FRAX597 treatment. Cells were transfected with Lipofectamine 3000 according to the manufacturer's instructions and treated with FRAX or DMSO. Apoptosis was measured with flow cytometry. (E) PAK inhibition prolongs survival in $Braf^{V600E}$ PTEN null mice. Melanoma was induced in adult mice at P21, P22, and P23 with topical treatment of 4-OHT (25mg/mL) as previously described (49). Vehicle or FRAX597 (100mg/kg P.O. Q.D.) was administered for six days between P28 and P33. Mice were euthanized when the tumor burden exceeded the minimum restrictions as advised by veterinary technicians, and Kaplan-Meier survival curves were generated for $Braf^{CA/+}$; $Pten^{fl/fl}$;$Tyr::Cre^{ERT2}$; $RhoJ^{+/+}$ vehicle (n=5) or FRAX597 (n=5) treated animals. Log-rank test demonstrates significant difference between the two groups (**$p<0.002$, Log-rank test). (F) PAK inhibition delays tumor formation. Mice were treated with 4-OHT at P21, P22, and P23 on their backs to induce melanoma. Tumors were allowed to progress for 2 weeks prior to drug treatment. Mice were either administered FRAX597 or Vehicle for six days. Mice were euthanized after six days of drug treatment and images were taken with a dissecting microscope. Tumors were visible in vehicle treated mice (arrows) but smaller lesions were visible FRAX597 treated mice (arrowheads). (G) Disruption of RhoJ-PAK signaling blocks the formation of nevi and the growth of melanoma. The area of pigmented lesions (developing melanomas) from F was quantified (A.U. arbitrary units) and analyzed (*$p=0.04$, n=3, Student t-test). Error bars indicate SEM. (H) RhoJ expression enables melanocytes to differentiate and

migrate out of the hair follicle during the process of nevogenesis and evolve into melanoma tumors. Perturbation of RhoJ-Pak signaling prevents melanocytes from differentiating normally, which leads to loss of pigment in hair, impairment of melanocytes to migrate out of the hair to form nevi, and prevent transformation into melanoma as efficiently.

CHAPTER 3: ATR Mutations Promote the Growth of Melanoma Tumors by Modulating the Immune Microenvironment

Introduction

Melanomas accumulate a high burden of UV-induced mutations (154). While genomic studies have identified some putative melanoma driver mutations, leading to the development of agents such as MAP kinase inhibitors that induce tumor regression (155), it is less understood how other UV-induced mutations and tumor heterogeneity as a whole modulates tumor growth. These questions are not easily addressed by existing *in vivo* models, as existing animal models are either genetically homogeneous or lack a functional immune system (156).

While UV-irradiation contributes to the high mutation burden in skin cancer (157), melanoma tumors accumulate even more mutations as they fail to repair UV-damaged DNA. Patients with the DNA repair disorder Xeroderma Pigmentosum have an increased risk of melanoma (158), while mutations that affect telomere maintenance are also linked to melanoma (159), and mutations in CDKN2a, which is commonly defective in melanoma (160), also regulates genome maintenance (161). Melanoma cells also have DNA damage checkpoint defects- 70% of cutaneous melanoma cell lines demonstrate defective G1 checkpoint arrest (162). Finally, some patients predisposed to melanoma have mutations in the MC1R receptor which is known to activate DNA repair mechanisms (163) by modulating the activity of the ATR kinase (164, 165).

The ATR kinase is essential for the viability of both human and mouse cells (166, 167). In response to single stranded DNA damage, the ATR kinase is recruited to damaged DNA, becomes activated, and then phosphorylates its downstream target

Chk1 (168). Activation of Chk1 results in cell cycle arrest and DNA repair to prevent damaged cells from progressing through the cell cycle (169). Chk1 is essential for the development of murine melanocytes (170), identifying a specific role for ATR-Chk1 in the melanocyte lineage. While ATR is essential for replication, hypomorphic mutations in ATR are observed in Seckel syndrome (171), a recessive disorder characterized by developmental delay and premature aging. Similarly, ATR mutant (ATR mt) mice develop signs of premature aging and hair greying (172). Partial loss-of-function ATR mutations also can cause an oropharyngeal cancer syndrome (173).

In this study, we sought to examine whether ATR mutations can contribute to the development of melanoma. We identify ATR loss of function mutations in human melanoma, and determine that introducing similar mutations into BRAF mt PTEN heterozygous mouse melanomas (49) accelerates both tumor growth and mutation accumulation. ATR mt tumors in this model recruited proinflammatory macrophages while repelling T cells important for the anti-tumor response, identifying ATR mutations that modulate the immune response to promote growth.

Materials and Methods

Mouse breeding, activation of *Tyrosinase::Cre^{ERT2}* transgene, and experimental endpoints.

Atr^{flox}, Tyrosinase::Cre^{ERT2}, *Braf^{Ca}*, and *Pten^{lox4-5}* mice were genotyped using established protocols. 3μl of a 25 mg/ml solution of 4-OHT (98% Z-isomer, Sigma-Aldrich, St. Louis, MO, USA) in DMSO was applied to the right flank, back skin and tail of mice on postnatal days 2, 3 and 4. Institutional Animal Care and Use Committee (IACUC) of the University of California Irvine approved our study protocols. The

decision to euthanize mice was determined by independent University Lab Animal Resource (ULAR) staffs that were blinded with respect to the mouse genotype. Mice were euthanized if the volume of their tumors exceeded 10% of total body volume, if tumors were significantly ulcerated, if mice were moribund, if they lost weight, if they were lethargic, or if they were unable to ambulate.

Multiphoton microscopy of mouse skin.

Experimental mice were shave depilated at p50 (second telogen), euthanized, and immediately imaged ex-vivo (no labeling) with multiphoton microscopy (MPM) to capture the fluorescence signal from keratin and melanins and second harmonic generated (SHG) signal from collagen using LSM 510 NLO Zeiss system. Fluorescence and second harmonic generation was excited by femtosecond Titanium: Sapphire (Chameleon-Ultra, Coherent) laser at 900 nm. Emission was detected at 390-465 nm for SHG channel (blue), and 500-550 nm (green) and 565-650 (red) fluorescence channels. Each animal was imaged at 8 to 10 randomly chosen locations on depilated skin of the lower back. Stacks of optical sections of 636μmx636μm at different depths ranging from 0 to 240 μm (5 μm steps) were obtained to allow for 3-D volume reconstruction (LSM Image Browser, Carl Zeiss GMBH).

Cell Culture and UVB irradiation.

A375, MeWo and MB435S were obtained from ATCC. JWCI-WGS01, JWCIWGS18, JWCI-WGS22, and JWCI-WGS31 were provided by the John Wayne Cancer Institute. WM983B, WM3211, and WM3248 were obtained from Coriell Institute for Medical Research. A375 and MB435 were grown in Dulbecco's MEM supplemented with 10% fetal bovine serum (FBS); WM983B, WM3211, and WM3248 were grown in

Tu medium with 2% FBS. MeWo was grown in Eagle's MEM supplemented with 10% FBS; and JWCIWGS01, JWCI-WGS18, JWCI-WGS22, and JWCI-WGS31 were cultured in RPMI medium with 10% FBS. For UV irradiation of cell cultures, the culture medium was removed and washed with phosphate-buffered saline (PBS). The source of the irradiation was a CLP-1000M UV Crosslinker with UV lamp F8T5 (efficiency of lamp is 1.5mW/min) for UVB (UVP 34-0042-01) (at 302 nm), (Upland, CA). Irradiation was controlled by monitor with the dose of 250J/M2. After irradiation, fresh medium was added to the culture and cells were incubated at 370C incubator for 40 mins.

Western blotting and antibodies

Lysates were prepared in RIPA lysis buffer (RIPA supplemented with protease inhibitor, Santa Cruz Biotechnology, Dallas, TX). Lysates were subjected to SDS-PAGE on 4-12% Bis-Tris gradient gels (Life technology, Grand Island, NY) under reducing conditions and transferred onto Immobilon-P membranes (EMD Millipore, Billerica, MA). Membranes were blocked in 5% non-fat milk with 1X TBS and 1% Tween-20, and probed with one of the following antibodies: rabbit polyclonal GAPDH, #5174; rabbit β-Actin(13E5), #4970S; rabbit polyclonal phospho-CHK1 S345, #2348s; rabbit polyclonal ATR, #2790s; (Cell Signaling Technology, Danver, MA), and mouse monoclonal ATR (2B5), GTX70109 (Genetex, Irvine, CA), and M2 (F1804) antibody (Sigma-Aldrich, St. Louis, MO). Protein levels were assessed using densitometry analysis (ImageJ, NIH, Bethesda, MD).

Western blotting analysis of mouse tumors.

End stage mouse tumors were obtained from BRAF*V600E* PTEN+/- ATR*mD/mD* or BRAF*V600E* PTEN+/- ATR+/+ mice. Tumors were surgically excised, and snap

frozen in liquid nitrogen. Tumors were minced with a scalpel and homogenized and lysed in RIPA buffer with Precellys lysing kit (Bertin technologies, Rockville, MD). Lysate from tumors were subjected to Western blotting analysis.

Expression of ATR wt and mt constructs in A375 melanoma cells.

pcDNA3-ATR WT expression construct was purchased form Addgene (plasmid #31611). The ATR mts were generated by site-specific mutagenesis. (Agilent Technologies, Santa Clara, CA). Plasmids were transfected into A375 cell line by Turbofect transfection reagent (Thermo Scientific, Waltham, MA). 48hrs after transfection, cells were selected by G418 selection for 7days. Selected cells were either exposed to UV irradiation as indicated or subjected to immunoprecipitation followed by western blotting as indicated.

EdU labeling and flow cytometry.

Cells were labeled with 10 μM Edu for 1h, then were irradiated with UVB (250J/m^2). At 0hr or 6hr post-UV cells were fixed and stained with Click-iT Plus EdU Alexa Fluor 647 Flow Cytometry assay kit (Life technology, Grand Island, NY, USA) according to the manufacture's protocol. Cells were subjected to Flow Cytometry with an Attune Acoustic Focusing Cytometer (Life technology, Grand Island, NY, USA) to analyze the EdU positive cells. The resulting data were analyzed using Acoustic Focusing Cytometer software (Life technology, Grand Island, NY, USA).

RNA-Seq.

Total RNA from WT 1-4 and mD 1-4 (Tumor samples) or WT 1-3 and mD- 1-3 (Nevi samples) was monitored for quality control using the Agilent Bioanalyzer Nano RNA chip. Library construction was performed according to the Illumina TruSeq RNA v2

protocol. The input quantity for total RNA was 1µg and mRNA was enriched using oligo dT magnetic beads. The enriched mRNA was chemically fragmented for four minutes. Firststrand synthesis used random primers and reverse transcriptase to make cDNA. After second strand synthesis, the ds cDNA was cleaned using AMPure XP beads and the cDNA was end repaired and then the 3' ends were adenylated. Illumina barcoded adapters were ligated on the ends and the adapter ligated fragments were enriched by nine cycles of PCR. The resulting libraries were validated by qPCR and sized by Agilent Bioanalyzer DNA high sensitivity chip. The concentrations for the libraries were normalized and then multiplexed together. The concentration for clustering on the flowcell was 12.5pM. The multiplexed libraries were sequenced on three lanes using paired end 100 cycles chemistry for the HiSeq 2500. The version of HiSeq control software was HCS 2.2.38 with real time analysis software, RTA 1.18.61. Paired-end sequencing reads were trimmed of adapter sequences, analyzed for quality using the Fastqc program (http://www.bioinformatics.babraham.ac.uk/projects/fastqc/), and aligned to the mouse reference genome version mm10 using the Tophat alignment software (version 2.0.12) (174). Fragments and exons were quantified using the Cufflinks program (version 2.2.1) (175). The edgeR library (176) of the R statistical environment was used for differential gene expression analysis of mapped read counts and R was used for hierarchical clustering of the normalized counts that aligned to genes. P-values and FDR values of differentially expressed genes are reported. Ingenuity Pathway Analysis (IPA) indicated that genes that are components of ATR canonical pathways were enriched in the ATR mutant tumors. Bars indicate the negative logarithm of the enrichment p-value. The orange dotted line indicates the

statistical threshold ($p<0.05$) for the enrichment canonical pathways. The orange squares represent the ratio (value of molecules in a given pathway that meet the cutoff criteria, divided by total number of molecules that make up that pathway) for each canonical pathway (QIAGEN, Redwood City, CA).

Genomic DNA-Seq.

Using a Covaris S2, gDNA was sheared using conditions to generate 300 - 500bp fragments. The Bio Scientific NEXTflex Rapid DNA-Seq kit for the Illumina platform was used. From 300 ng of sheared gDNA, the ends were repaired and then adenylated on the 3' ends. The repaired and adenylated fragments were then ligated with NEXTflex DNA-Seq adapters. After ligation, a dual size selection was performed using AMPure XP beads with a lower cutoff of 500bp and an upper cutoff of 700bp. The adapter ligated fragments were enriched using 11 cycles of PCR. The libraries were validated by qPCR and sized by Agilent Bioanalyzer DNA high sensitivity chip. The libraries were clustered on the flowcell at 12.5pM and sequenced on two lanes using paired end 100 cycles chemistry. The version of HiSeq control software was HCS 2.2.38 with real time analysis software, RTA 1.18.61. DNA sequencing reads were aligned to the reference mouse genome (mm10) using the BWA software (version 0.7.8) (177). Single nucleotide variants and indels were called using the GATK best practices pipeline (178, 179). Structural variation was identified using a combination of the programs BreaKDancer (version 1.1.2) (180, 181), Delly (version 0.6.1) (182) and a suite of software tools developed in house. VCF files containing all SNV calls were deposited on dbSNP after publication. The number of SNVs present in ATR mt and ATR wt tumors were determined, and the number of SNVs per kb was determined for each

chromosome. ATR independent variants were eliminated by removing SNVs that were present in any of the four BRAF*V600E* PTEN$^{+/-}$ ATR$^{+/+}$ tumors from the set of variants that occurred in any of the four BRAF*V600E* PTEN$^{+/-}$ ATR$^{mD/mD}$ tumors. Transitions and transversions were defined by the nucleotide change from the BRAF*V600E* PTEN$^{+/-}$ ATR$^{+/+}$ tumors. Variants on each chromosome were visualized utilizing iobio.io (183).

Tumor volume measurements.

Tumors were measure at postnatal day 75 or the end point of the study. An electronic caliper was used to measured tumor size. Tumor volume was evaluated using the following formula: TV = (width)2X length/2.

CD3, CD19and F4/80 flow cytometry analysis.

End stage of mouse tumors were obtained from BRAF^{V600E} PTEN$^{+/-}$ ATR$^{mD/mD}$, or BRAF^{V600E} PTEN$^{+/-}$ ATR$^{+/+}$. Tumors were surgically excised, washed with 70% ethanol and PBS. Tumors were minced with a scalpel and dissociated using a tumor dissociation kit (#130-096-730) and gentleMACs (Miltenyi Biotec, Auburn, CA) according to the manufacture's protocol. Dissociated tumor cells were labeled by CD3 (17A2)-PE/Cy7, CD19(6D5)-APC and F4/80 (BM8)-APC/Cy7 (BioLegend, San Diego, CA). Cells were subjected to flow cytometry using an Attune Acoustic Focusing Cytometer (Life technology, Grand Island, NY) to analyze the CD3, CD19 and F4/80 positive cells. The resulting data were analyzed using Acoustic Focusing Cytometer software (Life technology, Grand Island, NY, USA).

RAW264.7 culture and cytokine stimulation.

RAW264.7 macrophage-like cells (ATCC) were cultured in Dulbecco's MEM supplemented with 10% FBS. For cytokine stimulation, RAW culture was replaced with

fresh medium with a final concentration of 100ng/ml IFN-γ or 20 ng/ml IL-4 for 24hrs. RNA was harvested from treated cells using standard protocols.

mRNA preparation, reverse transcription, and real-time PCR.

Cells or tumor samples were lysed in Trizol reagent (Life technology, Grand Island, NY, USA) and homogenized with a Precellys lysing kit (Bertin techonologies, Rockville, MD). Purified mRNA was resuspended in RNase-free water, and the concentration was measured using a nanophotometer (Implen, Westlake Village, CA). Reverse transcription was performed using a high capacity cDNA reverse transcription kit (Applied Biosystems, Foster City, CA) per the manufacturer's protocol. Real-time PCR (real-time quantitative PCR "qPCR") was performed using the cDNA generated as described above. Primers (Supplemental Data File1-sheet3) were purchased from Integrated DNA Technologies, Inc (Coralville, IA). Quantitative real-time PCR was performed with a Power SYBR-Green master mix according to the manufacturer's instruction and analyzed on a StepOnePlus Real-Time PCR system (Applied Biosystems, Carlsbad, CA). Alternatively, probe-base q-PCR was performed with Taqman fast advanced master mix (Applied Biosystems, Carlsbad, CA). For all qPCR, cytokine stimulated RAW 264.7 cells (INF-γ alone or IL-4 alone) were the positive control for M1 or M2 macrophages. mRNA expression values were normalized to GAPDH expression. Expression fold changed were calculated by comparing to RAW 264.7 cells.

Immunohistochemistry.

Tumor samples were fixed in 10% formalin for 24hrs, washed in PBS followed by ethanol dehydration, and paraffin embedded. 8 μm thick sections were cut from paraffin

blocks and adhered to glass slides. Slides were dried overnight and paraffin was removed with xylene followed by rehydration. Antigen retrieval was carried out by heating slides to 95°C for 15 min in 0.01M sodium citrate buffer (pH 6). Endogenous peroxidase quenching and bleaching of pigmentation was performed using 3% H2O2 overnight at room temperature. Protein block was carried out using either 5% normal goat serum in 1x TBST, or M.O.M blocking reagent (Vector Laboratories, Burlingame, CA) for 1 hr. Tumor samples were then incubated with primary Ab F4/80 (1:100) (AbSerotec, Raleigh, NC) , CD3 (1:100), CD19 (1:100) (Santa Cruz Biotechnology, Dallas, TX) or Ki67 (1:100, Novocastra reagent, Leica Biosystems, Buffalo Grove, IL)) overnight at 4°C, followed by incubations with biotinylated secondary antibodies (1:200 anti-rat; 1:500 anti-mouse; Vector Laboratories) for 1 hour at room temperature. Slides were then treated with ABC-streptavidin-peroxidase (Vector Laboratories) for 30 mins and developed with DAB (Dako) followed by counterstaining in hematoxylin and dehydration before mounting with permount.

Statistical analysis

Kaplan Meier survival curves were generated and significance was assessed using the log-rank test, an unpaired t-test, or a two-way ANOVA test. Volume of pigmented lesions from MPM images were measured manually on orthogonal projections to access length, width and depth of a nevus as it is outlined by a bright luminescence from melanin. Four animals per group (wt vs mD/mD) were imaged. Other data was analyzed by GraphPad Prism6 statistical analysis software using an unpaired t-test or two way Anova test. Significances were as indicated.

Results

Loss of Function ATR mutations are present in human melanoma

Initial studies identified mutations in the ATR pathway in human melanoma. 7% of melanoma tumors in the TCGA have mutations in genes that affect the ATR pathway (ATR and CHK1), with most of these mutations occurring in the ATR gene (6%). Analysis of an independent set of primary tumors revealed a higher incidence of ATR mutations (13%). ATR mutations did not map to a specific hotspot within the open reading frame (Figure 3.1.A), and none of the ATR mutations observed were recurrent in the dataset analyzed. ATR mt tumor cell lines from this cohort were examined to determine whether they had defective cell cycle checkpoints. Upon UVB-irradiation, ATR is recruited to damaged DNA and initiates the phosphorylation of CHK1 at Serine 345, initiating cell cycle arrest (184). While UVB-irradiation was sufficient to induce CHK1 phosphorylation in ATR-WT melanomas (WM983B, A375, MNT1, WM3211, WM3428) (Figures 3.1.B, left panel and Figure 3.1.C), it did not induce the accumulation of phospho-CHK1 in ATR mt melanoma cell lines (JWCI-WGS18, JWCI- WGS22, MeWo, MB435S) as efficiently with the exception of JWCI-WGS01 and JWCI-WGS31 (Figure 3.1.B).

To assess whether ATR mt melanoma cell lines had defective cell cycle checkpoints, we examined whether UVB-irradiation induced cell cycle arrest in ATR WT (WM983B, A375) or mt melanomas. We excluded MNT-1 cells from this analysis as melanin in these cells interfered with the EdU assay. ATR mt cell lines incorporated less EdU after 1 hr of labeling as compared to ATR WT cells (Figure 3.1.D) whether or not they exhibited defects in Chk1 phosphorylation, suggesting that all of these mts have some defects in the activation of ATR downstream targets. UVB-irradiation

induced cell cycle arrest in ATR WT cells (A375), as similar percentages of EdU positive cells were observed in samples labeled for 1 hour followed by a 6 hr post UV chase as was observed in control cells labeled for 1 hr (Figure 3.1.E). Several ATR-mt cell lines (JWCI-WGS18, MeWo, MB435S) had defects in UV-induced cell cycle arrest, as cells were able to proliferate after UV-irradiation, diluting out the population of cells that were labeled with EdU during the first hour (Figure 3.1.D). The ability to overcome this replication block (Figure 3.1.E) correlated with the magnitude of defects in UVB-induced Chk1 phosphorylation (Figure 3.1.B). Taken together, these studies verify that subsets of melanoma tumors have ATR loss of function mutations.

Next, we verified that the ATR mutants in MB435S, MeWo, and JWCI-WGS18 cell lines, which exhibited altered UVB-induced checkpoints, interfered with the function of WT ATR. ATR mt constructs were generated and expressed at low levels in an A375 melanoma cell line that also express WT ATR. Initial studies verified that each WT or mt Flag-tagged ATR construct was expressed at a low level in A375 cells, and that these cell lines expressed similar levels of total ATR (Figure 3.1.FF, left panel). While UVB-irradiation induced Chk1 phosphorylation in cells that express WT ATR, UVB-irradiation was less efficient at inducing Chk1 phosphorylation in cells that express a kinase dead ATR mt (Figure 3.1.F, D2475A) (185) or in cells that express the ATR mts that had defective DNA damage checkpoints as identified in Figure 3.1.B and 3.1.E (Figure 3.1.F, right panel). These findings verify that the heterozygous ATR mutations observed in human tumors have functional consequences.

ATR mutations accelerate the growth and metastasis of melanomas *in vivo*

In order to determine whether ATR mutations contribute to tumor development and metastasis *in vivo*, we crossed *Atr*$^{flox/flox}$ mice in which the loxP sites flank the ATR kinase domain (186) (Figures 3.2.A, 3.2.B upper panel) with mice carrying a *Tyrosinase::Cre*^{ERT2} allele, a *Braf*^{CA} allele, and zero, one or two copies of a *Pten*$^{lox4-5}$ allele (49). The growth of nevi or tumors in this model could be modulated by altering the dosage of PTEN: melanocytes expressing mt BRAF and WT PTEN produce nevi but no melanoma, melanocytes expressing mt BRAF and one copy of PTEN form tumors that are visible after >75 days, while melanocytes that express mt BRAF and no PTEN rapidly develop melanomas that metastasize quickly (49). Initial studies verified that: 1) mice containing BRAF mt melanocytes had a normal lifespan and didn't develop tumors (Figure 3.2.C); and 2) tumor development was influenced by the absence of one PTEN allele but not by ATR mt (Figure 3.2.D).

In this set of experiments, we examined the consequences of ATR loss in nevi and melanoma using a published ATR flox model in which the excision of the ATR flox cassette is not 100% complete (172), resulting in the generation of mice that have some melanocytes with no functional ATR and others with WT ATR. Over time, a mixed population of ATR$^{-/-}$ and ATR$^{+/+}$ cells can then repopulate tissues of these animals. While this feature makes it difficult to measure the effect of complete ATR loss on tumor growth, it does generate tumors that have a mixture of different mutations as is observed in human melanoma. Induction of recombination with topical 4-OHT in these mice would result in the simultaneous BRAF^{V600E} mutation, generation of some cells with mixed deletion of the ATR kinase domain (termed ATR^{mD}), and *PTEN* deletion specifically in melanocytes (Figure 3.2.A). The ATR protein is very large (300 kDa), yet

the kinase domain of the protein is very small, making it impossible to distinguish truncated ATR from full length ATR by western blotting (Figure 3.2.E). RT-PCR (reverse transcriptase PCR) of tumor RNA successfully demonstrated that ATR mD (mD/mD) tumors contained the truncated ATR transcript of the appropriate size (Figure 2B, bottom left panel) while also containing the WT transcript. Additional studies verified that mRNA corresponding to the floxed form of ATR was expressed in melanoma tumors (Figure 3.2.B, bottom right panel). In order to verify that ATR mt melanomas had defects in cell cycle checkpoints, $ATR^{mD/mD}$ and $ATR^{+/+}$ tumors were lysed, and subjected to western blotting with p-Chk1(S345) Ab. $ATR^{mD/mD}$ tumor cells exhibited decreased phosphorylation of CHK1 (Figure 3.2.F), indicating that these tumors lacked normal cell cycle checkpoints. $ATR^{mD/mD}$ tumors also had less expression of ATR but no change in the expression of ATM (Figure 3.2.F) even though the ATR flox allele migrates at the same size of the WT allele (Figure 3.2.E). Taken together, these findings verify that the $ATR^{mD/mD}$ tumors had ATR signaling defects.

To examine whether ATR signaling influenced tumor progression, *Tyrosinase::Cre*^{ERT2}; *Braf*$^{CA/+}$; *Pten*$^{fl/+}$; *Atr*$^{fl/+}$ or *Atr*$^{fl/fl}$ mice were generated and tumor formation was induced by topical administration of 4-OHT. $PTEN^{+/-}$ tumors were specifically selected for these experiments as these tumors develop more slowly, making it easier to identify an effect of ATR on tumor growth. $BRAF^{V600E}$ $PTEN^{+/-}$ $ATR^{mD/+}$ tumors grew larger than $BRAF^{V600E}$ $PTEN^{+/-}$ $ATR^{+/+}$ tumors (Figure 3.2.G), ultimately resulting in the tumor growing so large that these mice had to be sacrificed prematurely for compassionate reasons (Figure 3.2.H) (decrease in median survival of 14 days). While $BRAF^{V600E}$ $PTEN^{+/-}$ $ATR^{mD/mD}$ tumors grew to a larger size than ATR

WT tumors (Figure 3.2.G), the BRAF^{V600E} PTEN$^{+/-}$ ATR$^{mD/mD}$ tumors did not reach a sufficient size that mice needed to be sacrificed sooner than mice carrying BRAF^{V600E} PTEN$^{+/-}$ ATR$^{mD/+}$ tumors (Figure 3.2.H). These observations are consistent with other studies that have indicated that ATR can have differing effects on tumor growth dependent on gene dosage (187).

Deletion of both copies of PTEN in mouse melanomas rapidly accelerates their growth, resulting in a high tumor burden that goes on to generate lung metastases (49). Deletion of one or both copies of the ATR kinase domain in BRAF^{V600E} PTEN null melanocytes did not result in an increased burden of tumors (Figure 3.2.I), consistent with the published observation that BRAF^{V600E} PTEN null tumors develop and metastasize rapidly. BRAF^{V600E} PTEN$^{-/-}$ ATR$^{mD/mD}$ tumors did, however, have a higher propensity to metastasize to the lung as compared to BRAF^{V600E} PTEN$^{-/-}$ tumors (Figures 3.2.J, 3.2.K). Taken together, these studies suggest that ATR mutations influence both the growth and metastasis of BRAF mt melanomas.

ATR mt promote the growth of BRAF mt nevi

As ATR mts modulate both tumor growth and metastasis, we next sought to examine the role of ATR mt in the growth of nascent tumors and nevi. First, we examined mice 75 days after birth when tumors are first readily visible. Both BRAF^{V600E} PTEN$^{+/-}$ ATR$^{mD/+}$ tumors and BRAF^{V600E} PTEN$^{+/-}$ ATR$^{mD/mD}$ tumors (Figure 3.3.A) were larger in size as compared to BRAF^{V600E} PTEN$^{+/-}$ ATR$^{+/+}$ tumors after 75 days. Moreover, a greater number of tumors were observed per mouse in mice carrying ATR$^{mD/+}$ tumors and *ATR*$^{mD/mD}$ tumors (Figure 3.3.A) when compared to ATR$^{+/+}$ tumors. *Tyrosinase::Cre*^{ERT2};*Braf*$^{CA/+}$ mice develop melanocytic nevi after 4-OHT administration

that can progress to melanoma after a prolonged duration (188). To more accurately assess whether ATR deficiency affects tumor initiation, we generated *Tyrosinase::Cre^{ERT2}*; *Braf$^{CA/+}$ Atr$^{fl/fl}$* mice and induced precancerous nevi formation using topical 4-OHT treatment. Initial experiments verified that *Tyrosinase::Cre^{ERT2}*; *Braf$^{CA/+}$ Atr$^{fl/fl}$* and *Tyrosinase::Cre^{ERT2}*; *Braf$^{CA/+}$* mice had no difference in overall survival, and validated that these mice had similar survival as WT mice as noted in earlier publications (49) (Figures 3.2.C, 3.2.D). The number of nevi after tamoxifen topical administration in *Tyrosinase::Cre^{ERT2}*; *Braf$^{CA/+}$ Atr$^{fl/fl}$* and *Tyrosinase::Cre^{ERT2}*; *Braf$^{CA/+}$* mice was quantified visually and using multiphoton microscopy (MPM), a technique that utilizes only intrinsic fluorescent signals to generate a three-dimensional image of melanoma tumors (138). *Tyrosinase::Cre^{ERT2}*; *Braf$^{CA/+}$ Atr$^{fl/fl}$* mice develop more nevi after 4-OHT treatment compared to *Tyrosinase::Cre^{ERT2}*; *Braf$^{CA/+}$* mice (Figure 3.3.B). By measuring the intrinsic fluorescent signals from melanin (red), keratin (green), and the second harmonic signals from collagen (blue) using MPM (138) (Figure 3.3.C), we were able to determine that the developing ATR mt nevi were larger in volume (Figure 3.3.D) and occupied a larger volume of the skin (Figure 3.3.E). There were also a larger number of nevi in *Tyrosinase::Cre^{ERT2}*; *Braf$^{CA/+}$ Atr$^{fl/fl}$* mice although this number was just below statistical significance ($p=0.0503$) (Figure 3.3.F). Taken together, these studies indicated that ATR deficiency affects tumor initiation.

ATR mt Melanomas Accumulate More Mutations

To investigate how ATR mutations affected mutation accumulation, the genomes of BRAF^{V600E} PTEN$^{+/-}$ ATR$^{mD/mD}$ and BRAF^{V600E} PTEN$^{+/-}$ ATR$^{+/+}$ mouse tumors were sequenced and compared. Initial studies identified single nucleotide variants (SNVs)

present in BRAF^{V600E} PTEN$^{+/-}$ ATR$^{mD/mD}$ and BRAF^{V600E} PTEN$^{+/-}$ ATR$^{+/+}$ tumors and determined that ATR mt tumors accumulated more SNVs. Comparison of the number of SNVs in these two tumors revealed that ATR mt tumors accumulated more single nucleotide variants (Figure 3.4.A). ATR SNVs had no predilection for specific transitions or transversions (Figure 3.4.B), and were randomly dispersed across the genome, including both coding and regulatory regions (Figure 3.4.C). In contrast, there was not a drastic increase in the number of translocations in ATR$^{mD/mD}$ tumors (two inversions and one area of LOH was observed, data not shown), suggesting that the ATR mutation was not a complete loss of function, as has been described by others (172), as it resulted in the accumulation of SNVs and not translocations as observed in ATR null cells (189). In addition, while ATR mt tumors accumulated more SNVs in chromosome 7 and 12 (Figure 3.4.A), these SNVs were evenly distributed across the chromosome and did not localize to any particular hotspot indicating that the altered growth properties of these tumors was unlikely to be driven by a specific mutation induced by ATR loss.

ATR mt Tumors Generate a Pro-Inflammatory Microenvironment that Supports Tumor Growth

Initial studies revealed that ATR mt melanoma cells do not proliferate more rapidly, as the number of Ki67 positive cells in ATR WT and mt tumors was similar (data not shown), consistent with published studies indicating that ATR function is required for cellular replication (186). In order to better understand how ATR deletion promotes the growth of tumors as a whole, RNA was collected from BRAF^{V600E} ATR$^{mD/mD}$ nevi and BRAF^{V600E} ATR$^{+/+}$ nevi and subjected to RNA-seq and differential expression analysis

(Figure 3.5.A). ATR mt nevi had decreased expression of *jun* and *fos* (Figure 3.5.B), serum response factors whose expression positively correlates with cellular proliferation (190), indicating that these tumors were not more proliferative (Figure 3.5.A). Notably, ATR mt nevi had decreased expression of SkinT genes (Figure 3.5.B), a class of genes known as butyrophilins (191) that promote T cell homing to epithelia (192). ATR mt nevi also had decreased expression of CD4, a marker for T- cells and other immune cells (Figure 3.5.A), indicating that ATR tumors downregulate T-cell homing mechanisms. Taken together, these studies suggested that ATR mt tumors do not proliferate more rapidly but instead promote tumor growth by modulating the immune response.

To better characterize the effect of ATR mt on the immune response, flow cytometry was utilized to quantify the number of infiltrating immune cells in ATR mt and ATR WT tumors. $ATR^{mD/mD}$ melanoma tumors had decreased numbers of infiltrating T-cells ($CD3^{+}$, pan T cell marker) and increased numbers of infiltrating macrophages ($F4/80^{+}$) and B cells (CD19, B cell marker) as compared to $ATR^{mD/+}$ and $ATR^{+/+}$ tumors (Figure 3.5.C). Interestingly, 40% of the cells in ATR^{mD} tumors were macrophages. Consistent with this observation, RNA-seq analysis of $BRAF^{V600E}$ $PTEN^{+/-}$ $ATR^{mD/mD}$ tumors and $BRAF^{V600E}$ $PTEN^{+/-}$ $ATR^{+/+}$ tumors did indicate that genes involved in immune activation were preferentially expressed in ATR mt tumors (Figures 3.5.D, 3.5.E). Immunohistochemical studies revealed that ATR mt tumors had increased numbers of infiltrating macrophages (Figure 3.5.F) and decreased number of infiltrating T cells (Figure 3.5.G), further verifying the flow cytometry results. Unfortunately, it was difficult to measure an effect on B cells histologically, as very few infiltrating B cells were present in either specimen (Figure 3.5.H).

Blood monocytes extravagate into target tissues where they differentiate into mature macrophages and polarize into diverse subsets depending on environmental challenge (193). While macrophage polarization is exceedingly complex, simplified *in vitro* models suggest that macrophages can polarize into “M1” subsets which are involved in generating an anti-tumor immune response or “M2” polarized subsets which can exert anti-inflammatory and pro-tumorigenic properties (194). Macrophages are detected in genetically heterogeneous tumors (195) and can promote melanoma invasion and metastasis (196). Gene expression studies revealed that $ATR^{mD/mD}$ tumors expressed high levels of “M2” macrophage markers (Arg1, CD206, PPARG) (197), consistent with the contention that these infiltrating cells had pro-tumorigenic properties. In contrast, $ATR^{mD/mD}$ tumors exhibited the same level of expression of markers known to be associated with “M1” anti-tumor macrophages (iNOS, TNF-α, IL-6) (197) (Figure 3.5 I). Melanoma cells are known to avoid the immune response by activating the expression of PD-L1 (198). $ATR^{mD/mD}$ tumors expressed higher levels of PD-L1 and lower levels of PD-1 as compared to $ATR^{+/+}$ tumors (Figure 3.5.J), indicating that ATR deficient tumors also modulated the PD1 immune checkpoint as is observed in human melanomas.

Discussion

Interactions between melanoma cells and immune cells are critical in promoting tumor initiation, tumor angiotropism (199), and therapy resistance (200). Cancer cells express PD-L1 and CTLA4, which prevents the immune system from recognizing and destroying tumor cells (201), and PD-1 and CTLA4 blocking antibodies can activate the anti-tumor response, leading to tumor regression (202, 203). Existing mouse melanoma models either generate clonal tumors with little diversity or examine the immune

response in syngeneic models that poorly mimic human disease (204). The autochthonous mouse melanoma model established here has an intact immune system and generates tumors with mutations in tumor drivers, tumor suppressors, as well as defects in DNA repair. The observation that M2 macrophages promote tumor growth in this model are consistent with clinical observations that melanomas with more tumor-infiltrating, M2-like macrophages have a poorer prognosis (205), and other observations that macrophages promote melanoma metastasis (196). Interestingly, ATR mosaic, p53 null mice also had an increased number of macrophages localized around the hair follicle (206), indicating that ATR deletion modulates macrophage function. Tumors from ATR mt mice also overexpress PD-L1, similar to what has been observed in human melanoma tumors that respond to PD1 inhibitors (198). In addition, ATR mt tumors downregulate the expression of butyrophilins (191), which normally promote T cell homing to epithelia (192).

Recent studies have highlighted that tumors that have a higher mutation load are more responsive to immunotherapies (207, 208). While some studies have suggested that this is the result of generating more tumor neo-antigens, it is currently unclear why a tumor that expresses a high load of neoantigens would be resistant to immunotherapy in the first place. The studies presented here identify novel mutations within tumor cells themselves that allow them to suppress the T cell immune response and recruit macrophages known to promote tumor growth. The novel mouse model described here is an ideal system to elucidate how melanoma tumors modulate the immune response in order to develop better immunotherapies.

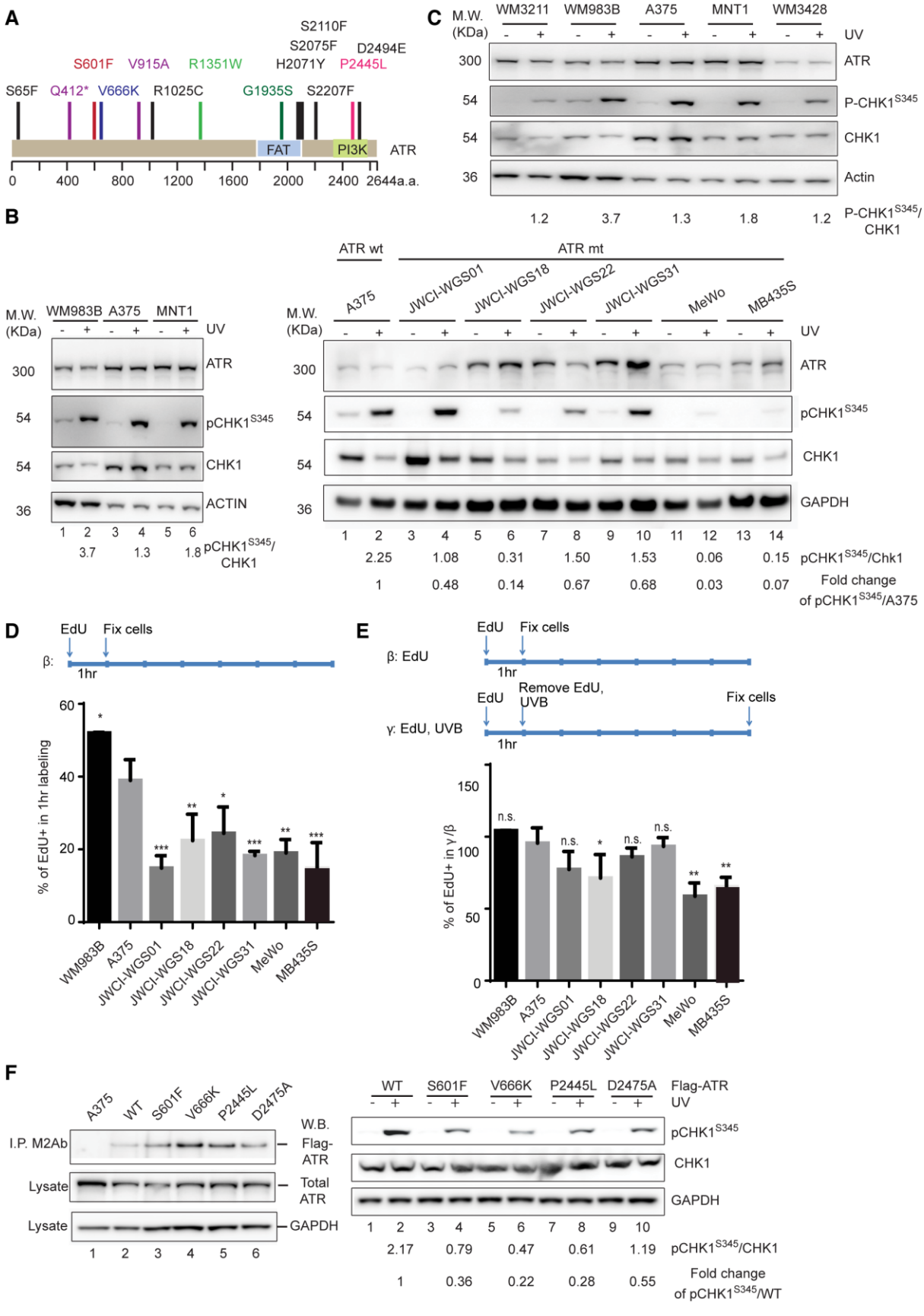
A
S2110F
S2075F
D2494E
S601F
V915A
R1351W
H2071Y
P2445L
S65F
Q412*
V666K
R1025C
G1935S
S2207F
FAT
PI3K
ATR
0
400
800
1200
1600
2000
2400
2644a.a.
C
M.W. (KDa)
WM3211
WM983B
A375
MNT1
WM3428
UV
300
ATR
54
P-CHK1S345
54
CHK1
36
Actin
1.2
3.7
1.3
1.8
1.2
P-CHK1S345/ CHK1
B
M.W. (KDa)
WM983B
A375
MNT1
UV
300
ATR
54
pCHK1S345
54
CHK1
36
ACTIN
1 2 3 4 5 6
3.7
1.3
1.8
pCHK1S345/ CHK1
ATR wt
ATR mt
A375
JWCI-WGS01
JWCI-WGS18
JWCI-WGS22
JWCI-WGS31
MeWo
MB435S
M.W. (KDa)
UV
300
ATR
54
pCHK1S345
54
CHK1
36
GAPDH
1 2 3 4 5 6 7 8 9 10 11 12 13 14
2.25 1.08 0.31 1.50 1.53 0.06 0.15
pCHK1S345/Chk1
1 0.48 0.14 0.67 0.68 0.03 0.07
Fold change of pCHK1S345/A375
D
EdU
Fix cells
β:
1hr
% of EdU+ in 1hr labeling
60
40
20
0
*
***
**
*
***
**
***
WM983B
A375
JWCI-WGS01
JWCI-WGS18
JWCI-WGS22
JWCI-WGS31
MeWo
MB435S
E
β: EdU
EdU
Fix cells
1hr
γ: EdU, UVB
EdU
Remove EdU, UVB
Fix cells
1hr
% of EdU+ in γ/β
150
100
50
0
n.s.
n.s.
*
n.s.
n.s.
**
**
WM983B
A375
JWCI-WGS01
JWCI-WGS18
JWCI-WGS22
JWCI-WGS31
MeWo
MB435S
F
A375
WT
S601F
V666K
P2445L
D2475A
I.P. M2Ab
W.B. Flag-ATR
Lysate
Total ATR
Lysate
GAPDH
1 2 3 4 5 6
WT
S601F
V666K
P2445L
D2475A
Flag-ATR
UV
pCHK1S345
CHK1
GAPDH
1 2 3 4 5 6 7 8 9 10
2.17 0.79 0.47 0.61 1.19
pCHK1S345/CHK1
1 0.36 0.22 0.28 0.55
Fold change of pCHK1S345/WT

Figure 3.1. Loss of function ATR mutations are present in human melanoma. (A) Tumor databases (TCGA, JWCI) were queried to identify ATR mutations, and the position of each ATR mutation is indicated. None of the observed mutations were recurrent in more than one tumor. (B) ATR mts have a defective DNA damage checkpoints. ATR WT melanoma cell cultures were irradiated with UVB followed by western blotting with the indicated antibodies (Ab) (left panel). Relative protein accumulation was measured by densitometry (see values) relative to a GAPDH loading control. (C) ATR wild type melanoma cell cultures (WM3211, WM983B, A375 and MNT1, WM3428) were irradiated with UVB followed by western blotting with the indicated antibodies. (D) ATR mutations do not accelerate the rate of proliferation of ATR mt human tumor cells. ATR WT or mts cells were labeled with EdU and the fraction of proliferating cells was determined. The graph represents the results of three independent experiments and error bars correspond to SEM. * $p<0.05$, **$p<0.01$; ***$p<0.005$ (E) ATR mts cells are more sensitive to UV-induced cell cycle arrest. ATR WT or mt cells were labeled with EdU for 1hr, irradiated with UVB, and the fraction of EdU+ cells was determined 0 and 6 hr post-UV as described. * $p<0.05$, **$p<0.01$ (F) Expression of ATR mts in A375 cells impaired the normal DNA damage response. A375 cells expressing either ATR FLAG tagged WT or mt constructs were lysed and immunoprecipitation with a FLAG antibody (M2) followed by western blotting with an ATR Ab to verify that each mt was expressed (left top panel). Total lysate from each culture expressing ATR WT or mt constructs was also immunoblotted with the indicated antibodies and relative accumulation of pChk1/Chk1 and pChk1/GAPDH was determined by densitometry.

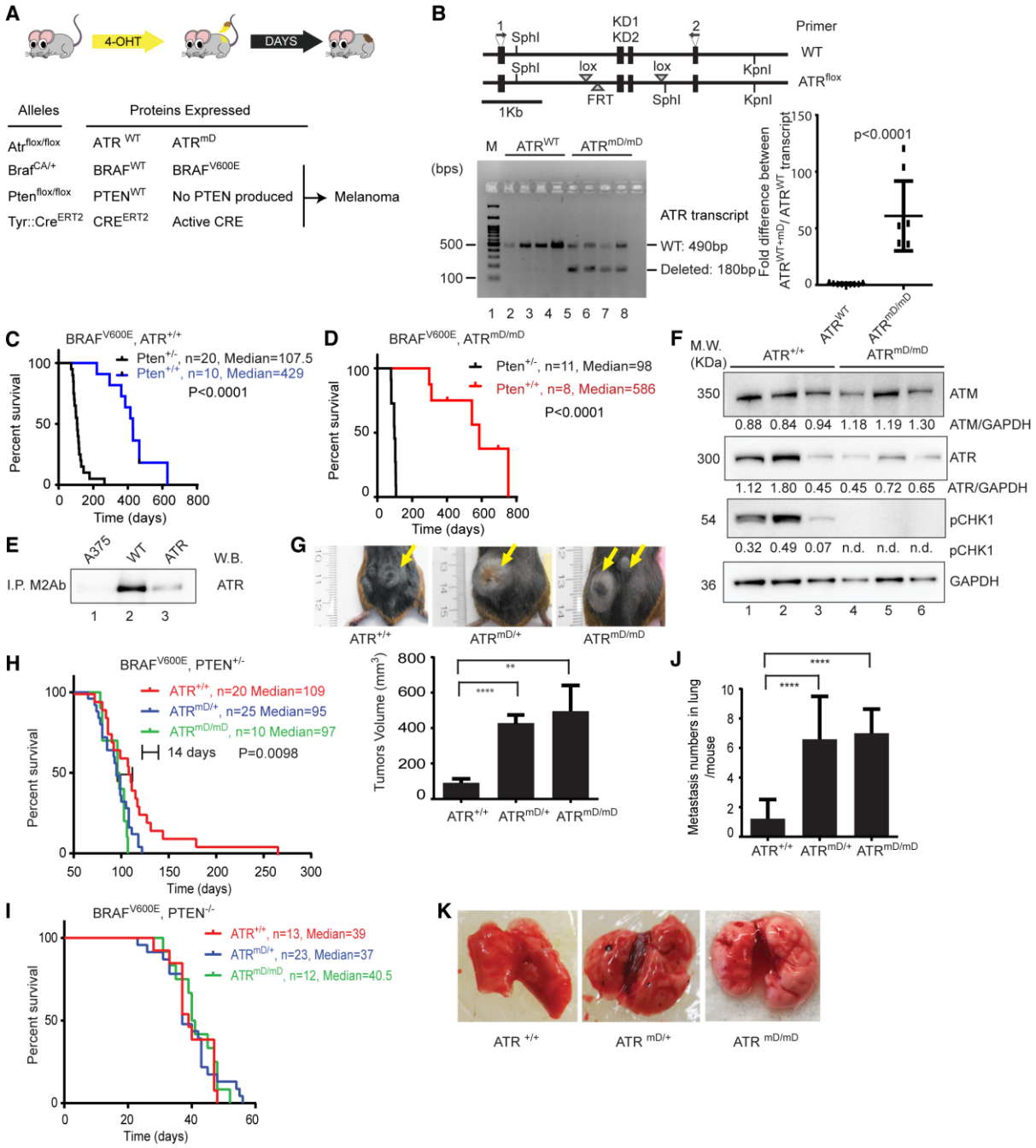

Figure 3.2. ATR haploinsufficiency promotes the invasion and metastasis of BRAF mt melanomas in mice. (A) Mice carrying various conditional alleles of *Braf* (*Braf*^{CA}), *Pten* (*Pten*$^{lox4-5}$) and/or *ATR* (*ATR*^{flox}) were crossed to *Tyr::CreER mice* with melanocyte-specific expression Cre recombinase (CreER^{T2}). Activation of CreER by 4-OHT leads to melanocyte-specific conversion of *Braf*^{CA} to *Braf*^{V600E}, *Pten* to null alleles

and *ATR*^{flox} to *ATR*^{mD}. (B) Schematic of the *ATR*^{flox} region (Brown and Baltimore, 2003). The kinase domain-encoding exons (KD1 and KD2) and primer locations were indicated (top panel). RT-PCR results are shown in the bottom panel. *ATR*$^{mD/mD}$ tumors expressed the floxed transcript. (C) Pten haploinsufficiency accelerates the demise of mice harboring BRAF^{V600E} ATR$^{+/+}$ tumors. Kaplan Meier survival curves for mice carrying BRAF^{V600E} ATR$^{+/+}$ with PTEN$^{+/+}$ or PTEN$^{+/-}$ with median life span of 429 days (n=10) and 107.5 days (n=20), respectively. (D) Pten haploinsufficiency does not accelerate the demise of mice harboring BRAF^{V600E} ATR$^{mD/mD}$ tumors. Kaplan Meier survival curves for mice carrying BRAF^{V600E} ATR$^{mD/mD}$ with PTEN$^{+/+}$ or PTEN$^{+/-}$ tumors with median life span of 586 days (n=8) and 98 days (n=20), respectively. (E) Expression of human ATR that mimics mouse ATR^{mD} (ATR^{hD}) in A375. A375 cells expressing either FLAG tagged wild-type or ATR^{hD} constructs were lysed and immunoprecipitated with a FLAG antibody (M2) followed by western blotting with an ATR Ab. (F) ATR$^{mD/mD}$ melanoma cells have defects in ATR signaling. Lysates from mouse tumors were subjected to western blotting with the indicated specific antibodies. Relative densitometry values are shown below each blot. n.d. means non-detectable. (G) ATR haploinsufficiency promotes the growth of BRAF^{V600E} PTEN$^{+/-}$ tumors. The mean tumor volume of ATR$^{+/+}$, ATR$^{mD/+}$, and ATR$^{mD/mD}$ tumors was 91.23$\pm$22.68 mm^3 (n=28), 428.6$\pm$57.95 mm^3 (n=28) ($p<0.0001$), and 495.4$\pm$145.8 mm^3 (n=27) ($p=0.0074$), respectively. Error bars represent SEM. Representative photographs are shown (top panel). (H) ATR haploinsufficiency accelerates the demise of mice harboring BRAF^{V600E} PTEN$^{+/-}$ tumors. Kaplan Meier survival curves for mice harboring BRAF^{V600E} PTEN$^{+/-}$ with ATR$^{+/+}$, ATR$^{mD/+}$, and ATR$^{mD/mD}$ tumors with median lifespan 109 days (n=20), 95

days (n=25), and 97 days (n=11), respectively. (I) ATR haploinsufficiency does not accelerate the demise of mice harboring $BRAF^{V600E}$ $PTEN^{-/-}$ tumors. Kaplan Meier survival curves for mice harboring $BRAF^{V600E}$ $PTEN^{-/-}$ with $ATR^{+/+}$, $ATR^{mD/+}$, and $ATR^{mD/mD}$ tumors with median lifespan 39 days (n=13), 37 days (n=23), and 40.5 days (n=12), respectively. (J) ATR haploinsufficiency promotes the metastasis $BRAF^{V600E}$ $PTEN^{-/-}$ tumors. Mice bearing $ATR^{+/+}$, $ATR^{mD/+}$, and $ATR^{mD/mD}$ tumors averaged 1.22 ± 0.43 (n=9), 6.60 ± 0.75 (n=15) and 7.00 ± 0.62 (n=7) metastases per mouse lung ($p<0.0001$), respectively. Error bars represent SEM. (K) Lung images from representative mice bearing $ATR^{+/+}$, $ATR^{mD/+}$, and $ATR^{mD/mD}$ tumor lung metastases at the end-stage.

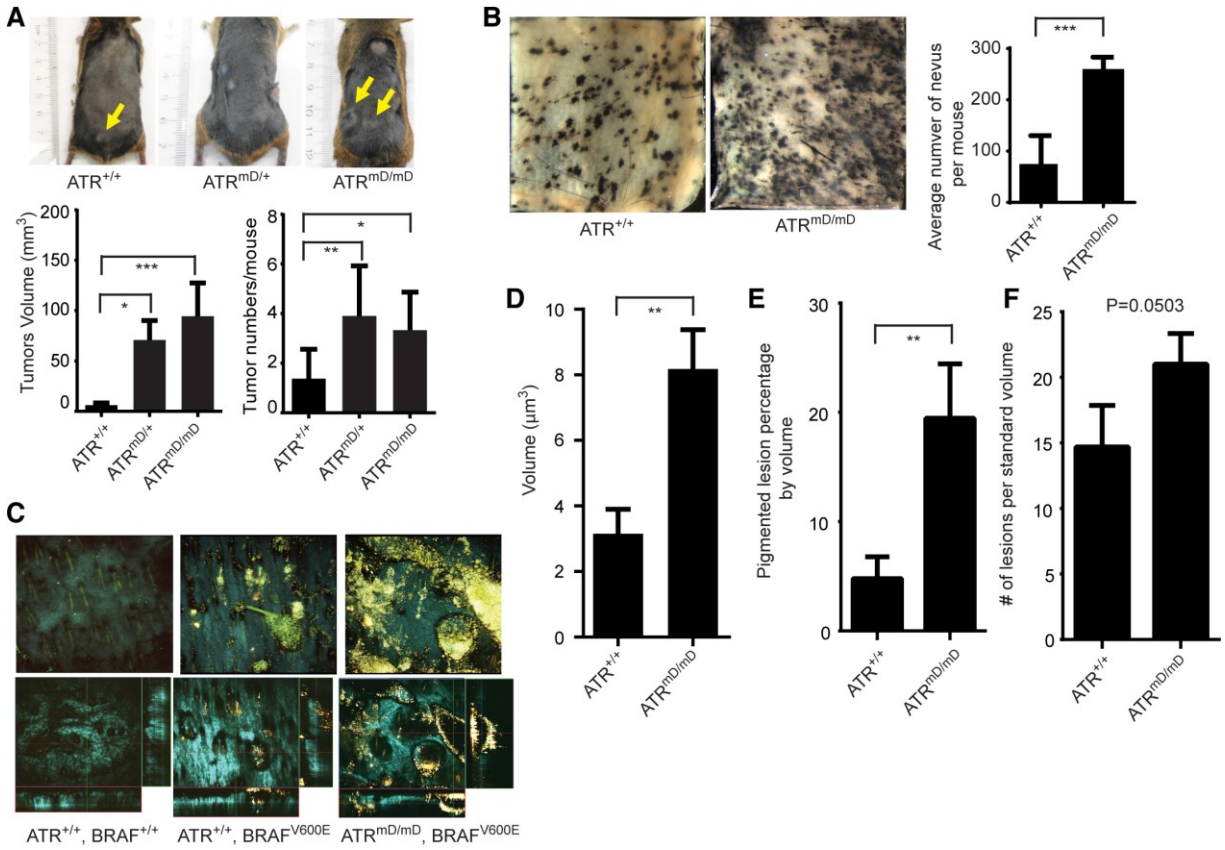

Figure 3.3. ATR mt promotes the growth of BRAF mt nevi and melanomas.

(A) ATR mt promotes the growth of developing melanoma tumors. Tumors were induced in *Braf*$^{CA/+}$ *Pten*$^{fl/+}$ *Atr*$^{fl/+}$ or *Braf*$^{CA/+}$ *Pten*$^{fl/+}$ *Atr*$^{fl/fl}$ mice and the size (bottom left panel) and number of tumors per mouse (bottom right panel) was determined after 75 days. Mice bearing ATR$^{+/+}$ tumors had an average of 1.38±0.42 (n=8) tumors per mouse with a mean volume of 6.06±2.31 mm^3 (n=13). Mice bearing ATR$^{mD/+}$ tumors had an average of 3.9 ±0.64 (n=10) tumors per mouse (p=0.0067) with a mean volume of volume of 70.69±19.42 mm^3 (n=19), (p<0.0001). ATR$^{mD/mD}$ mice had an average of 3.33±0.88 (n=4), (p=0.048) with a mean volume of 74.69±22.77 mm^3 (n=10), (p<0.0001). Error bars represent SEM. (B) ATR mutation promotes the growth of BRAF mt nevi. Nevi were induced in *Braf*$^{CA/+}$ *Atr*$^{+/+}$ and *Braf*$^{CA/+}$ *Atr*$^{fl/fl}$ mice and visualized 50 days after induction on the underside of the skin by standard photography.

Mice bearing $ATR^{mD/mD}$ and $ATR^{+/+}$ nevi had an average of 259.8 ±11.72 (n=4), and 74.75±27.69 (n=4) nevi per mouse, respectively. (p=0.0008). Error bars represent SEM. (C) ATR mt and ATR wt nevi visualized by label-free multiphoton microscopy of the mouse skin ex-vivo. MPM images from mice were obtained as described in methods, and a representative image from each genotype is shown. Top row (left to right): 3-D projections for normal skin, ATR wt and $ATR^{mD/mD}$. Bottom row: orthogonal projection from the stacks of images. Colored lines indicate positions being displayed as xy (blue), xz (red) and yz (green) planes. FOV is 636μm x 636μm Cyan: SHG of collagen; Green: fluorescence of keratin; Yellow and Red – fluorescence of melanin. (D) ATR mt nevi are larger than ATR wt nevi. Average volume of melanocytic nevi within the upper 50 μm of the skin was measured (μm^3) from 3-D skin reconstructions. (E) ATR mt nevi occupy a greater volume of the skin as compared to ATR wt nevi. Percentage of a volume occupied by pigmented lesions within the upper 50 μm of the skin compared to the total probed volume is reported and error bars represent S.D. (F) ATR mt promote the formation of BRAF mt nevi. Individual lesions were counted manually for all acquired stacks of images to the depth of 240 μm and then normalized to the volume of 10 stacks per each animal. A graph obtained from analyzing 5 mice in each group is shown.

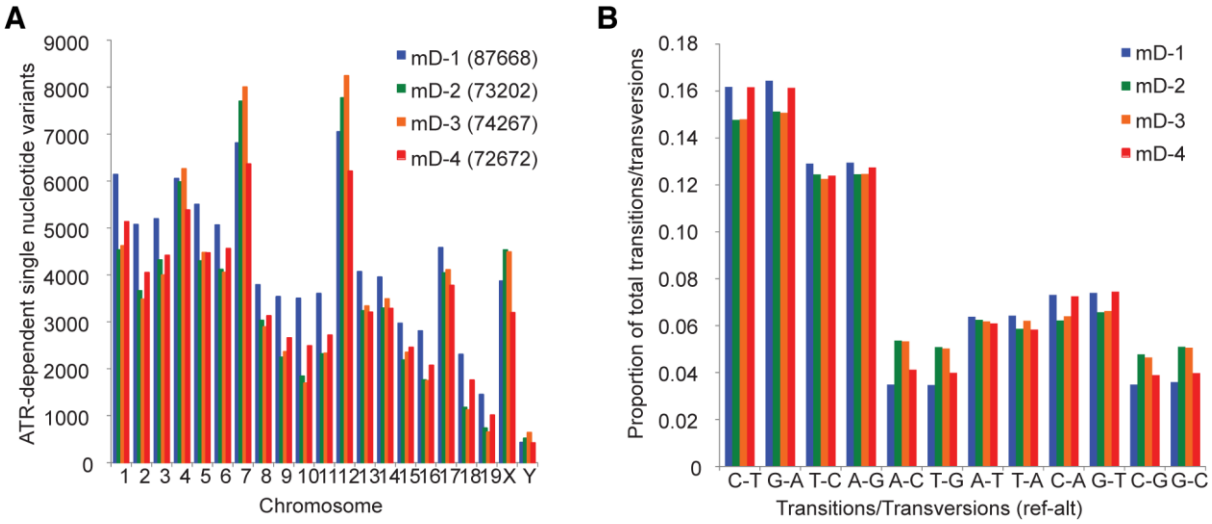

C

Mouse	tumor-specific variant	Exonic Variants	nonsynonymous variants	synonymous variants	Stop gain (nonsense)	Stop loss
mD1	87,668	412	252	154	6	0
mD2	73,202	312	176	142	2	1
mD3	74,267	417	223	187	7	0
mD4	72,672	308	167	134	6	1

Figure 3.4. ATR mt Leads to the Generation of a Genetically Heterogeneous Tumor. (A) ATR mt leads to the increased accumulation of single nucleotide variants in melanoma tumors. SNVs that were unique to $ATR^{mD/mD}$ tumors (not present in $ATR^{+/+}$ tumors) were identified as described in methods. The number of ATR-dependent SNVs (as defined in the methods section) at each chromosomal location is reported in the graph. mD denotes ATR mt tumor and WT denotes ATR WT tumors. (B) ATR mt does not lead to the increased accumulation of specific transitions or transversions. The number of specific transitions and transversions that were unique to $ATR^{mD/mD}$ tumors was determined, and the relative proportion of each transition/transversion (proportion of total) is indicated. (C) Mutation frequencies in ATR mt Tumors. The frequencies of single nucleotide variants in ATR mt tumors were determined as described in methods.

The number of coding and non-coding variants as well as the number of synonymous and non-synonymous variants was reported for each ATR mt tumor (mD1-mD4).

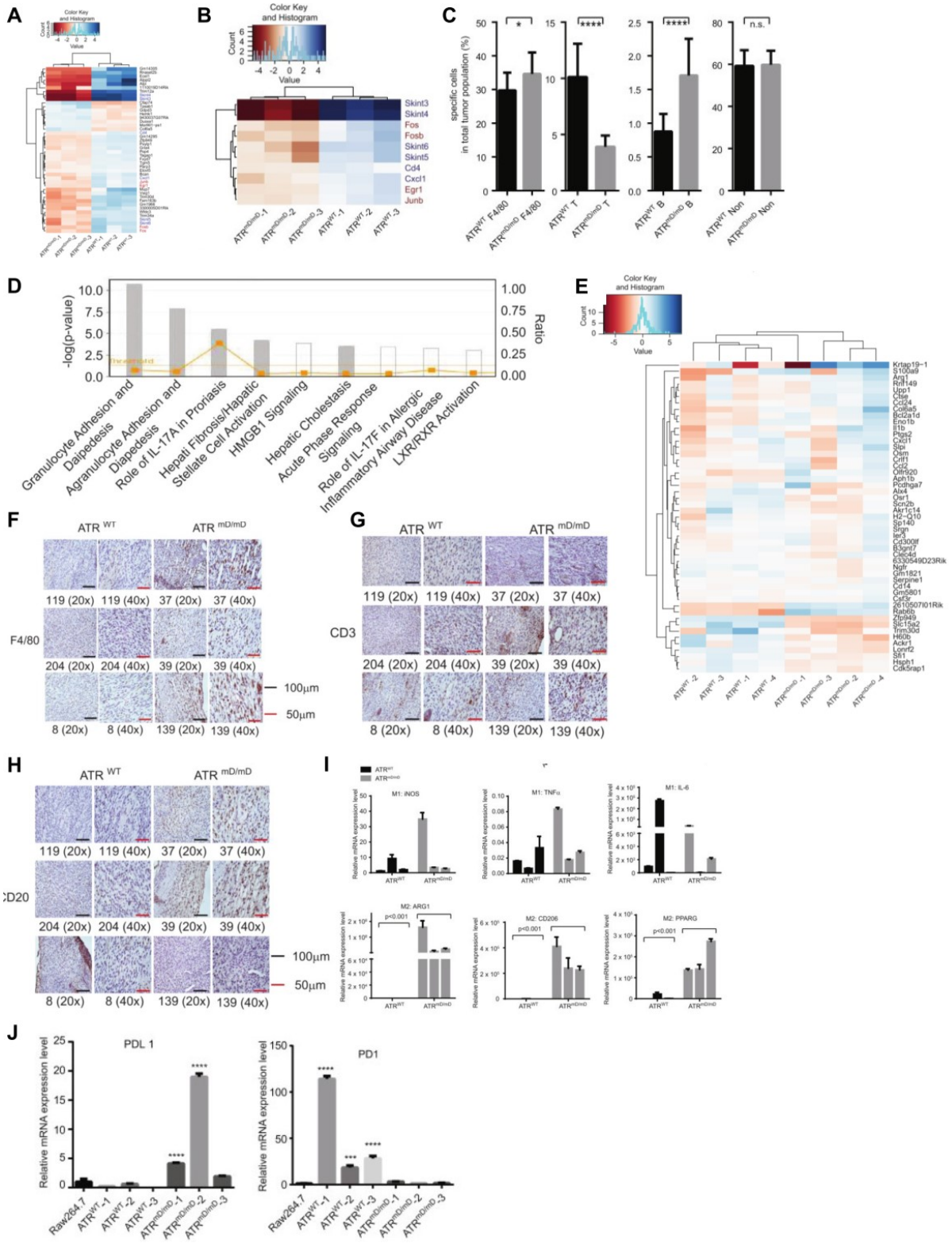

Figure 3.5. ATR mt tumors contain a greater number of infiltrating macrophages.

(A) RNA-sequencing and gene expression analysis from ATR wt and mt nevi was

performed as described. A heatmap of representative differentially expressed genes is presented. (B) ATR mt nevi modulate the immune response. RNA-sequencing and gene expression analysis was performed on ATR WT and ATR mt mouse nevi as described. Differentially expressed genes that regulate proliferation and the immune response identified in the dataset are shown. Hierarchical clustering of RNA-seq normalized read counts obtained from EdgeR ranging from less frequently expressed (dark blue) to highly (dark red) genes is shown. (C) ATR mt tumors recruit macrophages to create a pro-inflammatory tumor microenvironment. ATR wt and mt tumor cells were labeled by CD3 (T cell marker), CD19 (B cell marker) and F4/80 (macrophage marker) antibodies and sorted by flow cytometry as described in the supplement. * $p<0.05$, ***$p<0.001$. 5 tumors were analyzed per group. Error bars represent SEM. (D, E) ATR mt cells activate the expression of pathways involved in immune response and inflammation. RNA sequencing and gene expression analysis was performed as described. Differentially expressed gene classes identified using IPA are depicted (D), and a heatmap of representative differentially expressed genes is presented (E). (F), (G) and (H) ATR mt tumors recruit macrophages to create a proinflammatory tumor microenvironment. Mouse tumors were collected after experimental mice were euthanized and fixed in formalin. Paraffin-embedded tumor samples were stained with F4/80 Ab (F), CD3 Ab (G), and CD20 Ab (H). Three representative tumors from each genotype are shown. (I) ATR mt tumors are enriched in M2 like macrophages. RNA samples from ATR wt or mt tumors were subjected to RT-qPCR. The top panel represents of M1 macrophage expression of iNOS, TNFα and IL-6. The bottom panel represents of M2 macrophage expression of ARG1, CD206 and

PPARG. (J) ATR mt tumors express more PD-L1. RNA samples from ATR wt or ATR mt tumors were subjected to RT-qPCR using primers specific for PD-1 or PD-L1. ***p<0.001, ****p<0.0001, error bars represent SEM.

CHAPTER 4: Summary and Conclusions

The skin is a tissue that provides protection to internal organs from environmental factors, but the skin itself is susceptible to cancers such as basal cell carcinoma, squamous cell carcinoma, and melanoma. Basal cell carcinoma originates from basal cells in the skin and is usually caused by long-term sun exposure. This type skin cancer proliferates very slowly and usually never metastasizes which makes it possible to treat. Squamous cell carcinomas originate from squamous cells in the epidermis of the skin. This type of skin cancer also develops due to high exposure to UVR but chronic infections and inflammation of the skin also contribute to squamous cell carcinoma. Melanoma is the deadliest type of skin cancer because of its ability to metastasize throughout the body making it a challenge to treat. Unfortunately, the incidence rate of melanoma is on the rise especially among young people (7). Tanning has become a popular trend in the American culture and other European countries that is leading younger generations to lay out in the sun or visit tanning salons and exposing them to massive amounts of UVR. These fashion trends and other changes in the environment are causing melanoma incidence rates to increase dramatically while melanoma treatments remain unsuccessful.

Over the past 50 years, melanoma research has progressed significantly forward, albeit little progress has been made in terms of improving patient survival. Many new mutations were discovered because of the advances in NGS, with the third most prominent mutation being discovered in the last five years (154, 209-212). These new findings have led to the discovery of additional treatments from kinase inhibitors to immunotherapy extending the survival length minutely. Stage IV melanomas are the

most challenging melanomas to treat because they often spread throughout the body and metastasize. Metastasis to internal organs can be removed depending on their level of invasiveness but others might require treatment. Immunotherapy is the newest type of treatment recommend for late stage melanomas, which increases patient survival (66, 67). Alternative treatments include kinase inhibitors, chemotherapy, and radiation but tumors acquire resistance to some of these treatments making it a challenge to treat late stage melanoma. Unlike stage IV melanomas, stage III melanoma, which is characterized by cancer cells reaching a nearby lymph node, can be excised and treated with current therapies to prevent it from returning. Although patients with stage III melanoma have a higher survival rate, stage III melanomas are managing to escape treatment therapies and return more aggressively. Moreover, there are many more stage III than stage IV melanoma patients, and many patients could benefit from treatments targeting stage III disease. Additional work needs to continue in order to fully understand the mechanisms that regulate melanoma development.

While genomics studies have successfully identified both molecular drivers (154) and driver directed therapeutics (213) for stage IV melanoma, the pathways that cooperate with these oncogenes to promote tumorigenesis remains incomplete. The BRAF oncogene is the most common mutation in human melanoma (39), and therapies that inhibit BRAF signaling are effective at inducing tumor regression (122). Unfortunately, these tumors frequently recur and become unresponsive to treatment due to alterations in downstream BRAF signaling networks (71). BRAF mutations are also seen in common human nevi (129) that spontaneously arrest (119), suggesting that

events other than the BRAF mutation are required for tumor progression. In an effort to define signaling networks that drive the conversion of BRAF mutant cells into melanoma tumors, we focused on understanding the role of RhoJ, a Cdc42 family GTPase, in BRAF mutant cells.

Non-mutated gene products often times signal via established oncogenic pathways and contribute to therapeutic resistance. We utilized a synthetic lethal genomic screen in an effort to identify non-mutated gene products that would have a synergistic effect with chemotherapeutic agents and produce toxicity toward cancer cells (214, 215). A synergistic effect can exists between a gene product and a drug if depletion of that gene sensitizes cells to sub lethal doses of a drug (214, 215). With this approach we identified RhoJ as a regulator of melanoma chemoresistance that signals via PAK in response to cisplatin, an agent that produces DNA damage (113). Upon DNA damage the ATR (ataxia telangiectasia) pathway is activated (164, 165) in normal cells but we demonstrated that RhoJ suppressed ATR activity and led to a decrease in DNA damage-induced apoptosis resulting in an increase in survival *in vitro* (113). In addition to modulating DNA damage stress, we also demonstrated that RhoJ modulates actin cytoskeletal dynamics in melanoma cells (114). In this dissertation, we utilized an autochthonous mouse model of melanoma (49) to study the role RhoJ *in vivo*. Using this model, we determined that RhoJ accelerates the progression of BRAF mutant melanomas (Figure 2.1.C) and nevi growth (Figure 2.3.C) via the p21-activated kinase (PAK) pathway. PAK inhibitors selectively killed BRAF mutant melanoma cells that expressed RhoJ through the apoptotic BAD signaling pathway (Figure 2.5.C) and RhoJ knockout mice exhibited delayed formation of nevi (Figure 2.3.E). Interestingly, RNA-

seq analysis revealed that oxidative phosphorylation might be upregulated in melanoma tumors, which could contribute to survival and therapeutic resistance mechanisms, an area that will further be explored. Taken together, we demonstrated that supports the initiation and development of melanoma tumors *in vivo*.

To further understand how RhoJ regulates melanoma progression, we sought to determine how RhoJ signaling was linked to the BRAF network. Previously published work indicated that RhoJ activates PAK1 in melanoma cells (113, 114). PAK1, in turn, is known to phosphorylate MEK at serine-298 (211). Consistent with a role for RhoJ in activating Pak1, RhoJ knockdown or Pak inhibition, with FRAX597 an ATP-competitive inhibitor of group I Paks (132), both suppressed the accumulation of MEK phosphorylation at serine-298 *in vitro* (Figure 4.1.A). Chronic inhibition of RhoJ leads to a decrease in total MEK levels, which would further suppress accumulation of MEK^{Ser298} phosphorylation. Similarly, RhoJ knockout melanoma tumors had decreased accumulation of phoshpho-MEK^{Ser298} (Figure 4.1.B), consistent with a role for RhoJ in activating Pak1 *in vivo*. These observations coincide with previous reports demonstrating that the $RAC1^{P29S}$ mutation binds to Pak1 with an increased affinity (209) and that Pak1 amplification occurs in melanoma (216). Taken together, these results suggest that RhoJ or other Rac/Cdc42 family members can activate Pak1 signaling in melanoma tumors to provide a mechanism to avoid apoptosis.

We previously demonstrated that RhoJ suppressed ATR activity *in vitro* (113) and regulates the DNA damage response, but ATR role's *in vivo* had not been studied in melanoma. Loss-of-function mutations in ATR are found in seven percent of human melanomas (217) identifying a population of melanomas that could lead to a better

understanding of the disease. Using the previous described autochthonous mouse model of melanoma (49), ATR mutant nevi and melanomas grow larger (Figure 3.3.A) suggesting that mutant ATR maintains tumor stability. We demonstrated that ATR is able to maintain tumor stability by recruiting pro-tumorigenic macrophages that block T-cell recruitment, which accelerates tumor growth by regulating the tumor microenvironment (217). These studies revealed that ATR not only modulates the DNA damage response in melanoma tumors, but also induces immunosuppression near tumors to provide a mechanism for survival and maybe resistance. Intriguingly, our results also indicate that macrophages drive the process of tumor initiation, which will be the subject of future studies.

While RhoJ is highly expressed in subsets of melanoma cell lines (Figure 2.4.A) and mouse melanoma tumors (Figure 4.1.B), it is not clear how RhoJ expression affects survival in human cases. Using two clinically-well annotated melanoma tissue microarrays (139, 218), stage III melanoma tumors expressed significantly more RhoJ as compared to stage IV tumors even after correcting for stage of disease, age at time of surgery, and gender via multiple linear regression models. However, there was no correlation or RhoJ expression with gender and age. Additional correlative studies revealed that RhoJ positive stage IV melanomas had a slightly better prognosis with respect to disease-free and overall survival as compared to tumors that expressed less RhoJ (Figure 4.2.A, 4.2.B). There were no significant differences in the prognosis of RhoJ positive and negative stage III melanoma (Figure 4.2.C, 4.2.D). In breast cancer, estrogen receptor positivity portends a better prognosis (219) yet it is also an ideal therapeutic target (220) as it is expressed in a high proportion of breast tumors.

Similarly, RhoJ expression correlates with a slightly improved prognosis in stage IV disease suggesting that it may be a suitable therapeutic target in melanoma.

Oncogenic mutations alter conventional cellular signaling paradigms resulting in a selective dependence on non-mutated gene products to establish the tumorigenic platform (124). We sought to identify novel, tractable signaling networks that promote the growth of BRAF mutant melanocytes. We identify a novel signaling connection between RhoJ and MAPK that may influence the progression in distinct subsets of melanoma tumors. Intriguingly, while RhoJ is not mutated in melanoma tumors, the related GTPase RAC1 is mutated in a proportion of melanomas (209) and Pak is amplified in melanoma tumors (151), consistent with a general role for a Cdc42/Rac-Pak signaling axis in melanomagenesis.

Future Studies

Although oncogenic drivers like BRAF and PTEN promote melanoma due to their oncogenic potential, they also regulate cellular energy metabolism, which accompanies metastatic melanoma and resistance. The melanoma mouse model provided evidence that RhoJ further alters melanoma's metabolic signature (Figure 2.2.I). The majority of cellular energy is obtained mainly through glucose, which gets processed and converted to pyruvate through glycolysis. Pyruvate enters the mitochondria, when oxygen is present, and is converted to acetyl-CoA by pyruvate dehydrogenase, which is further broken down via the tricarboxylic acid cycle and oxidative phosphorylation to produce adenosine triphosphate (ATP). In the absence of oxygen, cells become dependent on glycolysis but pyruvate is converted into lactate as oppose to acetyl-CoA in order to generate the cofactor NAD^+ that is required for maintaining glycolysis during anaerobic

conditions. In melanoma, the most notable change in metabolism is a switch from mitochondrial oxidative phosphorylation to glycolysis *in vitro* (221, 222). Current melanoma drug treatments are encouraging, however the effectiveness of these new treatments might depend on mitochondrial function and metabolic drivers. Further research still needs to be done on melanoma to fully understand the metabolic network and how its plasticity allows cells to rewire to maintain tumor immunity. Currently melanoma cells utilize oncogenic compensatory mechanisms as a survival strategy might also be observed when utilizing metabolism-targeted therapy. Previous studies demonstrated that melanomas are able to utilize glucose and glutamine as a method to compensate for the inhibition of mitochondrial oxidation (223). This opens an area to study metabolic modifiers and their effects when used with current melanoma treatments.

In vivo studies show that tumors become more reliant on oxidative phosphorylation (224, 225). Studies have demonstrated that $BRAF^{V600E}$ inhibitors downregulate glycolytic enzymes and glucose transporters (221, 226). The constitutively active BRAF partially increases glycolytic activity via the transcription factor MYC (v-Myc avian myelocytomatosis viral oncogene homolog) (226), which is known to regulate lactate dehydrogenase A, glucose transporter 1, and hexokinase 2 (227). However, MYC also plays a role in mitochondrial metabolism by regulating mitochondrial biogenesis and production of acetyl-CoA. This process is important because it allows for the production of fatty acids and proliferation (228). The overarching goal of studying metabolism in melanoma is to determine whether metabolic rewiring due to RhoJ contributes not only to sustain tumor growth but to also

play a role in drug resistance. Our have identified cells that express high levels of RhoJ (Figure 2.4.A), and also characterized RhoJ knockout tumors. We can measure metabolites in these cells, and perform nutrient deprivation/add back experiments on human melanoma cells, cells from the RhoJ knockout or RhoJ wild type tumors, or mouse melanoma tumors. This leaves an open area to study metabolism as an alternative to or in combination with immune therapies.

Melanomas interact with their microenvironment to take advantage of interactions that promote tumor initiation and resistance. Recent studies have demonstrated that melanoma cells interact with immune cells by expressing PD-L1 and CTLA-4, which are both involved in immune checkpoint systems. Current therapies have aimed at developing antibodies targeting the ligands and receptors (61-63) of immune checkpoints. We demonstrated that ATR recruits M2 macrophages in an autochthonous melanoma mouse model promoted tumor-infiltrating cells providing evidence that melanomas use multiple mechanisms to promote survival (217). M1 macrophages can be described as classically activated, which leads to an inflammatory response, and alternatively activated which are considered M2 macrophages that exhibit an anti-inflammatory response. In some cancers M1 and M2 have been used as biomarkers for treatment and diagnosis (229). Using the autochthonous melanoma mouse model, the immune response can be studied in more depth to develop better immunotherapies.

An underlying question that arose from our studies was whether T-regulatory cells, cells that modulate the immune system, are regulating M1 and M2 macrophages and thus leading to more tumors in ATR mutant mice. We can approach this question

by utilizing single cell sequencing technology to determine whether T-regulator cells are present in ATR mutant cell. We also need to determine the signals that T-regulatory cells are releasing to either induce M2 macrophages and/or suppress M1 macrophages, which we could also obtain from single cell data. These results would be validated with either immunohistochemistry or single molecule fluorescence *in situ* hybridization. Understanding how T-regulatory cells modulate the immune microenvironment will provide a more clear understanding of tumor immunity. Unfortunately, previous studies demonstrated that suppression of T-regulatory cells leads to autoimmunity (230). Interestingly, the mechanism of action for CTLA4 immunotherapy is not completely understood, but CTLA4 is constitutively expressed in regulatory T-cells, unlike conventional effector T-cells, which suggest that this therapy could enhance anti-tumor immune responses. Selective depletion of T-regulatory cells is dependent on macrophages expressing the Fcγ receptor within the tumor microenvironment in melanoma (231), which might explain the role of M2 macrophages in our model. Our autochthonous mouse model shows in increase in PD-L1 (217) but it is unclear as to whether PD1 antibody treatment also possess a similar T-regulatory cell phenotype on tumors as CTLA4 making our model an excellent tool study PD1 immunotherapy. The long-term goal is to understand how the tumor microenvironment is rewiring itself to gain drug resistance. By understanding how the tumor microenvironment is regulated by other cells then we can have a better insight to drug resistance. Combining this direction with our metabolic hypothesis, we would further investigate how the tumor microenvironment might also contribute to metabolic rewiring and eventually lead to drug resistance.

In summary, we describe a role for RhoJ and ATR in the context of BRAF mutant and loss of PTEN autochthonous melanoma mouse model. Both RhoJ and ATR promote tumor progression via different mechanisms. RhoJ regulates tumor initiation via BAD signaling while ATR modulates the tumor microenvironment to recruit macrophages, which are important for tumor growth and progression. We hypothesize that these mechanisms could also lead to resistance mechanisms in melanomas. Previous studies reported RhoJ to be expressed in various tissues such as the heart, lung, and liver (102), but for the first time we are able perform single cell RNA-sequencing to identify different cell types within the skin in order to establish RhoJ expression at the single cell level (Figure 4.3.A). We were able to identify specific cell populations by using specific cell markers for melanocytes, bulge cells, endothelial cells, and upper hair follicle cells (Figure 4.3.B). Although RhoJ is expressed across all skin cells (Figure 4.3.C), it is expressed higher in specific populations such as melanocytes, hair bulge cells, hair follicle cells and endothelial cells (Figure 4.3.D). These studies are important because functional genomics studies lead to the identification of novel pathways that regulate tumor development and tumor immune microenvironment.

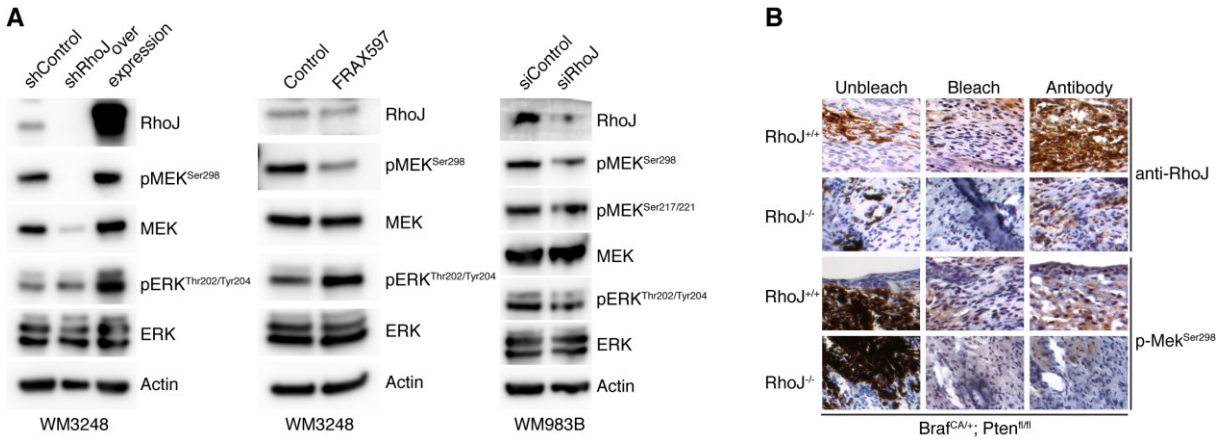

Figure 4.1. RhoJ cross talks with MAPK signaling pathway via MEK. (A) Knockdown of RhoJ with shRNA, siRNA, or inhibition of Pak with FRAX597 blocks activation of Pak1 targets in melanoma cells. Lysates were prepared by knocking down RhoJ with shRNA (ThermoScientific), siRNA, and immunoblotted with the indicated Abs. Samples were treated with 1μM of FRAX597 for 24 hrs before they were collected and analyzed with phospho-MEK^{Ser298}, a Pak1 specific phosphorylation site. (B) RhoJ signals to BRAF via MEK *in vivo*. Formalin-fixed paraffin embedded mouse melanoma skin was bleached with 3% hydrogen peroxide (overnight) to remove melanin and analyzed for expression of RhoJ. The phosphorylation of Mek^{Ser298} was measured via immunohistochemistry.

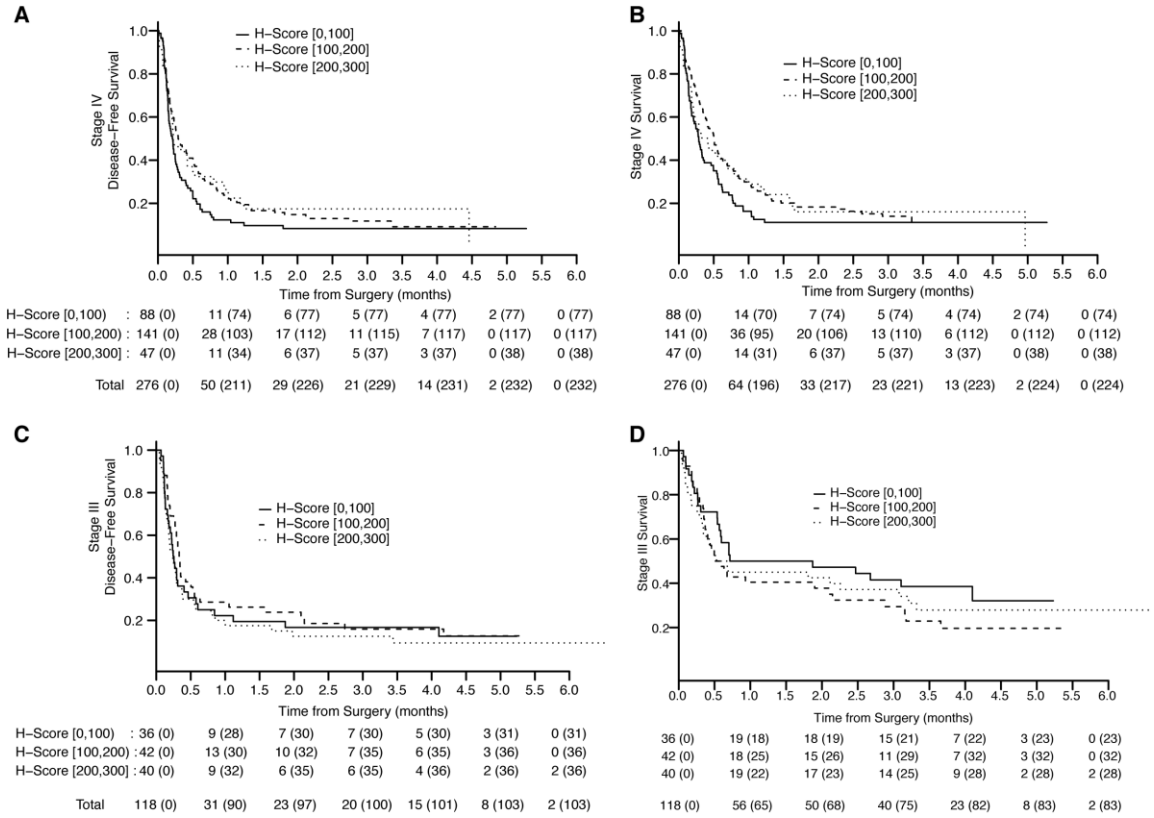

Figure 4.2. RhoJ has a better prognosis in stage IV melanomas. Kaplan-Meier estimates of (A) disease-free survival and (B) overall survival by Rho-J staining H-score among Stage IV patients. Patients were considered at risk from the time of surgery to the first of event occurrence (death or death/disease recurrence), loss-to-follow up, or end of study follow up. Kaplan-Meier estimates of (C) disease-free survival and (D) overall survival by Rho-J staining H-score among Stage III patients. Patients were considered at risk from the time of surgery to the first of event occurrence (death or death/disease recurrence), loss-to-follow up, or end of study follow-up.

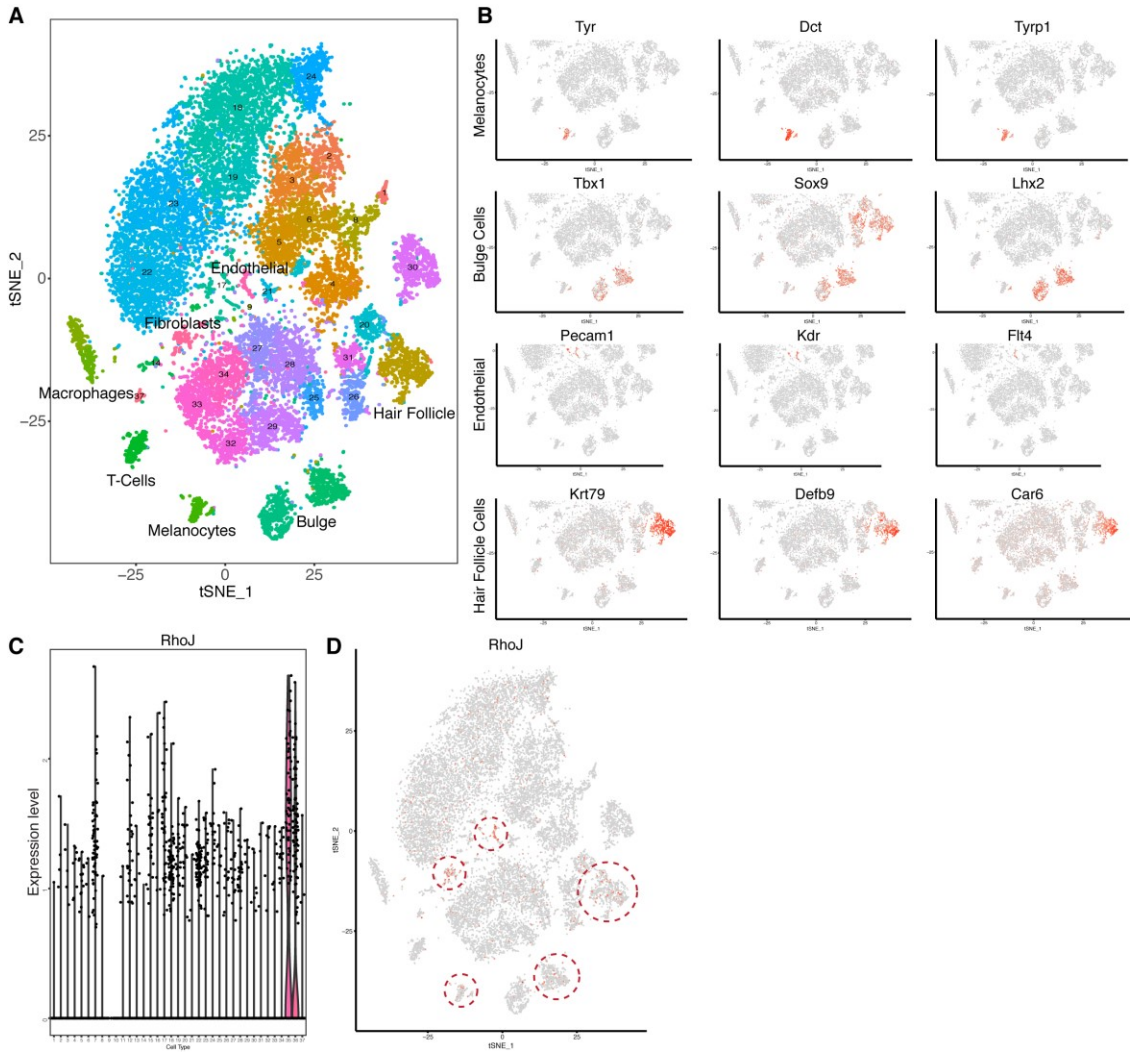

Figure 4.3. RhoJ is expressed in various cell types within the skin. (A) Single cell RNA sequencing from mouse skin (n=20,000) visualized with t-distributed stochastic neighbor embedding (t-SNE). (B) Expression of specific cell markers displayed on the t-SNE map identifies cell type. Orange color depicts expression of the gene noted. (C) RhoJ expression among all cell clusters. RhoJ is highly expressed in clusters 35 (endothelial cells) and 36 (fibroblasts). (D) RhoJ expression visualized onto the t-SNE. RhoJ is expressed in moderate number of cell in the melanocyte, bulge, hair follicle, fibroblasts, and endothelial clusters (outlined in red).

REFERENCES

1. Smalls LK, Randall Wickett R, and Visscher MO. Effect of dermal thickness, tissue composition, and body site on skin biomechanical properties. *Skin Res Technol.* 2006;12(1):43-9.
2. Oshima H, Rochat A, Kedzia C, Kobayashi K, and Barrandon Y. Morphogenesis and renewal of hair follicles from adult multipotent stem cells. *Cell.* 2001;104(2):233-45.
3. Price ER, Horstmann MA, Wells AG, Weilbaecher KN, Takemoto CM, Landis MW, et al. alpha-Melanocyte-stimulating hormone signaling regulates expression of microphthalmia, a gene deficient in Waardenburg syndrome. *J Biol Chem.* 1998;273(49):33042-7.
4. Levy C, Khaled M, and Fisher DE. MITF: master regulator of melanocyte development and melanoma oncogene. *Trends Mol Med.* 2006;12(9):406-14.
5. Armstrong BK, and Kricker A. The epidemiology of UV induced skin cancer. *J Photochem Photobiol B.* 2001;63(1-3):8-18.
6. Urteaga O, and Pack GT. On the antiquity of melanoma. *Cancer.* 1966;19(5):607-10.
7. . Bethesda, MD: National Cancer Institute.; 2014.
8. Gilchrest BA, Eller MS, Geller AC, and Yaar M. The pathogenesis of melanoma induced by ultraviolet radiation. *N Engl J Med.* 1999;340(17):1341-8.
9. You YH, Lee DH, Yoon JH, Nakajima S, Yasui A, and Pfeifer GP. Cyclobutane pyrimidine dimers are responsible for the vast majority of mutations induced by UVB irradiation in mammalian cells. *J Biol Chem.* 2001;276(48):44688-94.

10. Greinert R, Volkmer B, Henning S, Breitbart EW, Greulich KO, Cardoso MC, et al. UVA-induced DNA double-strand breaks result from the repair of clustered oxidative DNA damages. *Nucleic Acids Res.* 2012;40(20):10263-73.
11. Chudnovsky Y, Khavari PA, and Adams AE. Melanoma genetics and the development of rational therapeutics. *J Clin Invest.* 2005;115(4):813-24.
12. Clark WH, Jr., From L, Bernardino EA, and Mihm MC. The histogenesis and biologic behavior of primary human malignant melanomas of the skin. *Cancer Res.* 1969;29(3):705-27.
13. Breslow A. Prognostic factors in the treatment of cutaneous melanoma. *J Cutan Pathol.* 1979;6(3):208-12.
14. Aoude LG, Wadt KA, Pritchard AL, and Hayward NK. Genetics of familial melanoma: 20 years after CDKN2A. *Pigment Cell Melanoma Res.* 2015;28(2):148-60.
15. Hussussian CJ, Struewing JP, Goldstein AM, Higgins PA, Ally DS, Sheahan MD, et al. Germline p16 mutations in familial melanoma. *Nat Genet.* 1994;8(1):15-21.
16. Kamb A, Shattuck-Eidens D, Eeles R, Liu Q, Gruis NA, Ding W, et al. Analysis of the p16 gene (CDKN2) as a candidate for the chromosome 9p melanoma susceptibility locus. *Nat Genet.* 1994;8(1):23-6.
17. Sherr CJ. The INK4a/ARF network in tumour suppression. *Nat Rev Mol Cell Biol.* 2001;2(10):731-7.
18. Puntervoll HE, Yang XR, Vetti HH, Bachmann IM, Avril MF, Benfodda M, et al. Melanoma prone families with CDK4 germline mutation: phenotypic profile and associations with MC1R variants. *J Med Genet.* 2013;50(4):264-70.

19. Harland M, Taylor CF, Chambers PA, Kukalizch K, Randerson-Moor JA, Gruis NA, et al. A mutation hotspot at the p14ARF splice site. *Oncogene.* 2005;24(28):4604-8.

20. Mistry SH, Taylor C, Randerson-Moor JA, Harland M, Turner F, Barrett JH, et al. Prevalence of 9p21 deletions in UK melanoma families. *Genes Chromosomes Cancer.* 2005;44(3):292-300.

21. Rizos H, Puig S, Badenas C, Malvehy J, Darmanian AP, Jimenez L, et al. A melanoma-associated germline mutation in exon 1beta inactivates p14ARF. *Oncogene.* 2001;20(39):5543-7.

22. Bertolotto C, Lesueur F, Giuliano S, Strub T, de Lichy M, Bille K, et al. A SUMOylation-defective MITF germline mutation predisposes to melanoma and renal carcinoma. *Nature.* 2011;480(7375):94-8.

23. Yokoyama S, Woods SL, Boyle GM, Aoude LG, MacGregor S, Zismann V, et al. A novel recurrent mutation in MITF predisposes to familial and sporadic melanoma. *Nature.* 2011;480(7375):99-103.

24. Carbone M, Yang H, Pass HI, Krausz T, Testa JR, and Gaudino G. BAP1 and cancer. *Nat Rev Cancer.* 2013;13(3):153-9.

25. Harbour JW, Onken MD, Roberson ED, Duan S, Cao L, Worley LA, et al. Frequent mutation of BAP1 in metastasizing uveal melanomas. *Science.* 2010;330(6009):1410-3.

26. Matatall KA, Agapova OA, Onken MD, Worley LA, Bowcock AM, and Harbour JW. BAP1 deficiency causes loss of melanocytic cell identity in uveal melanoma. *BMC Cancer.* 2013;13:371.

27. Ismail IH, Davidson R, Gagne JP, Xu ZZ, Poirier GG, and Hendzel MJ. Germline mutations in BAP1 impair its function in DNA double-strand break repair. *Cancer Res.* 2014;74(16):4282-94.

28. Horn S, Figl A, Rachakonda PS, Fischer C, Sucker A, Gast A, et al. TERT promoter mutations in familial and sporadic melanoma. *Science.* 2013;339(6122):959-61.

29. Huang FW, Hodis E, Xu MJ, Kryukov GV, Chin L, and Garraway LA. Highly recurrent TERT promoter mutations in human melanoma. *Science.* 2013;339(6122):957-9.

30. Xin H, Liu D, Wan M, Safari A, Kim H, Sun W, et al. TPP1 is a homologue of ciliate TEBP-beta and interacts with POT1 to recruit telomerase. *Nature.* 2007;445(7127):559-62.

31. Robles-Espinoza CD, Harland M, Ramsay AJ, Aoude LG, Quesada V, Ding Z, et al. POT1 loss-of-function variants predispose to familial melanoma. *Nat Genet.* 2014;46(5):478-81.

32. Aoude LG, Pritchard AL, Robles-Espinoza CD, Wadt K, Harland M, Choi J, et al. Nonsense mutations in the shelterin complex genes ACD and TERF2IP in familial melanoma. *J Natl Cancer Inst.* 2015;107(2).

33. Riverso M, Montagnani V, and Stecca B. KLF4 is regulated by RAS/RAF/MEK/ERK signaling through E2F1 and promotes melanoma cell growth. *Oncogene.* 2017.

34. Demunter A, Stas M, Degreef H, De Wolf-Peeters C, and van den Oord JJ. Analysis of N- and K-ras mutations in the distinctive tumor progression phases of melanoma. *J Invest Dermatol.* 2001;117(6):1483-9.

35. Albino AP, Nanus DM, Mentle IR, Cordon-Cardo C, McNutt NS, Bressler J, et al. Analysis of ras oncogenes in malignant melanoma and precursor lesions: correlation of point mutations with differentiation phenotype. *Oncogene.* 1989;4(11):1363-74.

36. Omholt K, Karsberg S, Platz A, Kanter L, Ringborg U, and Hansson J. Screening of N-ras codon 61 mutations in paired primary and metastatic cutaneous melanomas: mutations occur early and persist throughout tumor progression. *Clin Cancer Res.* 2002;8(11):3468-74.

37. Milagre C, Dhomen N, Geyer FC, Hayward R, Lambros M, Reis-Filho JS, et al. A mouse model of melanoma driven by oncogenic KRAS. *Cancer Res.* 2010;70(13):5549-57.

38. Imielinski M, Greulich H, Kaplan B, Araujo L, Amann J, Horn L, et al. Oncogenic and sorafenib-sensitive ARAF mutations in lung adenocarcinoma. *J Clin Invest.* 2014;124(4):1582-6.

39. Davies H, Bignell GR, Cox C, Stephens P, Edkins S, Clegg S, et al. Mutations of the BRAF gene in human cancer. *Nature.* 2002;417(6892):949-54.

40. Dhomen N, and Marais R. BRAF signaling and targeted therapies in melanoma. *Hematol Oncol Clin North Am.* 2009;23(3):529-45, ix.

41. Long GV, Menzies AM, Nagrial AM, Haydu LE, Hamilton AL, Mann GJ, et al. Prognostic and clinicopathologic associations of oncogenic BRAF in metastatic melanoma. *J Clin Oncol.* 2011;29(10):1239-46.

42. El-Osta H, Falchook G, Tsimberidou A, Hong D, Naing A, Kim K, et al. BRAF mutations in advanced cancers: clinical characteristics and outcomes. *PLoS One.* 2011;6(10):e25806.

43. Lovly CM, Dahlman KB, Fohn LE, Su Z, Dias-Santagata D, Hicks DJ, et al. Routine multiplex mutational profiling of melanomas enables enrollment in genotype-driven therapeutic trials. *PLoS One.* 2012;7(4):e35309.

44. Nikolaev SI, Rimoldi D, Iseli C, Valsesia A, Robyr D, Gehrig C, et al. Exome sequencing identifies recurrent somatic MAP2K1 and MAP2K2 mutations in melanoma. *Nat Genet.* 2011;44(2):133-9.

45. Goetz EM, Ghandi M, Treacy DJ, Wagle N, and Garraway LA. ERK mutations confer resistance to mitogen-activated protein kinase pathway inhibitors. *Cancer Res.* 2014;74(23):7079-89.

46. Isshiki K, Elder DE, Guerry D, and Linnenbach AJ. Chromosome 10 allelic loss in malignant melanoma. *Genes Chromosomes Cancer.* 1993;8(3):178-84.

47. Herbst RA, Weiss J, Ehnis A, Cavenee WK, and Arden KC. Loss of heterozygosity for 10q22-10qter in malignant melanoma progression. *Cancer Res.* 1994;54(12):3111-4.

48. Healy E, Rehman I, Angus B, and Rees JL. Loss of heterozygosity in sporadic primary cutaneous melanoma. *Genes Chromosomes Cancer.* 1995;12(2):152-6.

49. Dankort D, Curley DP, Cartlidge RA, Nelson B, Karnezis AN, Damsky WE, Jr., et al. Braf(V600E) cooperates with Pten loss to induce metastatic melanoma. *Nat Genet.* 2009;41(5):544-52.

50. Guldberg P, thor Straten P, Birck A, Ahrenkiel V, Kirkin AF, and Zeuthen J. Disruption of the MMAC1/PTEN gene by deletion or mutation is a frequent event in malignant melanoma. *Cancer Res.* 1997;57(17):3660-3.

51. Teng DH, Hu R, Lin H, Davis T, Iliev D, Frye C, et al. MMAC1/PTEN mutations in primary tumor specimens and tumor cell lines. *Cancer Res.* 1997;57(23):5221-5.

52. Tsao H, Zhang X, Benoit E, and Haluska FG. Identification of PTEN/MMAC1 alterations in uncultured melanomas and melanoma cell lines. *Oncogene.* 1998;16(26):3397-402.

53. Dhawan P, Singh AB, Ellis DL, and Richmond A. Constitutive activation of Akt/protein kinase B in melanoma leads to up-regulation of nuclear factor-kappaB and tumor progression. *Cancer Res.* 2002;62(24):7335-42.

54. Stahl JM, Sharma A, Cheung M, Zimmerman M, Cheng JQ, Bosenberg MW, et al. Deregulated Akt3 activity promotes development of malignant melanoma. *Cancer Res.* 2004;64(19):7002-10.

55. Govindarajan B, Sligh JE, Vincent BJ, Li M, Canter JA, Nickoloff BJ, et al. Overexpression of Akt converts radial growth melanoma to vertical growth melanoma. *J Clin Invest.* 2007;117(3):719-29.

56. Crosby T, Fish R, Coles B, and Mason MD. Systemic treatments for metastatic cutaneous melanoma. *Cochrane Database Syst Rev.* 2000(2):CD001215.

57. Eggermont AM, and Kirkwood JM. Re-evaluating the role of dacarbazine in metastatic melanoma: what have we learned in 30 years? *Eur J Cancer.* 2004;40(12):1825-36.

58. Dutcher JP, Creekmore S, Weiss GR, Margolin K, Markowitz AB, Roper M, et al. A phase II study of interleukin-2 and lymphokine-activated killer cells in patients with metastatic malignant melanoma. *J Clin Oncol.* 1989;7(4):477-85.

59. Kirkwood JM, Strawderman MH, Ernstoff MS, Smith TJ, Borden EC, and Blum RH. Interferon alfa-2b adjuvant therapy of high-risk resected cutaneous melanoma: the Eastern Cooperative Oncology Group Trial EST 1684. *J Clin Oncol.* 1996;14(1):7-17.

60. Pardoll DM. The blockade of immune checkpoints in cancer immunotherapy. *Nat Rev Cancer.* 2012;12(4):252-64.

61. Ribas A, Camacho LH, Lopez-Berestein G, Pavlov D, Bulanhagui CA, Millham R, et al. Antitumor activity in melanoma and anti-self responses in a phase I trial with the anti-cytotoxic T lymphocyte-associated antigen 4 monoclonal antibody CP-675,206. *J Clin Oncol.* 2005;23(35):8968-77.

62. Phan GQ, Yang JC, Sherry RM, Hwu P, Topalian SL, Schwartzentruber DJ, et al. Cancer regression and autoimmunity induced by cytotoxic T lymphocyte-associated antigen 4 blockade in patients with metastatic melanoma. *Proc Natl Acad Sci U S A.* 2003;100(14):8372-7.

63. Dong H, Strome SE, Salomao DR, Tamura H, Hirano F, Flies DB, et al. Tumor-associated B7-H1 promotes T-cell apoptosis: a potential mechanism of immune evasion. *Nat Med.* 2002;8(8):793-800.

64. Freeman GJ, Long AJ, Iwai Y, Bourque K, Chernova T, Nishimura H, et al. Engagement of the PD-1 immunoinhibitory receptor by a novel B7 family member leads to negative regulation of lymphocyte activation. *J Exp Med.* 2000;192(7):1027-34.

65. Nishimura H, Nose M, Hiai H, Minato N, and Honjo T. Development of lupus-like autoimmune diseases by disruption of the PD-1 gene encoding an ITIM motif-carrying immunoreceptor. *Immunity.* 1999;11(2):141-51.

66. Hamid O, Robert C, Daud A, Hodi FS, Hwu WJ, Kefford R, et al. Safety and tumor responses with lambrolizumab (anti-PD-1) in melanoma. *N Engl J Med.* 2013;369(2):134-44.

67. Topalian SL, Sznol M, McDermott DF, Kluger HM, Carvajal RD, Sharfman WH, et al. Survival, durable tumor remission, and long-term safety in patients with advanced melanoma receiving nivolumab. *J Clin Oncol.* 2014;32(10):1020-30.

68. Sosman JA, Kim KB, Schuchter L, Gonzalez R, Pavlick AC, Weber JS, et al. Survival in BRAF V600-mutant advanced melanoma treated with vemurafenib. *N Engl J Med.* 2012;366(8):707-14.

69. Flaherty KT, Puzanov I, Kim KB, Ribas A, McArthur GA, Sosman JA, et al. Inhibition of mutated, activated BRAF in metastatic melanoma. *N Engl J Med.* 2010;363(9):809-19.

70. Carlino MS, Todd JR, Gowrishankar K, Mijatov B, Pupo GM, Fung C, et al. Differential activity of MEK and ERK inhibitors in BRAF inhibitor resistant melanoma. *Mol Oncol.* 2014;8(3):544-54.

71. Das Thakur M, Salangsang F, Landman AS, Sellers WR, Pryer NK, Levesque MP, et al. Modelling vemurafenib resistance in melanoma reveals a strategy to forestall drug resistance. *Nature.* 2013;494(7436):251-5.

72. Emery CM, Vijayendran KG, Zipser MC, Sawyer AM, Niu L, Kim JJ, et al. MEK1 mutations confer resistance to MEK and B-RAF inhibition. *Proc Natl Acad Sci U S A.* 2009;106(48):20411-6.

73. Nazarian R, Shi H, Wang Q, Kong X, Koya RC, Lee H, et al. Melanomas acquire resistance to B-RAF(V600E) inhibition by RTK or N-RAS upregulation. *Nature.* 2010;468(7326):973-7.

74. Shi H, Moriceau G, Kong X, Lee MK, Lee H, Koya RC, et al. Melanoma whole-exome sequencing identifies (V600E)B-RAF amplification-mediated acquired B-RAF inhibitor resistance. *Nat Commun.* 2012;3:724.

75. Poulikakos PI, Persaud Y, Janakiraman M, Kong X, Ng C, Moriceau G, et al. RAF inhibitor resistance is mediated by dimerization of aberrantly spliced BRAF(V600E). *Nature.* 2011;480(7377):387-90.

76. Perna D, Karreth FA, Rust AG, Perez-Mancera PA, Rashid M, Iorio F, et al. BRAF inhibitor resistance mediated by the AKT pathway in an oncogenic BRAF mouse melanoma model. *Proc Natl Acad Sci U S A.* 2015;112(6):E536-45.

77. Hauschild A, Grob JJ, Demidov LV, Jouary T, Gutzmer R, Millward M, et al. Dabrafenib in BRAF-mutated metastatic melanoma: a multicentre, open-label, phase 3 randomised controlled trial. *Lancet.* 2012;380(9839):358-65.

78. Falchook GS, Lewis KD, Infante JR, Gordon MS, Vogelzang NJ, DeMarini DJ, et al. Activity of the oral MEK inhibitor trametinib in patients with advanced melanoma: a phase 1 dose-escalation trial. *Lancet Oncol.* 2012;13(8):782-9.

79. Kim KB, Kefford R, Pavlick AC, Infante JR, Ribas A, Sosman JA, et al. Phase II study of the MEK1/MEK2 inhibitor Trametinib in patients with metastatic BRAF-mutant cutaneous melanoma previously treated with or without a BRAF inhibitor. *J Clin Oncol.* 2013;31(4):482-9.

80. Flaherty KT, Infante JR, Daud A, Gonzalez R, Kefford RF, Sosman J, et al. Combined BRAF and MEK inhibition in melanoma with BRAF V600 mutations. *N Engl J Med.* 2012;367(18):1694-703.

81. Robert C, Karaszewska B, Schachter J, Rutkowski P, Mackiewicz A, Stroiakovski D, et al. Improved overall survival in melanoma with combined dabrafenib and trametinib. *N Engl J Med.* 2015;372(1):30-9.

82. Kuenen BC, Tabernero J, Baselga J, Cavalli F, Pfanner E, Conte PF, et al. Efficacy and toxicity of the angiogenesis inhibitor SU5416 as a single agent in patients with advanced renal cell carcinoma, melanoma, and soft tissue sarcoma. *Clin Cancer Res.* 2003;9(5):1648-55.

83. Ding X, Zhang W, Zhao T, Yan C, and Du H. Rab7 GTPase controls lipid metabolic signaling in myeloid-derived suppressor cells. *Oncotarget.* 2017.

84. Al-Zoairy R, Pedrini MT, Khan MI, Engl J, Tschoner A, Ebenbichler C, et al. Serotonin improves glucose metabolism by Serotonylation of the small GTPase Rab4 in L6 skeletal muscle cells. *Diabetol Metab Syndr.* 2017;9:1.

85. Paglialunga S, Simnett G, Robson H, Hoang M, Pillai R, Arkell AM, et al. The Rab-GTPase activating protein, TBC1D1, is critical for maintaining normal glucose homeostasis and beta-cell mass. *Appl Physiol Nutr Metab.* 2017:1-9.

86. Joglekar M, Elbazanti WO, Weitzman MD, Lehman HL, and van Golen KL. Caveolin-1 Mediates Inflammatory Breast Cancer Cell Invasion via the Akt1 Pathway and RhoC GTPase. *J Cell Biochem.* 2017;118(5):1273.

87. Wen SJ, Zhang W, Ni NN, Wu Q, Wang XP, Lin YK, et al. Expression of Rho GTPases family in melanoma cells and its influence on cytoskeleton and migration. *Oncotarget.* 2017.

88. Boulter E, Estrach S, Garcia-Mata R, and Feral CC. Off the beaten paths: alternative and crosstalk regulation of Rho GTPases. *FASEB J.* 2012;26(2):469-79.

89. Garcia-Mata R, Boulter E, and Burridge K. The 'invisible hand': regulation of RHO GTPases by RHOGDIs. *Nat Rev Mol Cell Biol.* 2011;12(8):493-504.

90. Vetter IR, and Wittinghofer A. The guanine nucleotide-binding switch in three dimensions. *Science.* 2001;294(5545):1299-304.

91. Hancock JF, Cadwallader K, Paterson H, and Marshall CJ. A CAAX or a CAAL motif and a second signal are sufficient for plasma membrane targeting of ras proteins. *EMBO J.* 1991;10(13):4033-9.

92. Hancock JF, Paterson H, and Marshall CJ. A polybasic domain or palmitoylation is required in addition to the CAAX motif to localize p21ras to the plasma membrane. *Cell.* 1990;63(1):133-9.

93. Roberts PJ, Mitin N, Keller PJ, Chenette EJ, Madigan JP, Currin RO, et al. Rho Family GTPase modification and dependence on CAAX motif-signaled posttranslational modification. *J Biol Chem.* 2008;283(37):25150-63.

94. del Pozo MA, Alderson NB, Kiosses WB, Chiang HH, Anderson RG, and Schwartz MA. Integrins regulate Rac targeting by internalization of membrane domains. *Science.* 2004;303(5659):839-42.

95. Del Pozo MA, Kiosses WB, Alderson NB, Meller N, Hahn KM, and Schwartz MA. Integrins regulate GTP-Rac localized effector interactions through dissociation of Rho-GDI. *Nat Cell Biol.* 2002;4(3):232-9.

96. del Pozo MA, Price LS, Alderson NB, Ren XD, and Schwartz MA. Adhesion to the extracellular matrix regulates the coupling of the small GTPase Rac to its effector PAK. *EMBO J.* 2000;19(9):2008-14.

97. Lang P, Gesbert F, Delespine-Carmagnat M, Stancou R, Pouchelet M, and Bertoglio J. Protein kinase A phosphorylation of RhoA mediates the morphological and functional effects of cyclic AMP in cytotoxic lymphocytes. *EMBO J.* 1996;15(3):510-9.

98. Sauzeau V, Le Jeune H, Cario-Toumaniantz C, Smolenski A, Lohmann SM, Bertoglio J, et al. Cyclic GMP-dependent protein kinase signaling pathway inhibits RhoA-induced Ca2+ sensitization of contraction in vascular smooth muscle. *J Biol Chem.* 2000;275(28):21722-9.

99. Ellerbroek SM, Wennerberg K, and Burridge K. Serine phosphorylation negatively regulates RhoA in vivo. *J Biol Chem.* 2003;278(21):19023-31.

100. Tu S, Wu WJ, Wang J, and Cerione RA. Epidermal growth factor-dependent regulation of Cdc42 is mediated by the Src tyrosine kinase. *J Biol Chem.* 2003;278(49):49293-300.

101. Kwon T, Kwon DY, Chun J, Kim JH, and Kang SS. Akt protein kinase inhibits Rac1-GTP binding through phosphorylation at serine 71 of Rac1. *J Biol Chem.* 2000;275(1):423-8.

102. Vignal E, De Toledo M, Comunale F, Ladopoulou A, Gauthier-Rouviere C, Blangy A, et al. Characterization of TCL, a new GTPase of the rho family related to TC10 andCcdc42. *J Biol Chem.* 2000;275(46):36457-64.

103. Ackermann KL, Florke RR, Reyes SS, Tader BR, and Hamann MJ. TCL/RhoJ Plasma Membrane Localization and Nucleotide Exchange Is Coordinately Regulated by Amino Acids within the N Terminus and a Distal Loop Region. *J Biol Chem.* 2016;291(45):23604-17.

104. de Toledo M, Senic-Matuglia F, Salamero J, Uze G, Comunale F, Fort P, et al. The GTP/GDP cycling of rho GTPase TCL is an essential regulator of the early endocytic pathway. *Mol Biol Cell.* 2003;14(12):4846-56.

105. Aspenstrom P, Fransson A, and Saras J. Rho GTPases have diverse effects on the organization of the actin filament system. *Biochem J.* 2004;377(Pt 2):327-37.

106. Fukushima Y, Okada M, Kataoka H, Hirashima M, Yoshida Y, Mann F, et al. Sema3E-PlexinD1 signaling selectively suppresses disoriented angiogenesis in ischemic retinopathy in mice. *J Clin Invest.* 2011;121(5):1974-85.

107. Kaur S, Leszczynska K, Abraham S, Scarcia M, Hiltbrunner S, Marshall CJ, et al. RhoJ/TCL regulates endothelial motility and tube formation and modulates

actomyosin contractility and focal adhesion numbers. *Arterioscler Thromb Vasc Biol.* 2011;31(3):657-64.

108. Kim C, Yang H, Fukushima Y, Saw PE, Lee J, Park JS, et al. Vascular RhoJ is an effective and selective target for tumor angiogenesis and vascular disruption. *Cancer Cell.* 2014;25(1):102-17.

109. Kusuhara S, Fukushima Y, Fukuhara S, Jakt LM, Okada M, Shimizu Y, et al. Arhgef15 promotes retinal angiogenesis by mediating VEGF-induced Cdc42 activation and potentiating RhoJ inactivation in endothelial cells. *PLoS One.* 2012;7(9):e45858.

110. Leszczynska K, Kaur S, Wilson E, Bicknell R, and Heath VL. The role of RhoJ in endothelial cell biology and angiogenesis. *Biochem Soc Trans.* 2011;39(6):1606-11.

111. Takase H, Matsumoto K, Yamadera R, Kubota Y, Otsu A, Suzuki R, et al. Genome-wide identification of endothelial cell-enriched genes in the mouse embryo. *Blood.* 2012;120(4):914-23.

112. Yuan L, Sacharidou A, Stratman AN, Le Bras A, Zwiers PJ, Spokes K, et al. RhoJ is an endothelial cell-restricted Rho GTPase that mediates vascular morphogenesis and is regulated by the transcription factor ERG. *Blood.* 2011;118(4):1145-53.

113. Ho H, Aruri J, Kapadia R, Mehr H, White MA, and Ganesan AK. RhoJ and Pak Kinases Regulate Melanoma Chemoresistance by Suppressing Pathways that Sense DNA Damage. *Cancer Res.* 2012.

114. Ho H, Soto Hopkin A, Kapadia R, Vasudeva P, Schilling J, and Ganesan AK. RhoJ modulates melanoma invasion by altering actin cytoskeletal dynamics. *Pigment Cell Melanoma Res.* 2013;26(2):218-25.

115. Kim C, Yang H, Park I, Chon HJ, Kim JH, Kwon WS, et al. Rho GTPase RhoJ is Associated with Gastric Cancer Progression and Metastasis. *J Cancer.* 2016;7(11):1550-6.

116. Wilson E, Leszczynska K, Poulter NS, Edelmann F, Salisbury VA, Noy PJ, et al. RhoJ interacts with the GIT-PIX complex and regulates focal adhesion disassembly. *J Cell Sci.* 2014;127(Pt 14):3039-51.

117. Tybulewicz VL, and Henderson RB. Rho family GTPases and their regulators in lymphocytes. *Nat Rev Immunol.* 2009;9(9):630-44.

118. Campisi J. Suppressing cancer: the importance of being senescent. *Science.* 2005;309(5736):886-7.

119. Michaloglou C, Vredeveld LC, Soengas MS, Denoyelle C, Kuilman T, van der Horst CM, et al. BRAFE600-associated senescence-like cell cycle arrest of human naevi. *Nature.* 2005;436(7051):720-4.

120. Lowe SW, Cepero E, and Evan G. Intrinsic tumour suppression. *Nature.* 2004;432(7015):307-15.

121. Bild AH, Yao G, Chang JT, Wang Q, Potti A, Chasse D, et al. Oncogenic pathway signatures in human cancers as a guide to targeted therapies. *Nature.* 2006;439(7074):353-7.

122. Chapman PB, Hauschild A, Robert C, Haanen JB, Ascierto P, Larkin J, et al. Improved survival with vemurafenib in melanoma with BRAF V600E mutation. *N Engl J Med.* 2011;364(26):2507-16.

123. Horn HF, and Vousden KH. Coping with stress: multiple ways to activate p53. *Oncogene.* 2007;26(9):1306-16.

124. Bodemann BO, and White MA. Ral GTPases and cancer: linchpin support of the tumorigenic platform. *Nat Rev Cancer.* 2008;8(2):133-40.

125. Jones RG, and Thompson CB. Tumor suppressors and cell metabolism: a recipe for cancer growth. *Genes Dev.* 2009;23(5):537-48.

126. Bernards R. A missing link in genotype-directed cancer therapy. *Cell.* 2012;151(3):465-8.

127. Pessetto ZY, Yan Y, Bessho T, and Natarajan A. Inhibition of BRCT(BRCA1)-phosphoprotein interaction enhances the cytotoxic effect of olaparib in breast cancer cells: a proof of concept study for synthetic lethal therapeutic option. *Breast Cancer Res Treat.* 2012;134(2):511-7.

128. Satyamoorthy K, Li G, Gerrero MR, Brose MS, Volpe P, Weber BL, et al. Constitutive mitogen-activated protein kinase activation in melanoma is mediated by both BRAF mutations and autocrine growth factor stimulation. *Cancer Res.* 2003;63(4):756-9.

129. Pollock PM, Harper UL, Hansen KS, Yudt LM, Stark M, Robbins CM, et al. High frequency of BRAF mutations in nevi. *Nat Genet.* 2003;33(1):19-20.

130. Tsao H, Goel V, Wu H, Yang G, and Haluska FG. Genetic interaction between NRAS and BRAF mutations and PTEN/MMAC1 inactivation in melanoma. *J Invest Dermatol.* 2004;122(2):337-41.

131. Kaelin WG, Jr. The concept of synthetic lethality in the context of anticancer therapy. *Nat Rev Cancer.* 2005;5(9):689-98.

132. Licciulli S, Maksimoska J, Zhou C, Troutman S, Kota S, Liu Q, et al. FRAX597, a small molecule inhibitor of the p21-activated kinases, inhibits tumorigenesis of neurofibromatosis type 2 (NF2)-associated Schwannomas. *J Biol Chem.* 2013;288(40):29105-14.

133. Harris ML, Buac K, Shakhova O, Hakami RM, Wegner M, Sommer L, et al. A dual role for SOX10 in the maintenance of the postnatal melanocyte lineage and the differentiation of melanocyte stem cell progenitors. *PLoS Genet.* 2013;9(7):e1003644.

134. Haq R, Shoag J, Andreu-Perez P, Yokoyama S, Edelman H, Rowe GC, et al. Oncogenic BRAF regulates oxidative metabolism via PGC1alpha and MITF. *Cancer Cell.* 2013;23(3):302-15.

135. Dumaz N, Hayward R, Martin J, Ogilvie L, Hedley D, Curtin JA, et al. In melanoma, RAS mutations are accompanied by switching signaling from BRAF to CRAF and disrupted cyclic AMP signaling. *Cancer Res.* 2006;66(19):9483-91.

136. She QB, Ma WY, and Dong Z. Role of MAP kinases in UVB-induced phosphorylation of p53 at serine 20. *Oncogene.* 2002;21(10):1580-9.

137. Lidell ME, Seifert EL, Westergren R, Heglind M, Gowing A, Sukonina V, et al. The adipocyte-expressed forkhead transcription factor Foxc2 regulates metabolism through altered mitochondrial function. *Diabetes.* 2011;60(2):427-35.

138. Balu M, Kelly KM, Zachary CB, Harris RM, Krasieva TB, Konig K, et al. Distinguishing between benign and malignant melanocytic nevi by in vivo multiphoton microscopy. *Cancer Res.* 2014;74(10):2688-97.

139. Marzese DM, Liu M, Huynh JL, Hirose H, Donovan NC, Huynh KT, et al. Brain metastasis is predetermined in early stages of cutaneous melanoma by CD44v6 expression through epigenetic regulation of the spliceosome. *Pigment Cell Melanoma Res.* 2015;28(1):82-93.

140. Schurmann A, Mooney AF, Sanders LC, Sells MA, Wang HG, Reed JC, et al. p21-activated kinase 1 phosphorylates the death agonist bad and protects cells from apoptosis. *Mol Cell Biol.* 2000;20(2):453-61.

141. Harada H, Andersen JS, Mann M, Terada N, and Korsmeyer SJ. p70S6 kinase signals cell survival as well as growth, inactivating the pro-apoptotic molecule BAD. *Proc Natl Acad Sci U S A.* 2001;98(17):9666-70.

142. Gadea G, Sanz-Moreno V, Self A, Godi A, and Marshall CJ. DOCK10-mediated Cdc42 activation is necessary for amoeboid invasion of melanoma cells. *Curr Biol.* 2008;18(19):1456-65.

143. Hanahan D, and Weinberg RA. Hallmarks of cancer: the next generation. *Cell.* 2011;144(5):646-74.

144. Abildgaard C, and Guldberg P. Molecular drivers of cellular metabolic reprogramming in melanoma. *Trends Mol Med.* 2015;21(3):164-71.

145. Yuan P, Ito K, Perez-Lorenzo R, Del Guzzo C, Lee JH, Shen CH, et al. Phenformin enhances the therapeutic benefit of BRAF(V600E) inhibition in melanoma. *Proc Natl Acad Sci U S A.* 2013;110(45):18226-31.

146. Frisch SM, and Francis H. Disruption of epithelial cell-matrix interactions induces apoptosis. *J Cell Biol.* 1994;124(4):619-26.

147. Paoli P, Giannoni E, and Chiarugi P. Anoikis molecular pathways and its role in cancer progression. *Biochim Biophys Acta.* 2013;1833(12):3481-98.

148. Boisvert-Adamo K, and Aplin AE. Mutant B-RAF mediates resistance to anoikis via Bad and Bim. *Oncogene.* 2008;27(23):3301-12.

149. Menard RE, Jovanovski AP, and Mattingly RR. Active p21-activated kinase 1 rescues MCF10A breast epithelial cells from undergoing anoikis. *Neoplasia.* 2005;7(7):638-45.

150. Hooijkaas A, Gadiot J, Morrow M, Stewart R, Schumacher T, and Blank CU. Selective BRAF inhibition decreases tumor-resident lymphocyte frequencies in a mouse model of human melanoma. *Oncoimmunology.* 2012;1(5):609-17.

151. Pavey S, Zuidervaart W, van Nieuwpoort F, Packer L, Jager M, Gruis N, et al. Increased p21-activated kinase-1 expression is associated with invasive potential in uveal melanoma. *Melanoma Res.* 2006;16(4):285-96.

152. Ong CC, Jubb AM, Jakubiak D, Zhou W, Rudolph J, Haverty PM, et al. P21-activated kinase 1 (PAK1) as a therapeutic target in BRAF wild-type melanoma. *J Natl Cancer Inst.* 2013;105(9):606-7.

153. Babagana M, Johnson S, Slabodkin H, Bshara W, Morrison C, and Kandel ES. P21-activated kinase 1 regulates resistance to BRAF inhibition in human cancer cells. *Mol Carcinog.* 2017.

154. Hodis E, Watson IR, Kryukov GV, Arold ST, Imielinski M, Theurillat JP, et al. A landscape of driver mutations in melanoma. *Cell.* 2012;150(2):251-63.

155. Wellbrock C, and Arozarena I. The Complexity of the ERK/MAP-Kinase Pathway and the Treatment of Melanoma Skin Cancer. *Front Cell Dev Biol.* 2016;4:33.

156. Kuzu OF, Nguyen FD, Noory MA, and Sharma A. Current State of Animal (Mouse) Modeling in Melanoma Research. *Cancer Growth Metastasis.* 2015;8(Suppl 1):81-94.

157. Martincorena I, Roshan A, Gerstung M, Ellis P, Van Loo P, McLaren S, et al. Tumor evolution. High burden and pervasive positive selection of somatic mutations in normal human skin. *Science.* 2015;348(6237):880-6.

158. Masaki T, Wang Y, DiGiovanna JJ, Khan SG, Raffeld M, Beltaifa S, et al. High frequency of PTEN mutations in nevi and melanomas from xeroderma pigmentosum patients. *Pigment Cell Melanoma Res.* 2014;27(3):454-64.

159. Potrony M, Badenas C, Aguilera P, Puig-Butille JA, Carrera C, Malvehy J, et al. Update in genetic susceptibility in melanoma. *Ann Transl Med.* 2015;3(15):210.

160. Hayward NK. Genetics of melanoma predisposition. *Oncogene.* 2003;22(20):3053-62.

161. Box NF, and Terzian T. The role of p53 in pigmentation, tanning and melanoma. *Pigment Cell Melanoma Res.* 2008;21(5):525-33.

162. Carson C, Omolo B, Chu H, Zhou Y, Sambade MJ, Peters EC, et al. A prognostic signature of defective p53-dependent G1 checkpoint function in melanoma cell lines. *Pigment Cell Melanoma Res.* 2012;25(4):514-26.

163. Cassidy PB, Abdel-Malek ZA, and Leachman SA. Beyond Red Hair and Sunburns: Uncovering the Molecular Mechanisms of MC1R Signaling and Repair of UV-Induced DNA Damage. *J Invest Dermatol.* 2015;135(12):2918-21.

164. Jarrett SG, Wolf Horrell EM, Christian PA, Vanover JC, Boulanger MC, Zou Y, et al. PKA-mediated phosphorylation of ATR promotes recruitment of XPA to UV-induced DNA damage. *Mol Cell.* 2014;54(6):999-1011.

165. Jarrett SG, Wolf Horrell EM, Boulanger MC, and D'Orazio JA. Defining the Contribution of MC1R Physiological Ligands to ATR Phosphorylation at Ser435, a Predictor of DNA Repair in Melanocytes. *J Invest Dermatol.* 2015;135(12):3086-95.

166. Brown EJ, and Baltimore D. ATR disruption leads to chromosomal fragmentation and early embryonic lethality. *Genes Dev.* 2000;14(4):397-402.

167. Cortez D, Guntuku S, Qin J, and Elledge SJ. ATR and ATRIP: partners in checkpoint signaling. *Science.* 2001;294(5547):1713-6.

168. Cimprich KA, and Cortez D. ATR: an essential regulator of genome integrity. *Nat Rev Mol Cell Biol.* 2008;9(8):616-27.

169. Smits VA, and Gillespie DA. DNA damage control: regulation and functions of checkpoint kinase 1. *FEBS J.* 2015;282(19):3681-92.

170. Smith J, Larue L, and Gillespie DA. Chk1 is essential for the development of murine epidermal melanocytes. *Pigment Cell Melanoma Res.* 2013;26(4):580-5.

171. O'Driscoll M, Ruiz-Perez VL, Woods CG, Jeggo PA, and Goodship JA. A splicing mutation affecting expression of ataxia-telangiectasia and Rad3-related protein (ATR) results in Seckel syndrome. *Nat Genet.* 2003;33(4):497-501.

172. Ruzankina Y, Pinzon-Guzman C, Asare A, Ong T, Pontano L, Cotsarelis G, et al. Deletion of the developmentally essential gene ATR in adult mice leads to age-related phenotypes and stem cell loss. *Cell Stem Cell.* 2007;1(1):113-26.

173. Tanaka A, Weinel S, Nagy N, O'Driscoll M, Lai-Cheong JE, Kulp-Shorten CL, et al. Germline mutation in ATR in autosomal- dominant oropharyngeal cancer syndrome. *Am J Hum Genet.* 2012;90(3):511-7.

174. Trapnell C, Pachter L, and Salzberg SL. TopHat: discovering splice junctions with RNA-Seq. *Bioinformatics.* 2009;25(9):1105-11.

175. Trapnell C, Hendrickson DG, Sauvageau M, Goff L, Rinn JL, and Pachter L. Differential analysis of gene regulation at transcript resolution with RNA-seq. *Nat Biotechnol.* 2013;31(1):46-53.

176. Robinson MD, McCarthy DJ, and Smyth GK. edgeR: a Bioconductor package for differential expression analysis of digital gene expression data. *Bioinformatics.* 2010;26(1):139-40.

177. Li H, and Durbin R. Fast and accurate short read alignment with Burrows-Wheeler transform. *Bioinformatics.* 2009;25(14):1754-60.

178. DePristo MA, Banks E, Poplin R, Garimella KV, Maguire JR, Hartl C, et al. A framework for variation discovery and genotyping using next-generation DNA sequencing data. *Nat Genet.* 2011;43(5):491-8.

179. McKenna A, Hanna M, Banks E, Sivachenko A, Cibulskis K, Kernytsky A, et al. The Genome Analysis Toolkit: a MapReduce framework for analyzing next-generation DNA sequencing data. *Genome Res.* 2010;20(9):1297-303.

180. Chen K, Wallis JW, McLellan MD, Larson DE, Kalicki JM, Pohl CS, et al. BreakDancer: an algorithm for high-resolution mapping of genomic structural variation. *Nat Methods.* 2009;6(9):677-81.

181. Fan X, Abbott TE, Larson D, and Chen K. BreakDancer - Identification of Genomic Structural Variation from Paired-End Read Mapping. *Curr Protoc Bioinformatics.* 2014;2014.

182. Rausch T, Zichner T, Schlattl A, Stutz AM, Benes V, and Korbel JO. DELLY: structural variant discovery by integrated paired-end and split-read analysis. *Bioinformatics.* 2012;28(18):i333-i9.

183. Miller CA, Qiao Y, DiSera T, D'Astous B, and Marth GT. bam.iobio: a web-based, real-time, sequence alignment file inspector. *Nat Methods.* 2014;11(12):1189.

184. Marechal A, and Zou L. DNA damage sensing by the ATM and ATR kinases. *Cold Spring Harb Perspect Biol.* 2013;5(9).

185. Nghiem P, Park PK, Kim Y, Vaziri C, and Schreiber SL. ATR inhibition selectively sensitizes G1 checkpoint-deficient cells to lethal premature chromatin condensation. *Proc Natl Acad Sci U S A.* 2001;98(16):9092-7.

186. Brown EJ, and Baltimore D. Essential and dispensable roles of ATR in cell cycle arrest and genome maintenance. *Genes Dev.* 2003;17(5):615-28.

187. Gilad O, Nabet BY, Ragland RL, Schoppy DW, Smith KD, Durham AC, et al. Combining ATR suppression with oncogenic Ras synergistically increases

genomic instability, causing synthetic lethality or tumorigenesis in a dosage-dependent manner. *Cancer Res.* 2010;70(23):9693-702.

188. Dhomen N, Reis-Filho JS, da Rocha Dias S, Hayward R, Savage K, Delmas V, et al. Oncogenic Braf induces melanocyte senescence and melanoma in mice. *Cancer Cell.* 2009;15(4):294-303.

189. Chanoux RA, Yin B, Urtishak KA, Asare A, Bassing CH, and Brown EJ. ATR and H2AX cooperate in maintaining genome stability under replication stress. *J Biol Chem.* 2009;284(9):5994-6003.

190. Verde P, Casalino L, Talotta F, Yaniv M, and Weitzman JB. Deciphering AP-1 function in tumorigenesis: fra-ternizing on target promoters. *Cell Cycle.* 2007;6(21):2633-9.

191. Abeler-Dorner L, Swamy M, Williams G, Hayday AC, and Bas A. Butyrophilins: an emerging family of immune regulators. *Trends Immunol.* 2012;33(1):34-41.

192. Barbee SD, Woodward MJ, Turchinovich G, Mention JJ, Lewis JM, Boyden LM, et al. Skint-1 is a highly specific, unique selecting component for epidermal T cells. *Proc Natl Acad Sci U S A.* 2011;108(8):3330-5.

193. Murray PJ, and Wynn TA. Protective and pathogenic functions of macrophage subsets. *Nat Rev Immunol.* 2011;11(11):723-37.

194. Galdiero MR, Bonavita E, Barajon I, Garlanda C, Mantovani A, and Jaillon S. Tumor associated macrophages and neutrophils in cancer. *Immunobiology.* 2013;218(11):1402-10.

195. Bauer K, Michel S, Reuschenbach M, Nelius N, von Knebel Doeberitz M, and Kloor M. Dendritic cell and macrophage infiltration in microsatellite-unstable and microsatellite-stable colorectal cancer. *Fam Cancer.* 2011;10(3):557-65.

196. Wang T, Xiao M, Ge Y, Krepler C, Belser E, Lopez-Coral A, et al. BRAF Inhibition Stimulates Melanoma-Associated Macrophages to Drive Tumor Growth. *Clin Cancer Res.* 2015;21(7):1652-64.

197. Martinez FO, and Gordon S. The M1 and M2 paradigm of macrophage activation: time for reassessment. *F1000Prime Rep.* 2014;6:13.

198. Tumeh PC, Harview CL, Yearley JH, Shintaku IP, Taylor EJ, Robert L, et al. PD-1 blockade induces responses by inhibiting adaptive immune resistance. *Nature.* 2014;515(7528):568-71.

199. Bald T, Quast T, Landsberg J, Rogava M, Glodde N, Lopez-Ramos D, et al. Ultraviolet-radiation-induced inflammation promotes angiotropism and metastasis in melanoma. *Nature.* 2014;507(7490):109-13.

200. Holzel M, Bovier A, and Tuting T. Plasticity of tumour and immune cells: a source of heterogeneity and a cause for therapy resistance? *Nat Rev Cancer.* 2013;13(5):365-76.

201. Munn DH, and Bronte V. Immune suppressive mechanisms in the tumor microenvironment. *Curr Opin Immunol.* 2015;39:1-6.

202. Larkin J, Lao CD, Urba WJ, McDermott DF, Horak C, Jiang J, et al. Efficacy and Safety of Nivolumab in Patients With BRAF V600 Mutant and BRAF Wild-Type Advanced Melanoma: A Pooled Analysis of 4 Clinical Trials. *JAMA Oncol.* 2015;1(4):433-40.

203. Yang Y. Cancer immunotherapy: harnessing the immune system to battle cancer. *J Clin Invest.* 2015;125(9):3335-7.

204. Merlino G, Flaherty K, Acquavella N, Day CP, Aplin A, Holmen S, et al. Meeting report: The future of preclinical mouse models in melanoma treatment is now. *Pigment Cell Melanoma Res.* 2013;26(4):E8-E14.

205. Bronkhorst IH, Ly LV, Jordanova ES, Vrolijk J, Versluis M, Luyten GP, et al. Detection of M2-macrophages in uveal melanoma and relation with survival. *Invest Ophthalmol Vis Sci.* 2011;52(2):643-50.

206. Ruzankina Y, Schoppy DW, Asare A, Clark CE, Vonderheide RH, and Brown EJ. Tissue regenerative delays and synthetic lethality in adult mice after combined deletion of Atr and Trp53. *Nat Genet.* 2009;41(10):1144-9.

207. Snyder A, Makarov V, Merghoub T, Yuan J, Zaretsky JM, Desrichard A, et al. Genetic basis for clinical response to CTLA-4 blockade in melanoma. *N Engl J Med.* 2014;371(23):2189-99.

208. Van Allen EM, Miao D, Schilling B, Shukla SA, Blank C, Zimmer L, et al. Genomic correlates of response to CTLA-4 blockade in metastatic melanoma. *Science.* 2015;350(6257):207-11.

209. Krauthammer M, Kong Y, Ha BH, Evans P, Bacchiocchi A, McCusker JP, et al. Exome sequencing identifies recurrent somatic RAC1 mutations in melanoma. *Nat Genet.* 2012;44(9):1006-14.

210. Vu HL, Rosenbaum S, Purwin TJ, Davies MA, and Aplin AE. RAC1 P29S regulates PD-L1 expression in melanoma. *Pigment Cell Melanoma Res.* 2015;28(5):590-8.

211. Wang Z, Pedersen E, Basse A, Lefever T, Peyrollier K, Kapoor S, et al. Rac1 is crucial for Ras-dependent skin tumor formation by controlling Pak1-Mek-Erk hyperactivation and hyperproliferation in vivo. *Oncogene.* 2010;29(23):3362-73.

212. Watson IR, Li L, Cabeceiras PK, Mahdavi M, Gutschner T, Genovese G, et al. The RAC1 P29S hotspot mutation in melanoma confers resistance to pharmacological inhibition of RAF. *Cancer Res.* 2014;74(17):4845-52.

213. Carvajal RD, Antonescu CR, Wolchok JD, Chapman PB, Roman RA, Teitcher J, et al. KIT as a therapeutic target in metastatic melanoma. *JAMA.* 2011;305(22):2327-34.

214. Mizuarai S, Irie H, Schmatz DM, and Kotani H. Integrated genomic and pharmacological approaches to identify synthetic lethal genes as cancer therapeutic targets. *Curr Mol Med.* 2008;8(8):774-83.

215. Whitehurst AW, Bodemann BO, Cardenas J, Ferguson D, Girard L, Peyton M, et al. Synthetic lethal screen identification of chemosensitizer loci in cancer cells. *Nature.* 2007;446(7137):815-9.

216. Chow HY, Jubb AM, Koch JN, Jaffer ZM, Stepanova D, Campbell DA, et al. p21-Activated kinase 1 is required for efficient tumor formation and progression in a Ras-mediated skin cancer model. *Cancer Res.* 2012;72(22):5966-75.

217. Chen CF, Ruiz-Vega R, Vasudeva P, Espitia F, Krasieva TB, de Feraudy S, et al. ATR Mutations Promote the Growth of Melanoma Tumors by Modulating the Immune Microenvironment. *Cell Rep.* 2017;18(10):2331-42.

218. Wang J, Chong KK, Nakamura Y, Nguyen L, Huang SK, Kuo C, et al. B7-H3 associated with tumor progression and epigenetic regulatory activity in cutaneous melanoma. *J Invest Dermatol.* 2013;133(8):2050-8.

219. Holst F, Stahl PR, Ruiz C, Hellwinkel O, Jehan Z, Wendland M, et al. Estrogen receptor alpha (ESR1) gene amplification is frequent in breast cancer. *Nat Genet.* 2007;39(5):655-60.

220. Jensen EV, and Jordan VC. The estrogen receptor: a model for molecular medicine. *Clin Cancer Res.* 2003;9(6):1980-9.

221. Hall A, Meyle KD, Lange MK, Klima M, Sanderhoff M, Dahl C, et al. Dysfunctional oxidative phosphorylation makes malignant melanoma cells addicted to glycolysis driven by the (V600E)BRAF oncogene. *Oncotarget.* 2013;4(4):584-99.

222. Scott DA, Richardson AD, Filipp FV, Knutzen CA, Chiang GG, Ronai ZA, et al. Comparative metabolic flux profiling of melanoma cell lines: beyond the Warburg effect. *J Biol Chem.* 2011;286(49):42626-34.

223. Lim JH, Luo C, Vazquez F, and Puigserver P. Targeting mitochondrial oxidative metabolism in melanoma causes metabolic compensation through glucose and glutamine utilization. *Cancer Res.* 2014;74(13):3535-45.

224. Abildgaard C, Dahl C, Basse AL, Ma T, and Guldberg P. Bioenergetic modulation with dichloroacetate reduces the growth of melanoma cells and potentiates their response to BRAFV600E inhibition. *J Transl Med.* 2014;12:247.

225. Barbi de Moura M, Vincent G, Fayewicz SL, Bateman NW, Hood BL, Sun M, et al. Mitochondrial respiration--an important therapeutic target in melanoma. *PLoS One.* 2012;7(8):e40690.

226. Parmenter TJ, Kleinschmidt M, Kinross KM, Bond ST, Li J, Kaadige MR, et al. Response of BRAF-mutant melanoma to BRAF inhibition is mediated by a network of transcriptional regulators of glycolysis. *Cancer Discov.* 2014;4(4):423-33.

227. Zeller KI, Jegga AG, Aronow BJ, O'Donnell KA, and Dang CV. An integrated database of genes responsive to the Myc oncogenic transcription factor: identification of direct genomic targets. *Genome Biol.* 2003;4(10):R69.

228. Morrish F, Noonan J, Perez-Olsen C, Gafken PR, Fitzgibbon M, Kelleher J, et al. Myc-dependent mitochondrial generation of acetyl-CoA contributes to fatty acid biosynthesis and histone acetylation during cell cycle entry. *J Biol Chem.* 2010;285(47):36267-74.

229. Mukhtar RA, Nseyo O, Campbell MJ, and Esserman LJ. Tumor-associated macrophages in breast cancer as potential biomarkers for new treatments and diagnostics. *Expert Rev Mol Diagn.* 2011;11(1):91-100.

230. Sakaguchi S. Naturally arising CD4+ regulatory t cells for immunologic self-tolerance and negative control of immune responses. *Annu Rev Immunol.* 2004;22:531-62.

231. Simpson TR, Li F, Montalvo-Ortiz W, Sepulveda MA, Bergerhoff K, Arce F, et al. Fc-dependent depletion of tumor-infiltrating regulatory T cells co-defines the

efficacy of anti-CTLA-4 therapy against melanoma. *J Exp Med.* 2013;210(9):1695-710.